University of Alberta

The relationship between iceberg calving rates and ice flow dynamics for nine major tidewater glaciers draining the Agassiz and western Grant Ice Caps, in Nunavut, Canada, between 1959 and 2003

by

Scott Norman Williamson 

A thesis submitted to the Faculty of Graduate Studies and Research
in partial fulfillment of the requirements for the degree of

Master of Science

Earth and Atmospheric Science

Edmonton, Alberta
Spring 2007

Your file Votre référence
ISBN: 978-0-494-30039-8
Our file Notre référence
ISBN: 978-0-494-30039-8

ABSTRACT

This remote sensing study investigates the relationship between iceberg calving rates and ice flow dynamics for nine major tidewater glaciers draining the Agassiz and western Grant Ice Caps in Nunavut, Canada, between 1959 and 2003. Glacier calving rates and flow dynamic variability are largely unknown for much of the Arctic and must be quantified because the current warming trend occurring in the Arctic has the potential to change this regions ice caps contribution to sea-level change. The results reported here show that calving rates (1999 – 2003) are highly variable, with rates changing by up to a factor of two between successive years and summer calving rates ~2 – 8 times larger than the annual rates. The largest annual velocities recorded were ~ 400 – 700 m a^{-1}, but velocities of ~100 – 200 m a^{-1} were common. Summer velocities were up to an order of magnitude larger than annual values.

ACKNOWLEDGEMENTS

I would like to thank my supervisor, Dr. Martin Sharp, for his guidance throughout this project. Many thanks go to Dr. Dave Burgess, Dr. Gabriel Wolken, Dr. Fiona Cawkwell and Dr. Lindsey Nicholson for their assistance in bringing this thesis to fruition. I would like to thank my parents, Sue and Darrell, for their support and encouragement. I would like to thank Jason Young and Kristi Koons for their generous support without which finishing this thesis would have been extremely difficult. Lastly I would like to thank Zoé Stacey for her love and support.

Table of Contents

Introduction	1
Background	2
Glacier dynamics and iceberg calving	3
Iceberg calving mechanisms	7
The relation between icebergs and glacier type	10
Iceberg calving rate	12
Glacier flow dynamics, calving rates and climate change	12
Remote sensing, glacier dynamics and iceberg calving	16
Study Area	19
Methods	23
Image sources	23
Optical image preparation	25
Glacier surface feature delineation	28
Glacier velocity	31
Calving rate error analysis	35
Iceberg calving rate estimates	36
Results	39
Ice cap calving rates	107
Discussion	108
Glacier flow rates and flow rate variability	108
The implications of calving rate variation	113
Variations in glacier calving rate associated with changes in flow dynamics	114
Floating tidewater glacier tongues and mass balance	115
Further work	115

Conclusions 116
References 117

List of Tables

Table 1. Iceberg dominant characteristics and relative production from various Svalbard tidewater ice masses. 11

Table 2. Tidewater glaciers investigated in this study. All Glaciers drain the Agassiz Ice Cap, except the Otto Glacier which drains the western Grant Ice Cap (‡Indicates unofficial glacier name). 23

Table 3. Imagery details (See Figure 3 and Table 2 for ice cap locations). 24

Table 4. Glacier terminus area change error between 1999 and 2003. 30&31

Table 5. Otto Glacier Terminus Region Properties & Flow Characteristics 48

Table 6. Calving rates 51&52

Table 7. Eugenie Glacier Terminus Region Properties & Flow Characteristics 56

Table 8. Antoinette Glacier Properties & Flow Characteristics 64

Table 9. Lake Tuborg Glacier Properties & Flow Characteristics 72

Table 10. D'Iberville Glacier Properties & Flow Characteristics 78

Table 11. Cañon Glacier Properties & Flow Characteristics 85

Table 12. Parrish Glacier Properties & Flow Characteristics 91

Table 13. John Richardson Bay Glacier (East) Properties & Flow Characteristics 96

Table 14. Sawyer Bay Glacier Properties & Flow Characteristics 102

List of Figures

Figure 1. Crevasse orientation as a result of the stress field on a glacier's surface: (a) shear stress exerted by valley walls only, (b) shear stress exerted by valley walls and extending flow, (c) shear stress exerted by the valley walls and compressive flow. 4

Figure 2. Mechanisms of grounded tidewater glacier iceberg production: (a) terminus specific over-steepening, (b) thermal erosion at water-line, (c) preferential crevasse penetration in terminus region over-steepening, (d) buoyancy of sub-marine platform. 8

Figure 3. Iceberg calving tidewater glaciers investigated in this study – base imagery is July 10, 1999 Landsat 7 Panchromatic (Glaciers are identified by letter in Table 1). 22

Figure 4. Terminus area change (0.875 km^2 reduction) of John Richardson Glacier (East) between July 5, 1959 (yellow) and July 5, 2003 (blue) displayed on the 1959 aerial photograph (© A16604-020, July 5, 1959). 29

Figure 5. Glacier surface velocity map produced using Visi-Corr software for Parrish Glacier between the July 10, 1999 Landsat 7 panchromatic image and the July 21, 2001 Aster image displayed on the July 10, 1999 Landsat 7 panchromatic image. Examples of large locally anomalous flow vectors (red circles) indicate positions where the image cross-correlation software did not correctly measure displacement between images and are removed from results. 34

Figure 6. Segment of area (K) determined with glacier width (parameter c) and glacier centre-line depth (parameter h). 37

Figure 7. Otto Glacier velocities between 1959 and 2003. 40

Figure 8. Otto Glacier calving rates between 1999 and 2003. 40

Figure 9. Eugenie Glacier velocities between 1999 and 2003. 41

Figure 10. Eugenie Glacier calving rates between 1999 and 2003. 41

Figure 11. Antoinette Glacier velocities between 1999 and 2002. 41

Figure 12. Antoinette Glacier calving rates between 1999 and 2002. 41

Figure 13. Lake Tuborg Glacier velocities between 1999 and 2002. 42
Figure 14. Lake Tuborg Glacier calving rates between 1999 and 2002. 42
Figure 15. D'Iberville Glacier velocities between 1974 and 2003. 42
Figure 16. D'Iberville Glacier calving rates between 1974 and 2003. 42
Figure 17. Cañon Glacier velocities between 1999 and 2003. 43
Figure 18. Cañon Glacier calving rates between 1999 and 2003. 43
Figure 19. Parrish Glacier velocities between 1999 and 2003. 43
Figure 20. Parrish Glacier calving rates between 1999 and 2003. 43
Figure 21. Otto Glacier terminus position and surface feature displacement between July 7 and August 17, 1959 aerial photographs, displayed on the July 7, 1959 aerial photograph (© A16606-029, July 7, 1959). 49
Figure 22. Selected terminus positions, terminus region width measurement location, between 1959 and 2003 and examples of surface feature displacement between 1999 and 2003 and iceberg crevasse feature from Otto Glacier, displayed on the July 10, 1999 Landsat 7 panchromatic image. 50
Figure 23. 1959 aerial photograph (© A16612-049, July 7, 1959) of Eugenie Glacier indicating melt water channels and terminus width Measurement position. 57
Figure 24. Select terminus positions and examples of surface features used to determine surface displacement from Eugenie Glacier displayed on the July 10, 1999 Landsat 7 panchromatic image. 58
Figure 25. Selected image cross-correlation intra-annual velocity results (m a^{-1}) for Eugenie Glacier between June 23 to July 21, 2001 displayed on the July 21, 2001 Landsat 7 panchromatic image. Velocities indicated on the map are for the adjacent vectors. 59
Figure 26. August 15, 1966 Corona imagery of Eugenie Glacier showing image over-exposure typical of the 1966 Corona imagery. 60
Figure 27. 1959 aerial photograph (© A16694-040, July 27, 1959) of Antoinette (bottom of image) and Lake Tuborg Glaciers showing the terminus regions and the position of width measurements. 65

Figure 28. Selected terminus positions and examples of surface features from Antoinette Glacier displayed on the July 10, 1999 Landsat 7 panchromatic image. 66

Figure 29. Image cross-correlation velocity results (m a^{-1}) with approximate centre-line velocities at 1 km intervals indicated for Antoinette Glacier between July 10, 1999 and June 15, 2001 displayed on the July 10, 1999 Landsat 7 panchromatic image. 67

Figure 30. Image cross-correlation velocity results (m a^{-1}) with approximate centre-line velocities indicated at 1 km intervals for Antoinette Glacier between June 15 and July 19, 2001 displayed on the June 15 ASTER imagery. 68

Figure 31. Image cross-correlation velocity results (m a^{-1}) with approximate centre-line velocities indicated at 1 km intervals for Antoinette Glacier between July 19 and August 19, 2001 displayed on the July 19 ASTER imagery. 69

Figure 32. Lake Tuborg Glacier select terminus positions and an example of repeated crevasse patterns displayed on the July 10, 1999 Landsat 7 panchromatic image. 73

Figure 33. Image cross-correlation velocity results (m a^{-1}) for Lake Tuborg Glacier between July 10, 1999 and July 19, 2001 displayed on the July 10, 1999 Landsat 7 panchromatic image. 74

Figure 34. 1959 aerial photograph (© A16692-032, July27, 1959) showing the position at which the terminus region width was measured for d'Iberville Glacier. This imagery shows the fjord at the terminus to be sea-ice free. 79

Figure 35. Select terminus positions and examples of surface features from d'Iberville Glacier displayed on the August 4, 2003 ASTER image. This image shows the fjord at the terminus to be free of sea-ice. 80

Figure 36. Image cross-correlation velocity results (m a^{-1}) for d'Iberville Glacier between July 10, 1999 and June 27, 2001 displayed on the July 10, 1999 Landsat 7 panchromatic image. 81

Figure 37. D'Iberville Glacier's large iceberg with crevasse features captured on the July 2, 2002 Landsat 7 panchromatic image. 82

Figure 38. 1959 aerial photograph (© A16681-085, July 17, 1959) of Cañon Glacier showing the terminus width measurement position, a crevasse penetrating into the terminus and a sea-ice free Cañon Fjord. 86

Figure 39. Select terminus positions and examples of surface features on Cañon Glacier displayed on July 10, 1999 Landsat 7 panchromatic imagery. 87

Figure 40. Image cross-correlation velocity results (m a^{-1}) for Cañon Glacier between July 10, 1999 and July 31, 2000 displayed on the July 10, 1999 Landsat 7 panchromatic image. 88

Figure 41. Parrish Glacier July 15, 1959 aerial photograph displaying melt water channels and tabular icebergs (© A16721-086, July 15, 1959). 92

Figure 42. Parrish Glacier selected terminus positions with the terminus region width measured perpendicular to glacier flow adjacent to but not crossing the July 9, 2003 terminus position. Examples of surface features used to determine surface velocity are also shown. All features are displayed on the July 10, 1999 Landsat 7 panchromatic image. 93

Figure 43. Image cross-correlation velocity results (m a^{-1}) for Parrish Glacier between July 10, 1999 and July 21, 2001 displayed on the July 10, 1999 Landsat 7 panchromatic image. Centre-line velocities are displayed at the east margin. 94

Figure 44. 1959 aerial photograph (© A16604-020, July 5, 1959) of John Richardson Bay Glacier (East). 97

Figure 45. Select terminus positions, melt water channels and terminus region width measurement position for John Richardson Bay Glacier (East) displayed on July 31, 2003 ASTER imagery. 98

Figure 46. Image cross-correlation velocity results (m a^{-1}) for John Richardson Glacier (East) between July 10, 1999 and July 2, 2002 displayed on the July 10, 1999 Landsat 7 panchromatic image. Centre-line velocities are indicated on the map. 99

Figure 47. Benedict and Sawyer Bay Glaciers' terminus regions including Benedict Glacier's terminal moraine displayed on the July 4, 2003 ASTER imagery. 103

Figure 48. 1959 aerial photograph (© A16708-099, July 28, 1959) of Sawyer Bay Glacier. 104

Figure 49. Select terminus positions and terminus region width measurement position for Sawyer Bay Glacier displayed on July 4, 2003 ASTER imagery. 105

Figure 50. Image cross-correlation velocity results (m a^{-1}) for Sawyer Bay Glacier between July 10, 1999 and July 4, 2003 displayed on the July 10, 1999 Landsat 7 panchromatic image. 106

INTRODUCTION

Global climate models have predicted strong climate warming in northern high latitudes in the coming century (e.g., IPCC, 2001). There is now evidence that these predictions are accurate (Overpeck et al., 1997; Serreze et al., 2000). Increasing yearly air temperature in Greenland has been associated with widespread flow acceleration of glaciers at low elevations. This has occurred concurrently with an increase in mass loss related to increased surface melting, terminus retreat, and dynamic thinning (Abdalati et al., 2001; Krabill et al., 2004). This ongoing behaviour has been described in detail for two of Greenland's largest glaciers, Helheim Glacier (Howat et al., 2005) and Jakobshavn Isbræ (Joughin et al., 2004). These studies indicate that thinning is driving the larger retreat rates from floating and grounded termini alike, although likely through different mechanisms. Greenland's mass loss doubled between 1996 and 2005 with dynamic thinning accounting for as much as 2/3 of the increase (Rignot and Kanagaratnam, 2006. Furthermore, a glacier's velocity, and thus its ability to remove ice mass, may increase as summer surface melt water penetrates to the bed and enhances or activates sliding (e.g. Zwally et al., 2002) or may increase in relation to the removal of the buttressing effect caused by collapse of a floating glacier tongue (e.g. Joughin et al., 2004) or melting of sea-ice (e.g. Luckman and Murray, 2005). Longer periods of warmer summer air temperatures may make more melt water available for sliding and cause sea-ice coverage to be absent for longer durations. Although little variation in seasonal flow rate has been recorded on the major fast flowing glaciers in Greenland (Rignot and Kanagaratnam, 2006), an anomalously warm summer has been correlated with a flow regime shift to faster annual flow and dynamic thinning on a major outlet glacier (Luckman and Murray, 2005). Therefore if a significant dynamic glacier response to climate change is emerging, or is already underway as it appears to be in Greenland, then predictions of recent and future sea level change will need to take this into account. However, most current predictions of the glacial contribution to future sea level change in a warmer climate largely disregard the contribution by a response in flow dynamics, which could be a major contribution (Church et al., 2001).

Glaciers contribute to sea level change by adding water mass via melting and iceberg calving and removing water mass via precipitation (snowfall) that is sequestered

as glacier ice. The summation of water mass added to and removed from a glacier within a specified time period is a glacier's mass balance. Iceberg calving has recently been shown to be a significant ablation term in the mass balance of tidewater glaciers in Arctic regions (e.g. Burgess et al., 2005; Dowdeswell et al., 2002), potentially accounting for up to 40% of the mass lost from the ice caps studied. However, most calving rates have been estimated as temporal averages using the assumption of invariant flow velocities, typically on the order of decades (e.g. Burgess et al., 2005). Annual iceberg calving rates are not often measured, with only a few estimates available for tidewater glaciers on Ellesmere Island, Nunavut, Canada (e.g. Short and Gray, 2005). Furthermore, calving rates may be sensitive to changes in ice flow dynamics, but this aspect is relatively unknown because there are virtually no studies of the temporal variability in calving rates in this region (and the question of cause and effect is not resolved).

The aim of this study is to determine annual and seasonal iceberg calving rates and velocities of major tidewater valley glaciers draining the Agassiz and western Grant Ice Caps on northern Ellesmere Island, Nunavut, Canada. To accomplish this aim, glacier flow velocities and terminus area changes are determined from 1999 – 2003 satellite imagery and combined with glacier thickness measurements acquired by airborne radio-echo sounding to estimate iceberg calving rates. Lastly, to gain an appreciation of whether, and by how much, calving rates and flow dynamics have changed between 1959 and 2003, 1959 and 1966 aerial and satellite photographs are compared to 1999 – 2003 digital satellite imagery for differences in glacier terminus position, terminus region width and the presence and pattern of features such as crevasses, which are diagnostic of relative flow rate.

BACKGROUND

This section is intended to provide the reader with the necessary information to understand the relationship between glacier dynamics and iceberg calving. Glacier flow dynamics and iceberg calving rates are also explored in the context of a changing climate. Finally, the role of remote sensing in characterising glacier flow dynamics and estimating iceberg calving is discussed.

Glacier dynamics and iceberg calving

Tidewater glacier terminus thickness is strongly linked to a glacier's flow dynamics and iceberg calving rates. Thickness change near a tidewater terminus is driven by longitudinal gradients in ice flux, modified by 3 terms of mass balance: surface melt/accumulation, melt/freeze-on from the underwater part of the terminal cliff or base of a floating tongue, and iceberg calving. The longitudinal ice flux can dominate the thickness changes at the terminus compared to the thickness changes brought about by mass balance changes. An increasing longitudinal ice flux towards the terminus may result in thinning; a decreasing longitudinal ice flux towards the terminus may result in thickening (assuming constant glacier width). Variations in the other 3 components of the mass balance also affect thickness change. Water mass removal due to increased surface melting may act to thin a glacier; increased snow accumulation may serve to thicken it. Melting on the bottom of a floating ice tongue serves to reduce the thickness whereas water freezing to the bottom of a floating ice tongue serves to thicken it. Iceberg calving provides a means of ice mass removal that can cause terminus retreat and thinning because the ice removed at the terminus is larger than provided from up glacier.

Whether a region of a glacier is growing thicker or thinner is related to the type of flow it is experiencing. Nye (1952) used Alaskan glacier photographs to classify surface crevasse patterns into two general groups depending on whether the glacier is undergoing extending or compressive flow (Figure 1). Crevasses tend to form perpendicular to the direction of principal tensile stress at the glacier surface. When there is only lateral shear exerted by the glacier moving past valley walls (assuming negligible longitudinal stress), the crevasse patterns are as shown in Figure 1a. When no lateral friction is exerted by the valley walls, crevasses are aligned either across flow (longitudinal extending flow) or parallel to flow (longitudinal compressive flow). Lateral friction rotates these stresses to produce the crevasse patterns shown in Figure 1b (lateral shear superimposed on longitudinal extending flow) and Figure 1c (lateral shear superimposed on longitudinal compressive flow). In a region of extending flow, a glacier will tend to thin unless the longitudinal gradient in ice flux is offset by a positive surface or basal mass balance. In a region of compressive flow the compressive strain results in glacier thickening unless this is offset by a negative surface or basal mass balance.

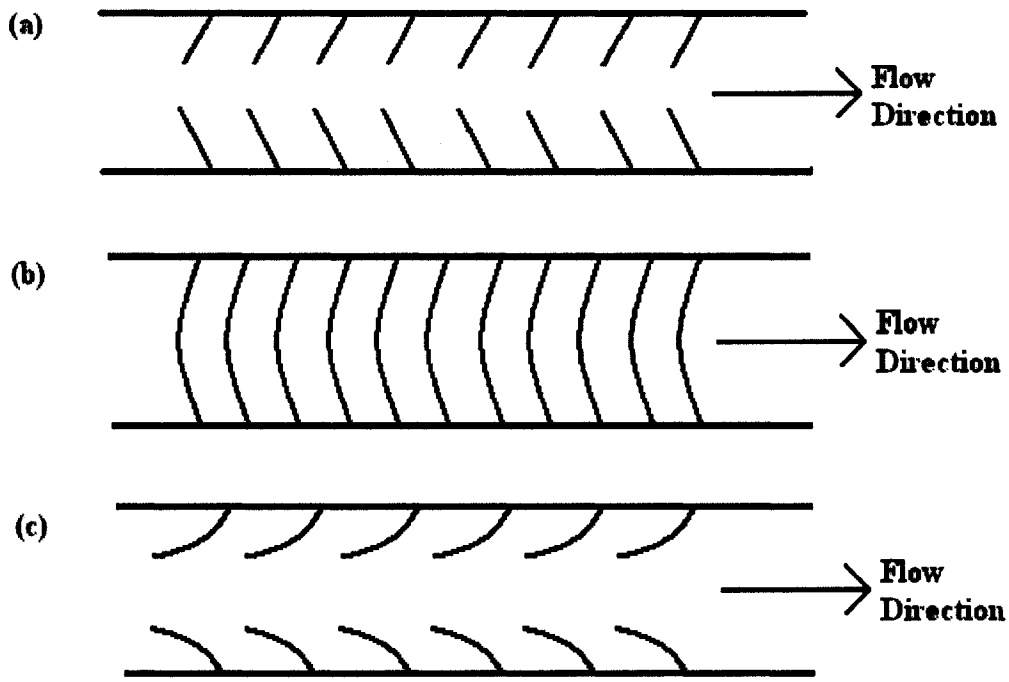

Figure 1. Crevasse orientation as a result of the stress field on a glacier's surface: (a) shear stress exerted by valley walls only, (b) shear stress exerted by valley walls and extending flow, (c) shear stress exerted by the valley walls and compressive flow.

Glacier flow can sometimes vary in a cyclical fashion. Two types of cyclical flow variation are widely recognised: glacier surges (e.g. Meier and Post, 1969; Murray et al., 2003a) and the tidewater glacier cycle (e.g. Meier and Post 1987). Both may result in advances and retreats of the glacier terminus. The classical glacier surge cycle consists of a relatively short period of high flow rates (years to decades) followed by a much longer quiescent phase (decades to centuries) during which flow rates are reduced by at least an order of magnitude. Climate seems to play a role in surge duration, but the role, if any, of climate in surge initiation is largely unknown. In Svalbard, for example, where the climate is relatively cold and arid, active phases of surge-type glaciers have durations of 7-11 years (Murray et al., 2003b). In the more temperate climate of maritime Alaska, however, active surge phases are typically shorter in duration and more intense (e.g. southeast Alaska; Lawson, 1997). Glacier surge duration in the Canadian Arctic is not well known compared to other regions, but evidence suggests that it is probably more

similar to (or even longer than) the long surge durations observed in Svalbard than to the short and intense Alaska surges (e.g. Copland et al., 2003a).

During the high velocity phase of a glacier surge, ice mass is transferred down-glacier from a reservoir area to a receiving area. When the surging ice reaches the terminus region, the terminus generally (but not always) advances rapidly, thickens, and becomes highly crevassed due to large spatial gradients in velocity. High calving rates can be associated with the high glacier velocity phase of actively surging tidewater glaciers (Post, 1969) even though the terminus tends to advance rapidly. During the quiescent phase, the lower region of the glacier tends to thin and the terminus may retreat, while ice thickens in the reservoir area. Furthermore, the calving rate tends to decrease due to reduced flow rates. The quiescent period is marked by reduced crevassing on the glacier's terminus due to decreases in spatial velocity gradients and this eventually allows the development of supra-glacial melt water channels. These melt water channels are obliterated by heavy crevassing during glacier surges.

Due to a paucity of field data from remote regions, including the Canadian Arctic, many glacier surges have not been observed directly. The occurrence of surge-type behaviour is, therefore, often inferred from glacier surface features that are visible on aerial photographs and/or satellite imagery. These features indicate whether a glacier has surged or has not surged during the residence time of the glacier ice within its drainage basin (e.g. Meier and Post, 1969). Copland and others (2003a) used diagnostic features identified on 1959 and 1999 imagery to identify recently active surge-type glaciers in the Canadian High Arctic. Features used to identify surge activity included: a) high ice surface velocity or a large change in velocity between two sets of images; b) large changes in terminus position (typically advances of the terminus during surges and retreats during quiescence); c) looped surface moraines and ice foliation; d) a heavily crevassed surface or change in the degree of surface crevassing between repeat imagery; e) features such as potholes, which are water-filled sealed crevasses (e.g. Sturm, 1987) and melt water channels on the glacier surface (which are typically indicative of the quiescent phase); f) shear margins that suggest a surging ice stream flowing within slower moving ice; g) the digitate nature of some tidewater glacier termini. A digitate terminus is typically the result of a glacier that has surged onto open water and has extended in a

shape akin to a crow's foot due to a lack of backpressure at the terminus. The length of a digitate terminus is usually on the order of several times greater than the glacier's width at the terminus. 51 glaciers on Northern Ellesmere Island were identified as surge type, likely surge type, or possibly surge type by Copland and others (2003a) based upon analysis of surge surface features on 1959 and 1999 imagery, and first hand documentation of surges. Where surges were documented (e.g. a rapidly advancing terminus, a migrating ice bulge, or extreme crevassing in the terminus region) the glacier was considered to be an active surge type glacier. If only surge indicators from imagery were used to determine the likelihood of surge type classification, then the intensity and number of indicators was used to distinguish between likely and possibly surge type. If the indicators became less evident through time then the surge type glacier was determined to be quiescent. If no surge features were identified then the glacier was deemed to be non-surge type.

The tidewater glacier cycle consists of a long period of very slow advance, on the order of 1000 years, followed by a period of rapid terminus disintegration and retreat, which usually takes less than 100 years (Meier and Post, 1987). This period is marked by high velocities and crevassing more typical of actively surging glaciers. The retreat phase of tidewater glaciers is marked by high calving rates that are often associated with the terminus retreating into deep water. The tidewater cycle is, therefore, described by the direction and rate of terminus position change. A feedback loop may also occur – retreat decreases the backpressure at the terminus, which causes stretching and increased velocity at the terminus, which in turn causes more stretching. Stretching of a glacier's terminus causes thinning, and is often also marked by flow acceleration in the terminus region. Because of the large velocity changes, rapid terminus retreat and heavy crevassing that can occur on non-surging tidewater glaciers (Meier and Post, 1987), Copland and others (2003a) used a combination of surface criteria to identify surge-type glaciers. This ensured better differentiation between surge type and non-surge type glaciers. High iceberg calving rates are often associated with terminus disintegration (rapid terminus retreat) of tidewater glaciers (Meier and Post, 1987). Much lower calving rates are associated with the gradual advance of non-surge type glaciers due to the low velocities and relatively stable terminus position.

In the Canadian Arctic, Short and Gray (2005) found significant short-term variations in the velocity of glaciers that were not considered to be surge type. This confirms the suggestion by Mayo (1978) that some glaciers may exhibit short-term increases in velocity for periods lasting up to several years that do not result in the volume of ice mass removal normally associated with a surge. Furthermore, some tidewater glaciers may flow at high velocities for long periods of time, but observations are insufficient to determine whether or not these fast-flow episodes are surges. Müller (1969) suggested that periods of increased tidewater glacier activity may last as long as 50 years, but whether or not there are multiple types of cyclical flow occurring in the tidewater cycle (as suggested by Short and Gray, 2005) is largely unknown. Periods of fast flow on tidewater glaciers can occur when they are grounded below sea level (Meier and Post, 1987). These periods of fast flow are related to buoyancy changes resulting from changes in glacier thickness or sea level. Furthermore, a glacier's velocity may increase as surface melt water penetrates to the bed in summer and enhances or activates sliding (e.g. Zwally et al., 2002). A glacier with a floating terminus may experience velocity increases as the buttressing effect of a floating tongue decreases during retreat or collapse (e.g. Joughin et al., 2004). However, these mechanisms should not be viewed as separate. A grounded tidewater terminus may, through thinning, approach flotation so that basal resistance to flow decreases and flow can accelerate. Increased velocity by sliding may propagate across the grounding line (the position where a glacier's terminus begins to float) and be recorded over the floating terminus.

Iceberg calving mechanisms

Glacier flow is affected by whether a tidewater terminus is floating or grounded and so too are the types of icebergs produced. Iceberg characteristics relate to the type of terminus from which they originate by calving mechanisms. Ice will float in water because it is less dense, thus producing features like floating glacier tongues and icebergs. However, if ice thickness relative to the depth of water in which it resides is greater than the thickness required for buoyancy, the ice will ground. Thinning may also cause a grounded terminus to approach flotation (van der Veen, 2002), which will likely increase iceberg production. The increase in buoyancy will decrease the basal resistance to flow

which leads to terminus region flow acceleration. Flow acceleration leads to enhanced iceberg calving or terminus advance (and terminus region stretching – extending flow), or a combination of the two. These responses to flow acceleration further reduce the thickness of the terminus region. When the terminus region becomes too thin to maintain its integrity, rapid retreat ensues through an increase in iceberg calving. The differences in glacier terminus geometry, thickness, flow and buoyancy create different calving mechanisms from floating and grounded termini.

Van der Veen (2002) identified several different mechanisms of iceberg production from a grounded terminus (Figure 2).

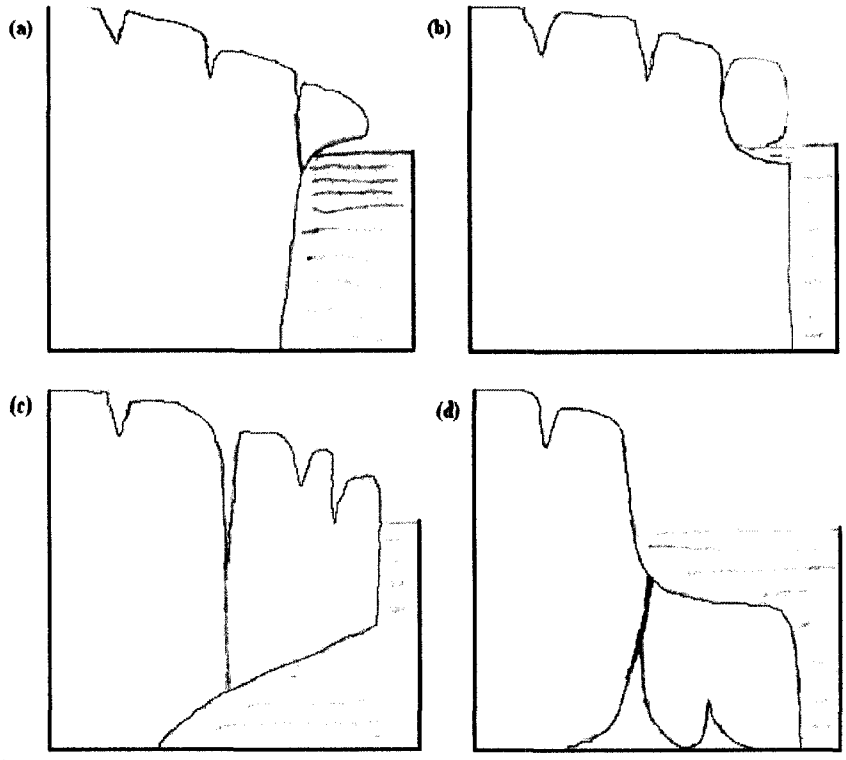

Figure 2. Mechanisms of grounded tidewater glacier iceberg production: (a) terminus specific over-steepening, (b) thermal erosion at water-line, (c) preferential crevasse penetration in terminus region over-steepening, (d) buoyancy of sub-marine platform.

Often a glacier will undergo thinning as a precursor to acceleration and terminus retreat. Crevasses will be involved in iceberg calving because of fracture propagation (Kirkbride and Warren, 1999) and will likely be formed in response to any velocity gradient induced by differential acceleration of flow. Maximum bed parallel shearing occurs during

periods of limited water lubrication, or in the absence of highly deformable materials at the base. Wave action can undercut the glacier at the waterline. These factors result in an over-steepened terminal ice cliff, which can cause sections of ice to calve (Figure 2a). Preferential crevasse penetration can produce icebergs with crevasse markings on their surface. Furthermore, crevasse depth can increase significantly if the crevasse is filled with water (Weertman, 1973) potentially decreasing the distance between crevasses that delineate icebergs. In the High Arctic, the period of increased availability of glacier surface melt water is in the summer, which generally equates to the months of June, July and August. However, the length of the summer period decreases progressively as latitude increases. During periods of increased melt water penetration to the bed, increased sub-glacial water pressure may promote glacier sliding and reduce bed-parallel shearing. Thermal erosion at the waterline may also cause iceberg calving (Figure 2b). Over-steepening may induce a bending moment at the terminus, causing preferential crevasse penetration to the full depth of the glacier, which produces relatively large icebergs (Figure 2c). Successive sub-aerial-calving events, defined by Hughes (2002) as slab-calving, will produce slab icebergs and leave an ice ledge below the water line. The buoyancy of this sub-marine platform or ledge creates a bending moment that will cause crevasses at the bottom to fracture upward, causing the sub-marine ledge to break off (Figure 2d) (Hughes, 2002).

Floating glacier termini are a common phenomenon in Arctic regions. Iceberg calving mechanisms from floating termini are not as well defined as those associated with grounded termini. Iceberg calving directly at the floating terminus is strongly linked to wave motion, diurnal tides, astronomical tides, and catastrophic impulses. These factors produce different levels of vertical oscillation in a floating ice tongue (Holdsworth, 1969), which creates a bending moment over the floating ice tongue. The bending moment caused by an imbalance of ice pressure and hydrostatic pressure at the ice front and along the edges of unconstrained ice tongues is a very effective mechanism for the production of strongly prismatic icebergs (Reeh, 1968). Crevasses on a glacier's surface may fill with water during the summer when surface melt is high. The melt water will deepen crevasses and thereby create planes of weakness from which icebergs will be produced. Tabular icebergs in Antarctica are associated with a specific type of fracture

propagation into floating termini termed "rifts". In Antarctica, rift propagation is the result of "glaciological" stress, or the effect of gravity on an ice shelf, and not tidal forcing (Joughin and MacAyeal, 2005). Although ice tongues in Arctic regions are smaller and experience more summer surface melt compared to ice shelves in Antarctica, a similar mechanism for rift propagation likely exists.

Recently, another mechanism, disarticulation, has been identified as producing large tabular icebergs as the result of large areas of floating termini breaking off tidewater glaciers in Alaska (Molnia, 2003). Large, rapidly-thinning glaciers that terminate in deep water undergo a change in buoyancy that can eventually lift a terminus from its bed. Once a terminus loses contact with the bed, the terminus region may begin to separate along pre-existing planes of weakness, perhaps through rifting. The planes of weakness can be more than a kilometre from the terminus and the disarticulation process may be facilitated by the presence of surface melt water. The result of disarticulation can be tabular icebergs sometimes greater than a kilometre in maximum dimension.

The relation between icebergs and glacier type

In a study of Svalbard icebergs, Dowdeswell (1989) determined that the number of icebergs produced, and their dominant geometric characteristics, were related to the type of ice mass from which they were calved (Table 1). This relationship is important because it provides a general picture of how calving relates to glacier type. Iceberg surface area and count have historically been used to determine calving rate. These methods have met with limited success because in-depth knowledge regarding lifetimes of the icebergs is required, and is generally lacking (Paterson, p.43). The ice mass types considered by Dowdeswell (1989) were surge type and non-surge type tidewater valley glaciers and ice cap/large outlets. Non-surge type tidewater valley glaciers were not described as advancing or retreating in this paper, but as having crevassed or predominantly non-crevassed terminus regions. The predominantly non-crevassed, non-surge type glaciers are hereafter referred to as non-crevassed. The non-surge type tidewater valley glaciers with a crevassed terminus region produce a moderate amount of a combination of small and large irregularly-shaped icebergs. Non-crevassed non-surge type tidewater valley glaciers produce small amounts of dominantly larger irregular

icebergs. Ice cap/large outlets and large outlet glaciers produce a small to moderate number of tabular icebergs. Surging glaciers produce many, dominantly small, irregularly-shaped icebergs. Quiescent surge-type glaciers produce few, dominantly larger, irregularly-shaped icebergs. Quiescent surge-type glaciers and the non-crevassed non-surge type glaciers produce similar amounts and types of icebergs.

Table 1. Iceberg dominant characteristics and relative production from various Svalbard tidewater ice masses.

Glacier or Ice Mass Type	**Relative Number of Icebergs Produced**	**Dominant Iceberg Characteristics**
Active Surge Type	Many	Bergy Bits and Small Irregular Icebergs
Quiescent Surge Type	Few	Larger Irregular Icebergs
Ice Cap or Large Outlet	Few – Moderate	Tabular Icebergs
Non-Surge Type Crevassed Margin	Moderate	Small and Large Irregular Icebergs, Bergy Bits
Non-Surge Type Uncrevassed Margin	Few	Larger Irregular Icebergs

Iceberg calving rate can be roughly estimated by combining the number of icebergs produced with knowledge of their size range. Iceberg size produced by different ice mass types was considered relatively and is not quantified in Table 1. Tabular icebergs are generally > 500 m in length, the larger irregular icebergs are generally > 50 m in length, with typical iceberg diameters of 100 m – 200 m being observed, and smaller irregular icebergs are generally < 50 m in length. Brash ice is less than ~2 m in length and bergy bits less than ~10 m in length, both of which are likely produced by disintegration of larger icebergs or are produced in combination with larger icebergs directly at the terminus (Dowdeswell, 1989). Thus the calving rate from active surge type and large outlet glaciers is potentially very large. It is smaller for tidewater valley glaciers that have little crevassing and quiescent surge type glaciers. Tidewater valley

glaciers that have a crevassed margin could have a large calving rate, potentially as large as an active surge type glacier.

Direct estimation of iceberg calving rate

The iceberg calving rate is an important quantitative component of a glacier's mass balance. A glacier's calving rate is the ice flux at the terminus modified to account for the volume of ice gained or lost as a result of terminus position change. Calving rates are often estimated over extended time periods using infrequently gathered data (e.g. Rignot and Kanagaratnam, 2006; Burgess et al., 2005). This method is the result of a paucity of data, especially regarding glacier velocity and ice thickness which are often only determined once during a study period of years to decades. The result is temporally averaged calving rates calculated assuming that no temporal changes in glacier velocity or thickness occur. Recent velocity measurements by Short and Gray (2005) from glaciers on Ellesmere Island indicate that there is significant inter-annual variation in glacier velocity, which influences calving rates. This should be taken into account in calculations of calving rates whenever possible.

Glacier flow dynamics, calving rates and climate change

Understanding the response of glacier flow dynamics and calving rates to climate change is necessary because the potential consequences, including sea level rise, are a significant concern to humanity. However, the relationships are complicated and not fully understood. Broad geographical trends in terminus advance and retreat seem to occur synchronously in response to climate change provided the duration of climate change is long enough (e.g. periods between minimum and maximum continental ice sheet extents during the Pleistocene). However, seemingly random fluctuations of terminus advance of some glaciers while others in the same region are retreating may occur from year to year during periods of climate change. Variation in local climates of individual glaciers may account for some of the differences in advance and retreat. However, the variability between glacier advance and retreat is also due to individual glaciers differing from one another in features such as size, steepness and velocity. Thus, glaciers that are in close

proximity could react differently to the same changes in mass balance over the short term. Moreover the effect of climate fluctuations on mass balance depends on the area-altitude distribution of the glacier (Paterson, p.317). This distribution can be radically different between glaciers, even for glaciers that are in close proximity (e.g. Burgess and Sharp, 2004). Furthermore, climate change will likely influence the mass balance of tidewater and land terminating glaciers differently, largely because they ablate mass in ways unique to their physical configuration. These variations allow differences in mass balance sensitivities and glacier responses to climate change.

To understand how climate change may affect glaciers with grounded and floating termini differently, it is necessary to discuss the types of ablation that each experience. Both tidewater and land terminating glaciers ablate mass by surface melt, with water being removed as run-off. Tidewater glaciers additionally lose ice mass by basal melting from floating tongues and iceberg production. Floating tongues may also increase in mass by basal ad-freezing. Although the mass gain by basal ad-freezing is poorly understood, mass loss by basal melting of floating glacier termini has been shown to be an important ablation term in North and Northeast Greenland (Rignot et al., 1997). The Petermann Glacier in Northern Greenland is a dramatic example of how significant this type of ablation can be, with basal melting accounting for 10 times more ablation than surface melting (Stewart et al., 2004). In a survey of 14 tidewater glaciers in North and Northeast Greenland, Steffen and others (2005) showed that ice discharge across the grounding line is 3.5 times that estimated from iceberg calving, and that basal melting is responsible for the bulk of the difference. Iceberg calving has recently been shown to be a significant ablation term in the mass balance of tidewater glaciers in the Arctic (e.g. Burgess et al., 2005; Dowdeswell et al., 2002), potentially accounting for up to 40% of the mass lost from the ice caps studied.

Greenland, which is experiencing increasing mean annual air temperatures, shows that glacier ablation related to dynamic thinning in conjunction with terminus retreat is as large as and potentially greater than surface melting (e.g. Krabill et al., 2004; Rignot and Kanagaratnam, 2006). Thinning however must be associated with a specific sink for the mass loss. The sink can be iceberg calving or melting, but mass loss is not necessarily the result of thinning. The importance of dynamic thinning as a mechanism for mass loss

indicates that glacier thickness is not related to climate forcing in a simple way (e.g. increased mass loss from increased surface melt). Flow increases and terminus retreat of large Greenland glaciers, with floating and grounded termini alike, is related to low elevation glacier thinning. Thinning, which can occur by melt increases or flow acceleration causes a decrease in resistance to flow and concentration of gravitational driving force (e.g. Howat et al., 2005; Joughin et al., 2004). Thus, under favourable climatic conditions, floating tidewater terminus positions are determined by lateral confinement by fjord walls. However, disintegration can occur rapidly when a decrease in glacier thickness, or change in terminus position, causes a change in buoyancy of the floating tongue, which causes the glacier to experience a reduction in back-pressure from lateral confinement.

An increase in melt water reaching a glacier's bed and causing flow acceleration is another possible mechanism for dynamic response of ice sheets to climate warming. Inter-annual flow rate variations have been correlated with the intensity of surface melting, which has been hypothesised to change the amount of melt water reaching the bed in the equilibrium zone of a Greenland glacier (Zwally et al., 2002). Melt water penetration provides a flow of heat (minor) and lubricating fluid to the glacier's base, which allows increased basal sliding rates and summer flow acceleration in some Greenland outlet glaciers (e.g. Joughin et al., 1996). However in terms of the large Greenland glaciers currently experiencing dynamic thinning, terminus retreat, and flow acceleration, the summer intra-annual velocity increases have been small, generally less than 10% (Rignot and Kanagaratnam, 2006). The large velocities on glaciers that are rapidly thinning are being sustained annually, which suggests that basal sliding is important throughout the year. In order to explain why these glaciers had high velocities throughout the year, Zwally and others (2002) hypothesised that glacier sliding on a wet base maintained at the pressure melting point (PMP) is important year round.

Unlike the flow of grounded terminus glaciers, floating ice tongues respond more quickly to changes in melting rates and to basal heat flux (Rignot et al., 2001). Thus, as mean annual sea-water and air temperatures increase, floating ice tongues may respond quickly. Increasing Northern Hemisphere ocean temperatures also account partly for the decreasing spring and summer sea-ice extent and summer and autumn Arctic sea-ice

thickness (IPCC, 2001). Changes in the force balance at the terminus of tidewater glaciers due to changes in basal melting rate induced by warmer temperatures may cause rapid disintegration of floating ice tongues. In Greenland the floating glacier ice is preserved because of the constraint of permanent sea-ice in the fjords (Koch, 1928). The more days a fjord experiences open water the less likely a floating terminus will form. If a floating terminus already exists the more days per year of open water it experiences the more likely it is to disintegrate. The decay of sea-ice is dependent on the amount of summer days that are above the freezing temperature of sea water and the growth of sea-ice is dependent on the number of days below the freezing temperature (Reeh et al., 1999). Thus, the maintenance of a stable floating tidewater glacier terminus position is directly related to the maintenance of permanent sea-ice coverage. Permanent sea-ice coverage is provided by a stable mean annual air temperature, a temperature that does not raise the freezing point of sea-ice above a threshold value. In Antarctica, Vaughan and Doake (1996) show a warming trend on both sides of the Antarctic Peninsula and a slow northward migration of annual-mean air isotherms. Moreover, ice shelves south of the -5°C mean annual isotherm show little terminus position change, whereas the ice shelves north of this isotherm have undergone dramatic retreat or complete collapse. In Greenland the majority of the floating glacier termini occur north of the -5°C mean annual isotherm. Therefore as the climate warms, causing the mean annual isotherm to migrate, floating glacier tongues will not be able to maintain their integrity and will potentially disintegrate rapidly (van der Veen, 2002). Larger glacier ablation could conceivably be caused by the reduced back-pressure provided by seasonally absent sea-ice, potentially through calving (e.g. dynamic thinning combined with terminus retreat). However an increase in ablation rates may be related to an increase in basal melting caused by warming ocean temperatures. To understand the potential magnitude of this issue Greenland glaciers indicate the amount of basal melting in relation to iceberg calving. In Northern Greenland (north of 77°N in 1999), ablation by basal melting from large floating glacier tongues is as large as ablation from iceberg calving from glaciers in Southern Greenland (south of 77°N in 1999), where the extensive floating tongues do not form.

Remote sensing, glacier dynamics and iceberg calving

This thesis is a study of the relationship between glacier flow dynamics and iceberg calving using remote sensing as the primary method of data acquisition. It is therefore important to assess how remote sensing data can be used to characterise glacier flow dynamics and quantify iceberg calving rates.

There are two types of remote sensing technologies – passive and active. The analysis of optical remote sensing imagery is the primary focus of this study, and is used in conjunction with and compared to results from published and unpublished active remote sensing studies. Active remote sensing involves the use of sensors to detect reflected responses from objects that are irradiated using artificially generated energy sources. Examples of active remote sensing pertinent to this thesis are radio-echo sounding (RES) and synthetic aperture radar (SAR) speckle tracking. Passive remote sensing uses sensors to detect the electro-magnetic radiation reflected or emitted from natural sources. The passive remote sensing data used in this thesis consist of optical satellite imagery and aerial photography. Optical remote sensing makes use of visible, near infrared and short-wavelength infrared sensors to form images of the earth's surface by detecting the solar radiation reflected from targets on the ground. Radio-echo sounding provides an estimate of glacier thickness, usually along the glacier centre-line, which is necessary for the estimation of glacier calving rates and to determine whether a glacier's terminus is floating or grounded. The optical remote sensing satellite imagery used in this study are recorded digitally and stored as 8-bit raster data. The optical imagery is used to determine glacier terminus area change, surface displacement and identify surface features indicative of flow behaviour. Specific details regarding the wavelengths of received energy and methods used for rectification of imagery for analytical use are presented in the methods section. A common problem in using optical systems to image highly reflective surfaces like ice caps, snow and glaciers is radiometric saturation. Radiometric saturation occurs when the input signal exceeds the dynamic range of the detector. Thus portions of an image that correspond to the most strongly reflecting portions of a surface that has been imaged have been assigned the largest reflectance value and thus any variation in this bins reflectance is lost. Although modern sensor systems are generally able to discern between features on an uncovered glacier

surface, earlier, primitive film systems may not show variation across a glacier's summer surface.

Glacier velocities reported in this study were determined by tracking the displacement of a glacier surface feature or features between pairs of optical satellite images and dividing the displacement by the time elapsed between imagery. Displacement can be measured manually from successive positions of identifiable surface features, such as crevasses, in successive optical images (e.g. MacDonald et al., 1989), and by using the image cross-correlation software Visi-Corr to automate the process of surface displacement determination (Scambos et al., 1992). The manual method was required here because the Visi-Corr software could not always successfully determine displacements.

In this study, glacier displacement between optical images was determined in part with the image cross-correlation software Visi-Corr. Visi-Corr is the Im-Corr software package (e.g. Bernstein, 1983) developed using C++ programming language for use in a visual environment for the Microsoft Windows platforms. The Im-Corr software was originally ported for visual use using the C programming language from the original FORTRAN LAS 5.0 software developed at NASA/Goddard Space Flight Centre. These software packages use a normalised cross-correlation method to measure displacement of distinct gray-scale moving surface features between successive images, provided the features show little change in their appearance (Scambos and others, 1992). Furthermore the chips' intensity values are normalised so that they have zero mean and unit standard deviation, which allows better correlation between images with differences in illumination. Features contained in a square reference chip of a preset pixel size are compared to a larger search chip, of preset size, at every centre-pixel location in which the reference chip will fit entirely within the search chip (Scambos and others, 1992). At every pixel in which the reference chip fits entirely within the search chip a correlation index is calculated. The correlation values near the best integer-pixel match are then used to interpolate a maximum correlation, potentially to sub-pixel precision. Finally, vector displacement results from the best match (providing that successful correlations occurred) for each reference and search pairs are output by the Visi-Corr software.

Displacement between glacier surfaces can also be determined with the speckle tracking technique applied to SAR imagery. This active remote sensing technique was used by Short and Gray (2005) to determine surface velocity very accurately in late winter for several of the glaciers for which velocities were also determined from optical imagery in this study. The speckle tracking technique provides a comprehensive picture of a glacier's velocity field, including velocity directly at the terminus. Speckle tracking using repeat-pass SAR imagery involves tracking the relative displacement of small image chips, thereby allowing the determination of glacier surface movement. If interferometric coherence conditions are satisfied, the image chip's radar speckle will correlate and a relative displacement estimate will be achieved (Gray et al., 1998). The speckle tracking process uses a two-dimensional cross-correlation function, utilizing small image chips to determine relative displacement along satellite track (azimuth) and across satellite track (slant range) directions (e.g. Gray et al., 2001) between coarsely registered, repeat-pass, single-look complex SAR images. A digital elevation model (DEM) is used to remove the topographic component in slant range displacement and to convert the measurements from slant range to ground range. The azimuth displacements and ground range are then calibrated using a stationary reference such as a nunatak. Assuming that glacier flow is parallel to the ice surface (Joughin et al., 1998), down slope surface velocity estimates are calculated from the corrected displacements (Short and Gray, 2005). The SAR data utilised in Short and Gray (2005) were obtained using the RADARSAT – 1 satellite, using the 5.6 cm wavelength, horizontal-transmit horizontal-receive mode with a repeat pass of 24 days. For reasons related to coherence, the use of speckle tracking was restricted to late winter, which in this case corresponds to the months of February and March. Thus the 24 day repeat pass, SAR speckle tracking provides displacements which are extrapolated to annual velocities for the calculation of annual calving rates. The error associated with velocity determination was determined to be in the 2 – 10 m a^{-1} range. When strong image features like crevasses are present, speckle tracking tracks the strong image features, which increases the error associated with the velocity determination to 10 – 20 m a^{-1} range (Short and Gray, 2005).

RES systems, operating at frequencies of 35 and 110 MHz, were flown over the centre-line of larger tidewater and land terminating outlet glaciers including those

draining western Grant and Agassiz Ice Caps in 1966 by Hattersley-Smith and others (1969). Over-flights of many of the same glaciers plus additional glaciers draining Agassiz Ice Cap were flown in 2000 using a 100 MHz radio-echo sounding system (Dowdeswell, personal communication – 2006). These radio-echo sounding over-flights cover all of the major tidewater glaciers considered in this study excepting the Otto Glacier. The Otto Glacier's centre-line terminus depth was acquired in 1995 by Gogineni (1995; ftp://tornado.rsl.ukans.edu/pub/greenland/1995/pdf/may26_95.pdf (accessed May 2004; cited in Short and Gray, 2005) using an airborne 150 MHz Improved Coherent Radar Depth Sounder (referred to hereafter generally as RES). The strongest return echoes correspond to the glacier surface and sub-glacial bedrock and the time lag between the returns from these two reflectors can be converted into a measure of ice thickness. On radar traces, a sharp break in reflectivity indicates the abrupt transition between floating and grounded ice near the termini of tidewater glaciers. Furthermore, a strong basal reflectivity which appears where water is present below ice and a relatively flat elevation profile at the end of a glacier are also suggestive of a floating ice tongue. Sources of error inherent in the aerial collection of radio-echo sounding data include oblique echoes from rough ice, valley walls and nunataks. These echoes may overlap in range with the bottom echo producing incoherent thickness results. These sources can make the determination of thickness and assessment of whether termini are floating or grounded difficult or impossible depending on the amount of interference.

STUDY AREA

Ice caps, ice fields and glaciers cover a large fraction of the Canadian Arctic islands. On Ellesmere Island, glacier ice covers about 84,000 km^2. This is approximately one-third of all Arctic ice outside Greenland. The nine tidewater valley glaciers analyzed in this thesis are located on Ellesmere Island between ~79° N and ~81° N (Figure 3; Table 2). These outlet glaciers are up to 70 km long, are generally confined between steep valley walls and have a maximum ice thickness as large as 500 to 800 m (Hattersley-Smith et al., 1969). All of the glaciers contained in this study drain from Agassiz Ice Cap (about 19,500 km^2) except Otto Glacier which drains from the west side of the western Grant Ice Cap (about 2,000 km^2). Several of the glaciers contained do not have official names

registered in the Canadian Geographical Names Database (http://gnss.nrcan.gc.ca/gnss-srt/searchName.jsp). Therefore, unofficial names have been assigned according to related geographical features. The rationale for choosing this study area results from its close proximity to Greenland and because little is known about the flow dynamics and iceberg calving rates for the glaciers in the study region. In Greenland, climate change induced changes in glacier flow dynamics are occurring. Whether such changes have also been occurring in the study area is largely unknown. The large geographical extent of the study area enables monitoring for widespread simultaneous changes in flow dynamics, which may indicate external forcing by climate change. The summation of the calving rate estimates will provide an estimate of the mass loss rate by calving from the Agassiz Ice Cap and a large portion of western Grant Ice Cap, because Otto Glacier is one of the few major tidewater glaciers draining this ice cap. Although several smaller tidewater glaciers on Agassiz Ice Cap were not included in this study, their contribution to ice cap calving rate is likely negligible because of their small size and lack of activity. For example on Devon Ice Cap eight major tidewater glaciers accounted for ~90% of the total ice mass discharged by calving with ~50% originating from one glacier alone (Burgess et al., 2005).

The interior regions of the Agassiz and western Grant Ice Caps are moderately mountainous. The highest elevation in the study area is the summit of the Agassiz Ice Cap at 2201 m a.s.l. (80.17° N, 75.5° W). The geology of the Agassiz and western Grant ice cap region is primarily Palaeozoic and Mesozoic sedimentary rock (Trettin, 1989). Climate data from the weather stations situated near sea level at Alert (located on the north eastern tip of Ellesmere Island; 82.51° N, 62.35° W) and Eureka (located on the west coast of Ellesmere Island, ~500 km south of Alert; 79.98° N, 85.93° W) indicate small annual amounts of precipitation (in the range of 100 to 200 mm per year) and a mean annual temperature that fluctuates around -17° Celsius over the last several decades. The mean monthly temperatures generally rise above 0° Celsius in July and August at Alert, and June, July and August at Eureka. Comparison of summer temperature reconstructions from two ~20 m ice cores from the south and north summits of Prince of Wales ice cap, located at 77° 52' N, 80° 48' W and 78° 29' N, 79° 25' W, respectively, with instrumental records and re-analysis records of July temperature

records in conjunction with measures of glacier mass balance indicate a warming trend between the late 1960s and late 1990s (Koch et al., Submitted).

A limited number of studies of the dynamics of individual glaciers in the study area have been undertaken (e.g. Holdsworth, 1977; Hattersley-Smith, 1969; Short and Gray, 2005). Calving rates have been estimated for a smaller number of glaciers (Short and Gray, 2005) on the Canadian Arctic islands including Otto Glacier which is contained in the study area here. Radio echo sounding surveys, which are used to determine ice thicknesses and the distribution of floating glacier termini, were flown in the spring of 1966 (Hattersley-Smith et al., 1969) and again for many of these glaciers in the summer of 2000 (Dowdeswell, personal communication – 2006). The Otto Glacier's centre-line terminus depth was measured in May 1995 by Gogineni (1995; ftp://tornado.rsl.ukans.edu/pub/greenland/1995/pdf/may26_95.pdf (Accessed May 2004; cited in Short and Gray, 2005).

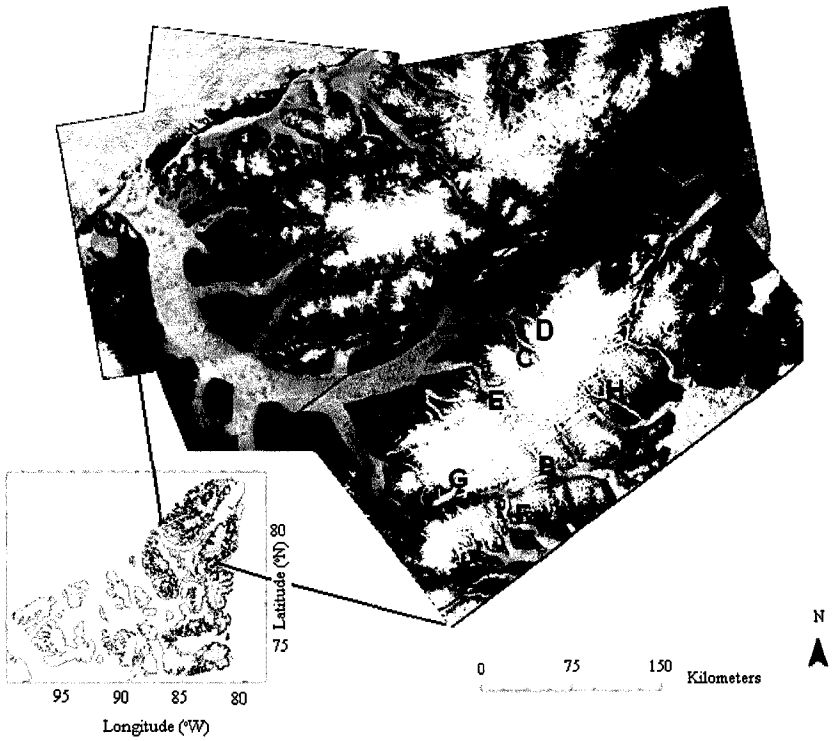

Figure 3. Iceberg calving tidewater glaciers investigated in this study – base imagery is July 10, 1999 Landsat 7 Panchromatic (Glaciers are identified by letter in Table 2).

Table 2. Tidewater glaciers investigated in this study. All Glaciers drain the Agassiz Ice Cap, except the Otto Glacier which drains the western Grant Ice Cap (‡Indicates unofficial glacier name).

Glacier Name	1999 Terminus Location	Figure 4: Glacier Identification Letter
Otto	81° 17' N, 84° 47' W	A
Eugenie	79° 48' N, 74° 42' W	B
Antoinette	80° 49' N, 76° 20' W	C
Lake Tuborg‡	80° 54' N, 76° 20' W	D
D'Iberville	80° 34' N, 78° 20' W	E
Parrish	79° 33' N, 77° 90' W	F
Cañon	79° 41' N, 79° 47' W	G
John Richardson Bay– East‡	80° 13' N, 72° 22' W	H
Sawyer Bay‡	79° 21' N, 77° 57' W	I

METHODS

Flow velocities and calving rates of nine major tidewater glaciers draining the Agassiz and western Grant Ice Caps were determined using optical remotely sensed imagery from 1999 – 2003. Flow characteristics were assessed from glacier surface appearances on aerial photographs from 1959 and 1966 and compared with assessments for the period 1999 – 2003 derived from satellite imagery. Calving rates were estimated for periods of differing length in the 1999-2003 window. These periods varied from several months in the summer to up to four years for the slower flowing glaciers. Calving rates were estimated using surface velocities derived from optical imagery and centre-line thicknesses derived from radio-echo sounding.

Image sources

The optical image data used in this study include: Landsat 7 Enhanced Thematic Mapper Plus (ETM+) panchromatic mode satellite imagery acquired in 1999, 2001 and 2002; ASTER (Advanced Spaceborne Thermal Emission and Reflectance Radiometer) VNIR bands 1, 2 and 3 satellite imagery acquired in 2000, 2001, 2002 and 2003; KH-4A Corona 1:305,000 photographs acquired in 1966; and 1:60,000 aerial photographs acquired in 1959/1960 (Table 3). The digital elevation model used in this study was

Table 3. Imagery details (See Figure 3 and Table 2 for ice cap locations).

Sensor	Image Path-Row (Landsat 7), Serial #-Exposure (Aerial Photograph) and Image I.D. (Aster & Corona)	Date	Time (GMT)	Location (Ice cap)
Landsat 7	049-001	10 July, 1999	18:56:23	Northern Agassiz
Landsat 7	049-002	10 July, 1999	18:56:47	Southern Agassiz
Landsat 7	049-001	2 July, 2002	18:52:17	Northern Agassiz
Landsat 7	049-002	2 July, 2002	18:52:41	Southern Agassiz
Landsat 7	043-003	21 July, 2001	18:17:09	South-West Agassiz
Landsat 7	051-247	24 July, 1999	20:46:51	Western Grant
Landsat 7	051-247	11 June, 2001	20:43:55	Western Grant
Aerial Photograph	A16612-049	7 July, 1959	~16:00	Eastern Agassiz
Aerial Photograph	A16691_032	29 July, 1959	~12:29	Western Agassiz
Aerial Photograph	A16694-040	27 July, 1959	~13:46	Western Agassiz
Aerial Photograph	A16681-085	17 July, 1959	~13:30	Southwest Agassiz
Aerial Photograph	A16721-086	15 July, 1959	~18:25	Southern Agassiz
Aerial Photograph	A16604-020	5 July , 1959	~21:08	Eastern Agassiz
Aerial Photograph	A16708-099	28 July, 1959	~15:58	Southern Agassiz
Aerial Photograph	A16609-023	6 July, 1959	~14:01	Eastern Agassiz
Aerial Photograph	A16606-029	7 July, 1959	~17:22	Western Grant
Aerial Photograph	A16734-030	17 August, 1959	~18:05	Western Grant
Aster	00307042003183843_07212003085644	4 July, 2003	18:38:43	Southern Agassiz
Aster	00206272001225721_04072001384116	27 June, 2001	22:57:21	Western Agassiz
Aster	00308042003193258_08262003110342	4 August, 2003	19:32:58	Western Agassiz
Aster	00207312000200643_02022001399241	31 July, 2000	20:06:43	Southwest Agassiz
Aster	00307092003185649_07242003180536	9 July, 2003	18:56:49	Southwest Agassiz
Aster	00207312000020626_02022001399238	31 July, 2000	20:06:26	Eastern Agassiz
Aster	00307082003000221_07232003144509	8 July, 2003	00:02:21	Eastern Agassiz
Aster	00106152001223322_12272002160900	15 June, 2001	22:33:22	Eastern Agassiz
Aster	00106152001223340_12272002160930	15 June 2001	22:33:40	Eastern Agassiz
Aster	00107192001190517_11182003185909	19 July 2001	19:05:17	Eastern Agassiz
Aster	00108192001195937_07292001899941	19 August 2001	19:59:37	Eastern Agassiz
Aster	00307052003192131_07222003085606	5 July, 2003	19:21:31	Eastern Agassiz
Aster	02207312000200608_02022001399227	31 July, 2000	20:06:08	Eastern Agassiz
Aster	00307092003185649_07242003180536	9 July, 2003	18:56:49	Southern Agassiz
Aster	00206252000220955_01212001298104	25 June, 2000	22:09:55	Western Grant
Aster	00306152002233403_07012002254563	15 June, 2002	23:34:03	Western Grant
Aster	00306272003232626_07152003190942	27 June, 2003	23:26:26	Western Grant
Aster	00307042003183843_07212003085644	4 July, 2003	18:38:43	Southern Agassiz
Corona: KH-4A	DS1036-1098DF010	15 August, 1966	Classified	Central Agassiz
Corona: KH-4A	DS1036-1082DF012	14 August, 1966	Classified	Southern Agassiz
Corona: KH-4A	DS1036-1098DA015	15 August, 1966	Classified	Southern Agassiz
Corona: KH-4A	DS1036-1098DF010	15 August, 1966	Classified	Southern Agassiz
Corona: KH-4A	DS1036-1082DF009	14 August, 1966	Classified	Southern Agassiz

subsetted from the Canadian Digital Elevation Dataset (CDED). The CDED was produced from the National Topographic System (NTS) 1:250,000 map sheets, which were derived from the previously mentioned 1959/1960 aerial photographs. The subsetted DEM was re-projected from WGS-84 geographic co-ordinate system to a 100 m resolution NAD 83 UTM grid system. The DEM has a vertical accuracy of ±20 m at ice cap margins and over exposed bedrock (Gagne, personal communication – 2002 (cited in Burgess and Sharp, 2004)).

Landsat 7 panchromatic imagery utilizes reflectance across the whole of the visible spectrum (0.5 μm to 0.9 μm) to produce one digital value per pixel (15 m resolution). ASTER image pixels, which also have 15 m resolution, are split into three bands representing visible and near infrared portions of the electro magnetic spectrum: band-1 (0.52-0.60 μm); band-2 (0.63-0.69 μm); and band-3 (0.76-0.86 μm). ASTER imagery can be viewed as composite colour whereas Landsat 7 panchromatic is viewed as grey scale. Aerial and Corona photographs are captured on film and must be developed and digitally scanned to allow use in a computerized environment. Photographic films are sensitive to light from 0.3 μm to 0.9 μm in wavelength, which includes the ultraviolet (UV), visible, and near-infrared (NIR) wavelengths. Image quality and film scanning resolution affect the spatial resolution assigned to the aerial photographs and Corona imagery. These details are discussed in the image rectification section.

Optical image preparation

1999 Landsat 7 panchromatic scenes covering the Agassiz and western Grant Ice Caps were ortho-rectified using the 1:250,000 NTS maps as geo-reference and the subsetted CDED DEM to correct for terrain distortion. All images contained in this study were projected to UTM (Universal Transverse Mercator) zone 17, NAD (North American Datum) 83. Ground control points (GCPs) were used as a means of linking the image being rectified to the subsetted CDED DEM and the NTS map sheets using identifiable landforms. Approximately 40 GCPs were used to ortho-rectify each of the 1999 Landsat 7 images to the NTS map sheets. The associated RMS errors were no more than 3 pixels, with no one GCP having an error in excess of 4 pixels. Identifying suitable landforms on

both the NTS map sheets and the Landsat 7 imagery was difficult, which made ortho-rectification using the NTS map sheets as the base level impractical. Prominent landforms were more easily identifiable in the 1999 Landsat 7 imagery than on the map sheets. Therefore all ASTER and Landsat 7 panchromatic images, other than the 1999 Landsat panchromatic imagery, were ortho-rectified using the 1999 Landsat 7 as reference and the subsetted CDED DEM as elevation reference using ~15 GCPs. 1959 aerial photographs of the High Arctic Islands were scanned at a 300 dpi resolution and ortho-rectified against the 1999 Landsat 7 imagery using the subsetted CDED DEM data and individual camera calibration information provided by the National Aerial Photograph Library located in Ottawa, Canada. The aerial photographs were assigned a 5.5 m ground resolution. The error in rectifying the aerial photographs to the 1999 Landsat 7 base imagery is approximately 3 pixels or 16.5 m using ~12 GCPs. Recently declassified Corona program imagery from 1966 partially fills the gap in imagery between the 1959 aerial photographs and 1999 when satellite coverage of Arctic regions became readily available at high spatial resolution. The Corona program was a CIA program from 1959 to 1972 that launched a series of short-term satellites into orbit with the intention of taking photographs of the earth. The 1966 KH-4A images used in this study were exposed through a key-hole camera before the film was ejected and returned to earth. The 1966 Corona program film was scanned at 300 dpi resolution. Corona images were subsetted to cover an area extending from approximately 10 km up glacier to 10 km down-fiord from glacier termini and then rectified to the Landsat 7 1999 base imagery using a third order polynomial geometric model. A third order polynomial rectification was used because the KH-4A series camera calibration files were unavailable. Unlike the Corona imagery, the camera calibration files have not yet been declassified, therefore making aerial photograph ortho-rectification in the traditional sense impossible. The best theoretical ground resolution that could be obtained from the Corona program images was 2.74 m. However, the Corona program images were re-sampled to a 15 m ground resolution because the imagery was of poor quality (e.g. image saturation due to film over exposure). The rectification error associated with the Corona imagery was approximately 3 pixels or 45 m, with no one GCP having an error in excess of 4 pixels based on using ~12 GCPs.

The accuracy of glacier surface velocities derived from manual feature tracking between repeat images (the process of determining glacier velocity and the errors involved is discussed in a subsequent section) is directly related to the precision of rectification between two images. Moreover, calving rate estimates require precise rectification to ensure the error associated with terminus area change is kept to a minimum. Therefore a second rectification process was applied to the previously rectified satellite imagery (collected after 1999) to enhance the precision of rectification and thus increase the accuracy of glacier surface displacement determination. The ortho-rectified ASTER and Landsat 7 images extending approximately 10 km up-glacier and down-fjord from calving tidewater glacier termini in the study area were subsetted for the second stage of rectification. A third order polynomial geometric model rectification was applied to the subsetted images using the base Landsat 7 imagery as the reference. The purpose of rectifying these smaller regions of interest was to decrease the rectification error for the subsets compared to the rectification error for a whole Landsat 7 or Aster Scene. Use of a polynomial rectification was deemed acceptable in this case because the areas being rectified were relatively small with limited elevation variation. This process was not applied to the 1959 aerial photographs or 1966 Corona imagery because surface features required for displacement determination between 1959 and 1966 could not be identified on the over exposed 1966 imagery. In addition the time separation between 1959 and 1999 was too large to leave any identifiable surface features on these glaciers from which surface displacement could be determined. Following the second round of rectification the root-mean-square (RMS) rectification error within the images was reduced from approximately 3 pixels to 1 pixel, or 15 m based on using ~12 GCPs (at least 10 GCPs are required to solve a third order polynomial model). Error associated with the digitization of glacier features is a function of the accuracies of image rectification and feature identification and digitization. Coregistration error was estimated to be ±15 m between all satellite images and the 1999 Landsat 7 ortho-rectified imagery, 16.5 m for the aerial photographs, and 45 m for the Corona imagery. The error associated with comparing satellite images other than 1999 base imagery is estimated to be ± 30 m (e.g. 2000 to 2001). However for this maximum error to occur, the imagery would have to be offset in opposite directions by the maximum co-registration error. Since the errors are

likely random, an error of ±15 m was chosen to better reflect the error associated with satellite image comparisons. The error associated with digitization of surface features and the glacier terminus is estimated to be ± one pixel, which is ±15 m for the Landsat 7, ASTER, and Corona imagery and ±5.5 m for the aerial photographs. All ortho and aerial photograph rectifications were performed using PCI Geomatica version 8.2 Ortho Engine software. The 3rd order polynomial and geometric rectifications were performed using ERDAS Imagine version 8.6.

Glacier surface feature delineation

Glacier surface features were either described or digitised from the rectified imagery. Features described included crevasse patterns, crevasse orientation, melt water channel size and number, and terminus shape. These features provide insight into glacier flow characteristics. Other glacier features (terminus area, icebergs, terminus region width and prominent crevasses) were digitised from the ortho-rectified imagery. To maintain consistency between the digitized products, digitization was undertaken at a scale of ~1:24,000.

The determination of glacier area change was accomplished without resorting to the delineation of the entire glacier drainage basin. For each glacier, a straight line was digitized perpendicular to glacier flow further up glacier than the most up-glacier terminus position recorded during the period covered by available imagery. From this arbitrary line, the glacier terminus region in each image was digitised and converted to a polygon. The area of each polygon was calculated using a visual basic script. Terminus area change was determined as the change in digitized glacier surface area between terminus area polygons from successive epochs. As an example, Figure 4 shows the terminus area change for John Richardson Glacier (East) from 1959 (yellow) to 2003 (blue) super-imposed on the 1959 aerial photograph. The terminus area change is a polygon as in Figure 4 (or series of polygons if one or more portions of the terminus advanced while others retreated between two images) produced by the subtraction of terminus region polygons that were discussed above. The terminus area change polygon or polygons have a total segment length that was calculated using a visual basic script. The error in terminus area change is the product of the total length of the terminus area

change polygon and the rectification error (see Table 4). Icebergs within 2 km of each terminus were digitised as polygon shape files. The area of each iceberg was calculated using a visual basic script. All vector files were created and analysed using the ESRI ArcGIS 8.3 software package.

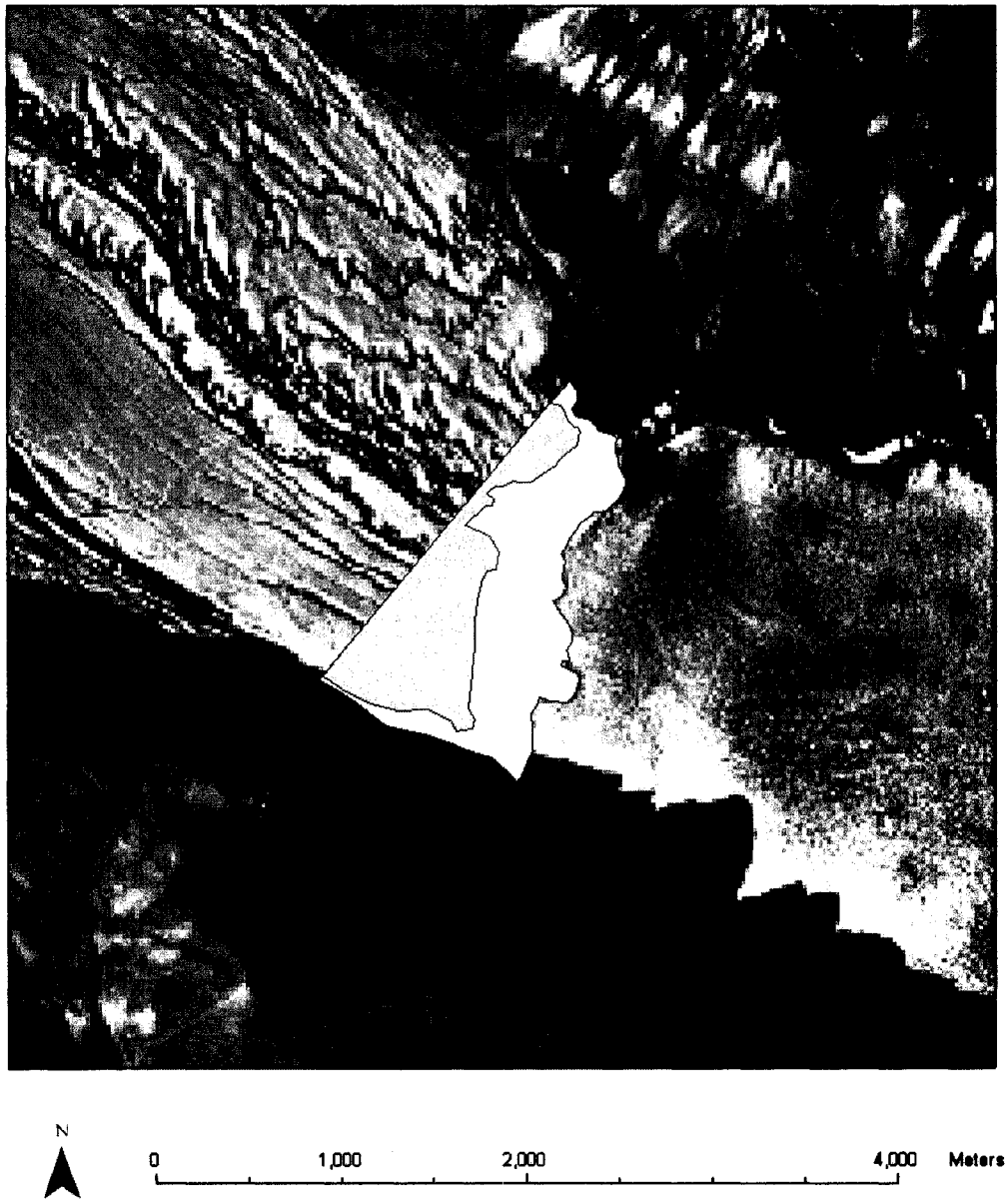

Figure 4. Terminus area change (0.875 km^2 reduction) of John Richardson Glacier (East) between July 5, 1959 (yellow) and July 5, 2003 (blue) displayed on the 1959 aerial photograph (© A16604-020, July 5, 1959).

Table 4. Glacier terminus area change error between 1999 and 2003.

Glacier	Image Dates	Error Sources	Terminus Area Change Length (km)	Terminus Area Change Identification Error (m)	Area Change Error ($\pm km^2$)
Otto	1999, July 24 to 2000, June 25	Digitization (1999) & Digitization + Coregistration	14.701	15 (1999) & 22	0.271
	2000, June 25 to 2001, June 11	Digitization + Coregistration	14.056	22	0.309
	2001, June 11 to 2002, June 15	Digitization + Coregistration	14.774	22	0.325
	2002, June 15 to 2003, June 27	Digitization + Coregistration	17.018	22	0.374
Eugenie	1999, July 10 to 2000, July 31	Digitization (1999) & Digitization + Coregistration	24.356	15 (1999) & 22	0.434
	2000, July 31 to 2001, July 21	Digitization + Coregistration	20.863	22	0.459
	2001, July 21 to 2002, July 2	Digitization + Coregistration	20.498	22	0.451
	2002, July 2 to 2003, July 8	Digitization + Coregistration	19.553	22	0.430
Eugenie – Intra-annual	June 23 to July 21, 2001	Digitization + Coregistration	20.738	22	0.456
Antoinette	July 10, 1999 to June 15, 2001	Digitization (1999) & Digitization + Coregistration	7.131	15 (1999) & 22	0.128
	July 19, 2001 to July 2, 2002	Digitization + Coregistration	6.148	22	0.135
Antoinette Intra-annual	June 15 to July 19, 2001	Digitization + Coregistration	5.766	22	0.127
Antoinette Intra-annual	July 19 to August 19, 2001	Digitization + Coregistration	5.339	22	0.117

Table 4. Glacier terminus area change error between 1999 and 2002-2003 – continued.

Lake Tuborg	July 10, 1999 to July 19, 2001	Digitization (1999) & Digitization + Coregistration	27.227	15 (1999) & 22	0.510
	July 19, 2001 to July 2, 2002	Digitization + Coregistration	30.568	22	0.672
Lake Tuborg – Intra-annual	June 15 to July 19, 2001	Digitization + Coregistration	28.831	22	0.634
Lake Tuborg – Intra-annual	July 19 to August 19, 2001	Digitization + Coregistration	29.640	22	0.652
d'Iberville	July 10, 1999 to June 27, 2001	Digitization (1999) & Digitization + Coregistration	10.396	15 (1999) & 22	0.191
	July 20, 2001 to August 4, 2003	Digitization + Coregistration	8.346	22	0.183
d'Iberville – Intra-annual	June 27 – July 20, 2001	Digitization + Coregistration	9.982	22	0.220
Parrish	1999, July 10 to 2001, July 21	Digitization (1999) & Digitization + Coregistration	5.213	15 (1999) & 22	0.0973
	2001, July 21 to 2002, July 2	Digitization + Coregistration	5.320	22	0.117
	2002, July 2 to 2003, July 9	Digitization + Coregistration	5.227	22	0.115
Cañon	July 10, 1999 to July 31, 2000	Digitization (1999) & Digitization + Coregistration	20.611	15 (1999) & 22	0.380
	July 31, 2000 to July 9, 2003	Digitization + Coregistration	19.055	22	0.419
John Richardson Bay (East)	July 10, 1999 to July 5, 2003	Digitization (1999) & Digitization + Coregistration	4.507	15 (1999) & 22	0.0843
Sawyer Bay	July 10, 1999 to July 4, 2003	Digitization (1999) & Digitization + Coregistration	9.897	15 (1999) & 22	0.184

Glacier velocity

Glacier surface velocity is an important descriptor of flow dynamics and an essential component in estimating calving rate. Moreover, the longitudinal velocity gradient near the glacier terminus adds insight into how flow may affect glacier thickness and thus buoyancy. An increasing velocity gradient towards the terminus indicates a tendency for ice to thin and a decreasing gradient towards the terminus indicates a tendency for the ice to thicken.

In this study, glacier surface velocity was determined using the FORTRAN LAS 5.0 software ported to the windows environment as the Visi-Corr image cross-correlation software (Scambos et al., 1992) or by manually measuring the glacier feature displacement that occurs between successive images and dividing by the elapsed time between image acquisitions. Copland and others (2003a) indicated that actively surging glaciers that flow at high velocities (e.g. >~500 m a^{-1}) sometimes result in inconsistencies in the velocity fields produced using image cross-correlation software, even though velocities of ~1000 m a^{-1} were determined between images taken approximately one year apart. Thus unsuccessful image cross-correlation results are likely related to one of several factors which may not be directly related to the elapsed time between images: reflectance changes between images may be related to the time of day at which the images were captured; the absence of surface features that the cross-correlation algorithm can track; or large velocity gradients at the scale of the features that are being searched for (Scambos et al., 1992). Results from this study reveal that surface displacements greater than ~370 m produced inconsistent velocity fields using the Visi-Corr software. However, some displacements which were less than ~370 m also produced inconsistent results, likely due to one or more of the reasons listed above. Vector results were considered inconsistent and therefore unusable if many large localized vectors of anomalous flow directions appeared across the whole extent of the map, or if the majority of the vector orientations were not physically realistic. Manual measurement of surface features is required to estimate centre-line terminus velocity for glaciers where Visi-Corr did not produce satisfactory results. Under circumstances that allowed velocity determination by both manual and image cross-correlation techniques the results obtained agreed within error, which indicates that this method is providing robust surface displacement results. The manual method of feature tracking on optical imagery only works where there are distinctive features, which are not always found near the terminus. Manual feature tracking may thus provide estimates of velocities up to several kilometres from the terminus. The coarse nature of this form of velocity gradient estimation only allows an assessment of whether the velocity is increasing, decreasing or constant towards the terminus, because the velocity gradient over the path the feature or features have followed may be spatially variable.

The centre-line longitudinal displacement gradient is determined from the Visi-Corr displacement map by reading the digital values of displacement at two centre-line correlation positions and dividing by the distance between the points. Technically a velocity gradient could be determined between any two locations on the glacier where velocities were established, however it is the velocity gradient at, or as near as possible to, the terminus that is of importance in this study and that is reported here. Figure 5 shows a velocity map produced by Visi-Corr for Parrish Glacier between 1999 and 2001. Velocity arrows are displayed as categories of ~25 m divisions in Figure 5. However the actual velocity for each vector can be individually queried from the map in the ArcGIS 8.3 software package, thus velocity maps with centre-line velocity and terminus velocity drawn directly on the map at 1 km intervals are presented in the results instead of providing categories of velocities as discussed above. The velocities drawn on the results maps are the average value of ~6 of the surrounding adjacent correlations. The Visi-Corr software does not always correctly identify surface displacement and thus velocity. Examples of inconsistent velocity vectors are indicated in Figure 5 with red circles. These types of inconsistent vectors have been removed from velocity maps found in the results section.

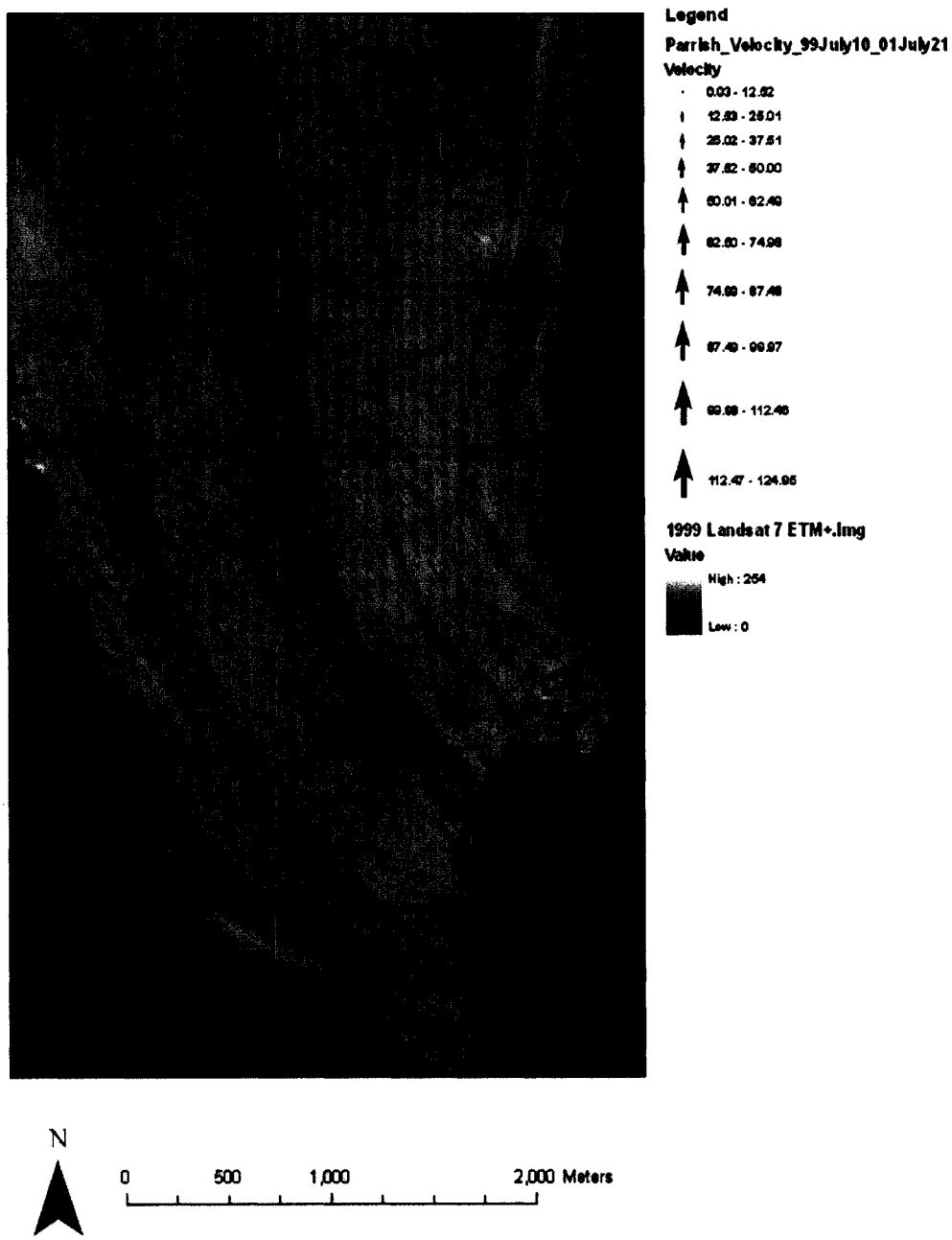

Figure 5. Glacier surface velocity map produced using Visi-Corr software for Parrish Glacier between the July 10, 1999 Landsat 7 panchromatic image and the July 21, 2001 Aster image displayed on the July 10, 1999 Landsat 7 panchromatic image. Examples of large locally anomalous flow vectors (red circles) indicate positions where the image cross-correlation software did not correctly measure displacement between images and are removed from results.

Image preparation for image cross-correlation involves several steps. A requirement for image cross-correlation by the Visi-Corr software is that images are in an 8-bit greyscale TIFF (Tagged Information File Format) format. Therefore ASTER bands 1, 2 and 3 were radiometrically merged to produce an 8-bit grey scale image with digital number values equal to the mean of the three separate bands for each pixel. The Landsat 7 panchromatic images are 8-bit grey scale format and do not require further processing. The greyscale images were subjected to a high pass filter to remove brightness variations related to large-scale topographic features (Scambos et al., 1992). Experimentation to determine the optimal kernel size was undertaken using filter sizes up to 7x7 pixels. A 3x3 pixel size high pass filter produced images that produced the fewest spurious correlations (e.g. adjacent correlations with radically different direction or intensity) and was applied to all imagery before image sets were cross-correlated with the Visi-Corr software.

The manual feature tracking technique has previously been shown to be effective for the determination of glacier velocity (e.g. MacDonald et al., 1989) but the results contain a higher amount of error due to the uncertainty in identifying surface features (Scambos et al., 1992) compared to image cross-correlation or SAR speckle tracking. However, when clear surface features, such as crevasses, appear on fast flowing glaciers imaged with SAR, speckle tracking of SAR image pairs will track the displacement of these features instead of the speckle. The tracking of features increases the error in displacement determined with SAR speckle tracking (Strozzi et al., 2002). In the Canadian Arctic, speckle tracking of February and March RADARSAT – 1 imagery of fast flowing glaciers with strong surface features degraded errors in velocity determinations to the 10 – 20 m a^{-1} range from the typical 2 – 10 m a^{-1} range for glaciers without prominent surface features (Short and Gray, 2005). Thus on fast flowing glaciers, where strong surface features exist, the manual method of velocity determination from optical imagery provides a comparable estimate of displacements to estimates derived using speckle tracking of SAR imagery.

Calving Rate error analysis

The error associated with estimates of calving rates derived from 1999 – 2003 satellite imagery is a function of the errors in measurements of glacier displacement, terminus position change, and ice thickness. The image cross-correlation process uses small rectangular image areas (chips) instead of individual pixels, producing up to sub-pixel accuracy in displacement determination (Scambos et al., 1992). The sub-pixel accuracy in displacement is therefore a function of tracking the displacement of groups of pixels that represent an unchanging shape. The error in displacement used here is ±15 m, is therefore likely to be a conservative estimate of the error associated with image cross-correlation. The error associated with glacier displacement calculated manually using the same easily identifiable features digitised on successive images is a function of feature digitization error and coregistration error, which is ±22 m. The error in terminus position change for images after 1999 is taken to be the product of both the coregistration error and terminus digitization error and the perimeter length of the polygon that defines terminus area change; the error in 1999 terminus position is taken to be a function of terminus identification only (Table 4). The error associated with glacier terminus thickness used here determined from RES returns is ±10 m (Dowdeswell et al., 2004). In relation to estimates of iceberg calving rate, the error associated with the measurement of glacier width is considered insignificant. However an error of ±30 m was chosen to account for the uncertainty in identifying the lateral edges of the glaciers. The above mentioned uncertainties define the error components with respect to calving rate. The next section identifies the method by which calving rates are estimated including the resulting error estimates.

Iceberg calving rate estimates

Iceberg calving rate is an important but poorly understood term in the mass balance of tidewater glaciers on Ellesmere Island. Repeat optical imagery was used to estimate iceberg calving rates using several inputs: glacier surface width at the terminus; depth averaged displacements; terminus area changes; and width averaged depth.

Width averaged depths for all glaciers were found by modeling glacier beds as a semi-circular parabolic cross section (after Nye, 1965). The parabolic cross section was calculated as the segment of a circle with area (K) from the glacier parameters width (c)

and centre-line depth (h) (Equations 1-5; Figure 6). The width averaged glacier depth is solved for by dividing the parabolic cross-sectional area by glacier width and results in a depth that is approximately 2/3 the centre-line depth.

$$r = (c^2+4h^2) / (8h) \quad (1)$$

$$\theta = 2 \arcsin (c / 2r) \quad (2)$$

$$s = (r)(\theta) \quad (3)$$

$$d = r - h \quad (4)$$

$$K = r^2 [\theta - \sin(\theta)] / 2 \quad (5)$$

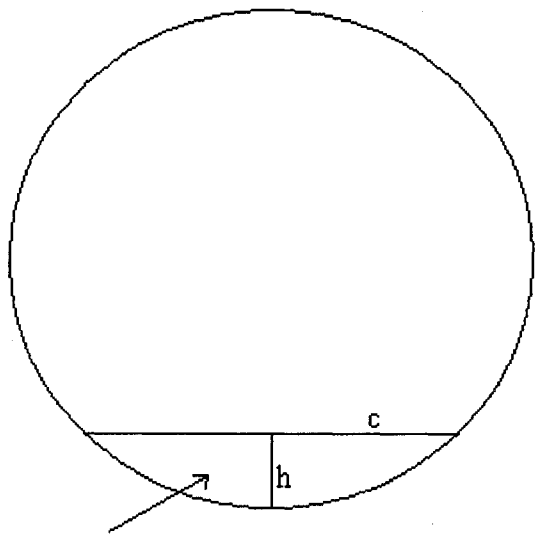

Figure 6: Segment of area (K) determined with glacier width (parameter c) and glacier centre-line depth (parameter h).

Glacier displacement between any two images was multiplied by glacier width to give the surface area that the glacier has moved through a flux gate, which is then modified by either subtracting terminus area change (if the terminus area has increased) or adding terminus area change (if the terminus area has decreased). Calving rate is calculated by multiplying the displacement area corrected for terminus area change by the width averaged depth and dividing by the time elapsed between images.

The upper and lower bounds of calving rate (CR_{upper} and CR_{lower}) were estimated with the following formulae (6 – 10):

$$CR_{upper} = (CV_{upper} +/- TV_{change}) / \text{repeat image elapse time} \quad (6)$$

$$CR_{lower} = (CV_{lower} +/- TV_{change}) / \text{repeat image elapse time} \quad (7)$$

where

$$CV_{upper} = (D_{sliding} + D_{error}) * (T + T_{error}) * (W) \quad (8)$$

and

$$CV_{lower} = (D_{depth\ ave} - D_{error}) * (T - T_{error}) * (W) \quad (9)$$

and

$$TV_{change} = (TA_{change}) * (T) \quad (10)$$

The calving volume (CV) of ice mass is the result of the displacement (D) resulting from flow multiplied by width averaged thickness (T) derived and terminus width (W). The terminus volume change is the result of terminus area change (TA_{change}) and terminus thickness. Terminus volume change (TV_{change}) is the result of terminus area change and width averaged thickness. In relation to calving rate estimates, a terminus retreat is considered a positive volume contribution and an advance is a negative volume contribution. The errors in glacier surface displacement (D_{error}) and thickness (T_{error}) are incorporated into the calving rate estimates. The errors associated with terminus volume change are not incorporated into the calving rate estimate in order to maintain continuity between relative rates of terminus advance and retreat. The ratio of basal sliding to ice deformation for the glaciers studied is unknown. Basal sliding likely increases in importance in summer as an effect of melt water reaching the glaciers bed and deformation likely regains importance in the winter when melt water production and penetration ceases (e.g. Zwally et al., 2002). Assuming that internal glacier ice deformation contributes to glacier flow, the depth-averaged velocity would be up to 80% of the surface velocity (Paterson, p.252). Therefore the contribution of depth averaged

velocity to calving rate is bounded at the upper end by assuming that there is no vertical velocity gradient and bounded at the lower end by a depth averaged velocity equivalent to 0.8 of the surface velocity. However, where a floating glacier tongue exists the vertical gradient in velocity is negligible (Sanderson and Doake, 1979), making the upper estimates of calving rate likely closer to the actual values in these cases. Furthermore near terminus buoyancy would make basal sliding the dominant process in this region and also suggests that the actual calving rates are closer to the upper calculated limit. No bathymetry data are available for areas down fjord of the calving termini studied. The volume changes associated with terminus advance or retreat were therefore calculated using the measured terminus ice thickness. The terminus area changes which were calculated between 1999 and 2003 correspond to small (~<0.5 km) terminus centre-line position changes and likely do not correspond to significant fjord bottom elevation changes. Therefore the changes in glacier volume that correspond to terminus area change are considered insignificant.

RESULTS

1999 – 2003 annually averaged velocities on the nine large tidewater glaciers draining the Agassiz and western Grant Ice Caps were as high as ~700 m a^{-1} and as low as ~14 m a^{-1}, with velocities of ~100 – 200 m a^{-1} being common (Figures 7, 9, 11, 13, 15, 17 and 19). The slow flowing John Richardson Bay and Sawyer Bay Glaciers had velocity and calving rate estimated once between 1999 and 2003. The 1999 – 2002 velocity and calving rate from John Richardson Bay Glacier was ~14 m a^{-1} and 0.004 km^3 a^{-1}. The 1999 – 2003 velocity and calving rate from Sawyer Bay Glacier was ~42 m a^{-1} and 0 km^3 a^{-1}. Furthermore, the available summer imagery indicates that summer velocity is up to an order of magnitude larger than the annual velocity and that velocities increase as summer progresses. Six of the nine glaciers studied terminate at a position where their constraining fjords widen, which suggests that fjord topography may be preventing further advance. Terminus positions of eight of the nine glaciers studied fluctuated by <1 km between 1959 and 2003.The largest terminus retreat during this time period (~2 km) occurred at Parrish Glacier. The terminus positions of all nine glaciers studied fluctuated by <0.5 km between 1999 and 2003. The terminus region widths (which are used here as

a proxy for ice thickness change) varied inconsistently across the study area. Some glaciers showed a width increase, some showed a width decrease and some showed no measurable change. The highest annually averaged calving rate measured between 1999 and 2003 (0.36 ± 0.03 km^3 a^{-1}) was found at Otto Glacier (2002-2003). The lowest rate (zero) was found for several of the slower flowing glaciers. The annually averaged calving rates were highly variable, with 2 fold changes being recorded (Figures 8, 10, 12, 14, 16, 18 and 20). The summer calving rates were ~2 – 8 times larger than the annual values.

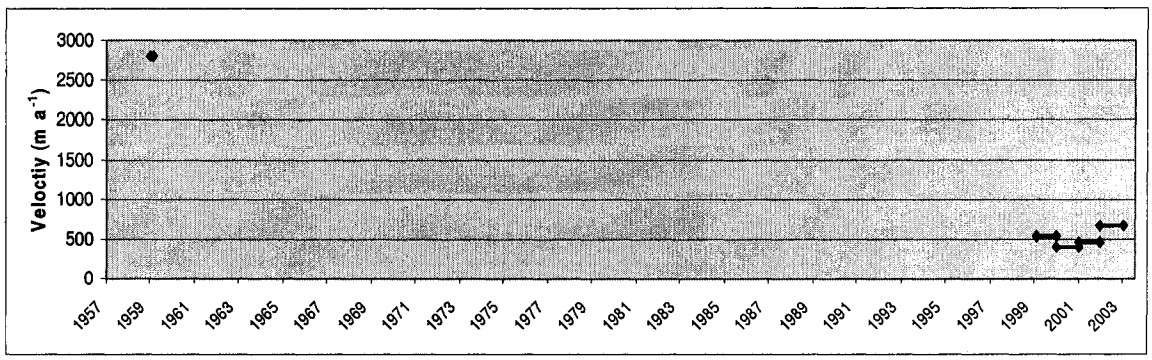

Figure 7. Otto Glacier velocities between 1959 and 2003.

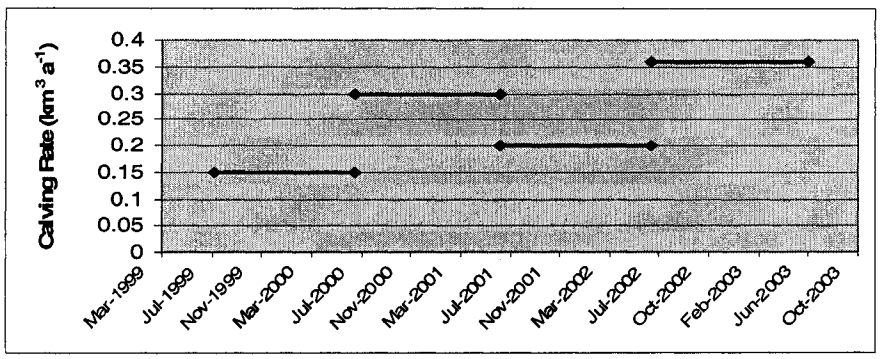

Figure 8. Otto Glacier calving rates between 1999 and 2003.

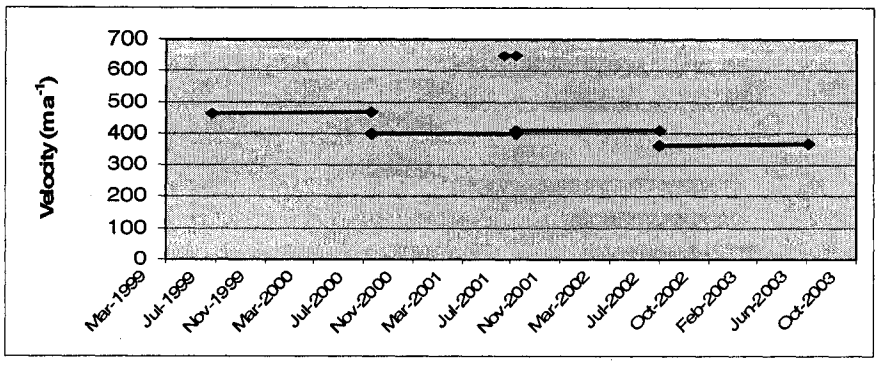

Figure 9. Eugenie Glacier velocities between 1999 and 2003.

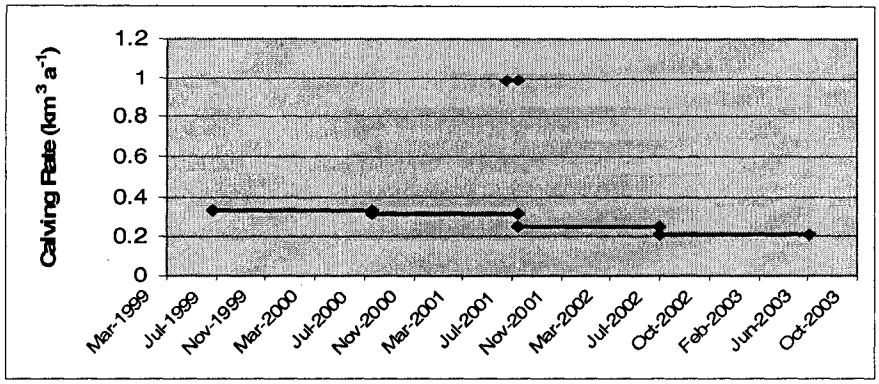

Figure 10. Eugenie Glacier calving rates between 1999 and 2003.

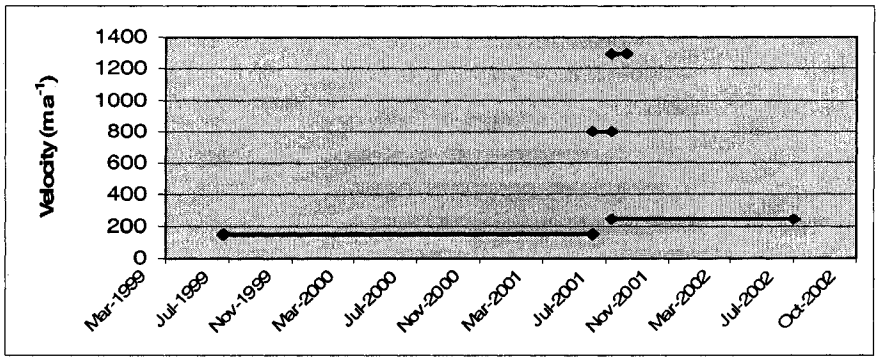

Figure 11. Antoinette Glacier velocities between 1999 and 2002.

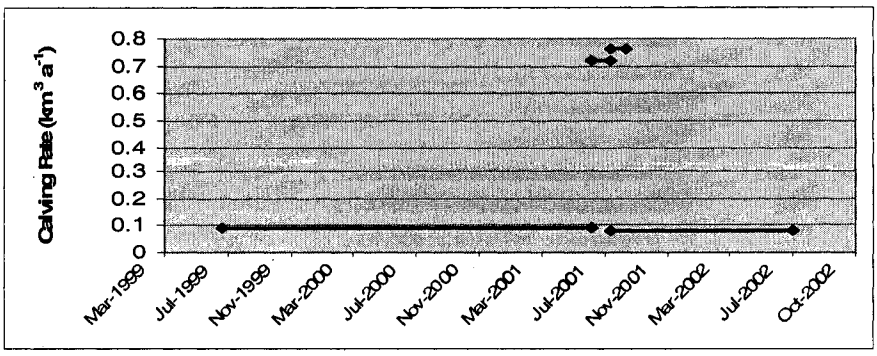

Figure 12. Antoinette Glacier calving rates between 1999 and 2002.

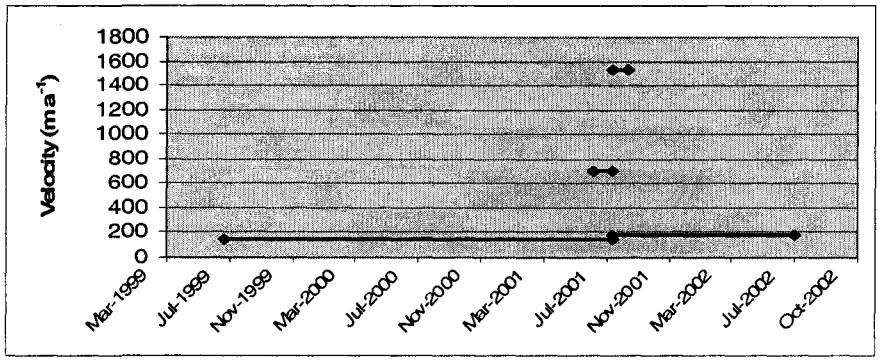

Figure 13. Lake Tuborg Glacier velocities between 1999 and 2002.

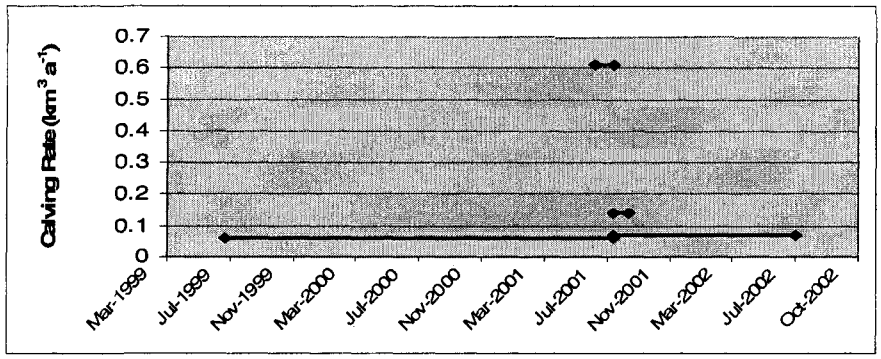

Figure 14. Lake Tuborg Glacier calving rates between 1999 and 2002.

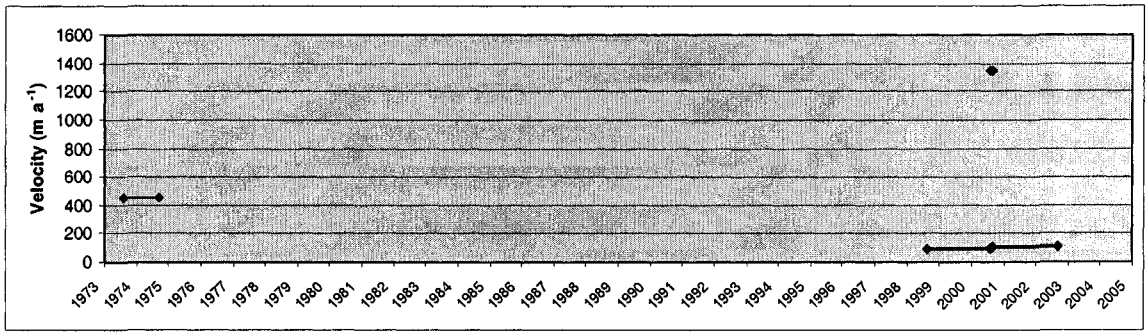

*1974-1975 velocity from Holdsworth, 1977

Figure 15. D'Iberville Glacier velocities between 1974 and 2003.

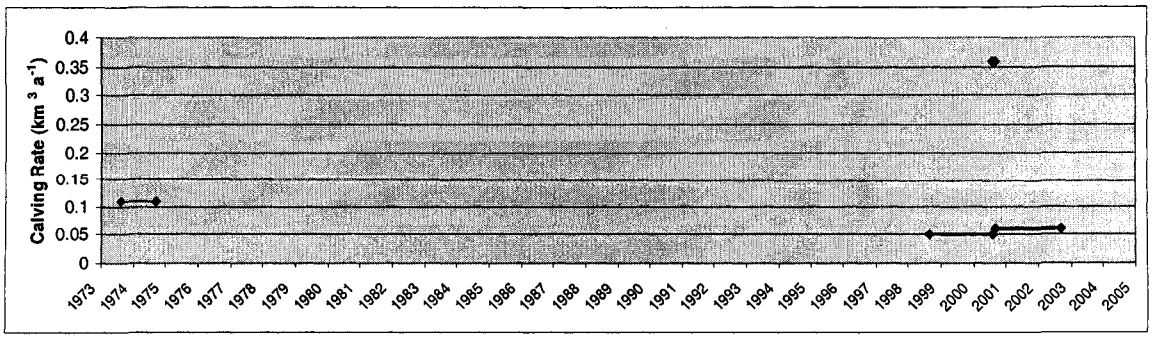

*1974-1975 calving rate from Holdsworth, 1977

Figure 16. D'Iberville Glacier calving rates between 1974 and 2003.

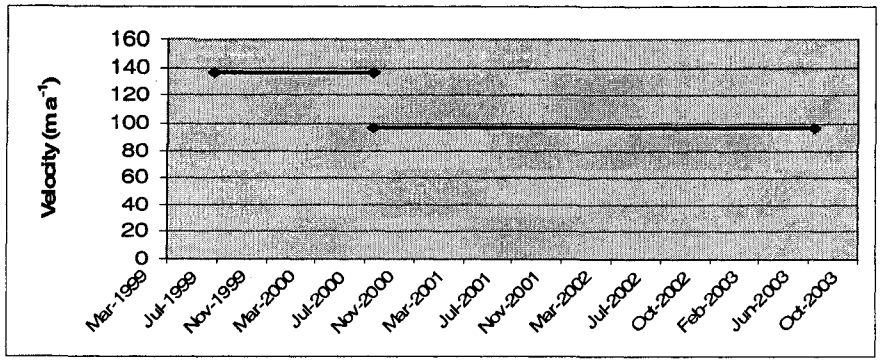

Figure 17. Cañon Glacier velocities between 1999 and 2003.

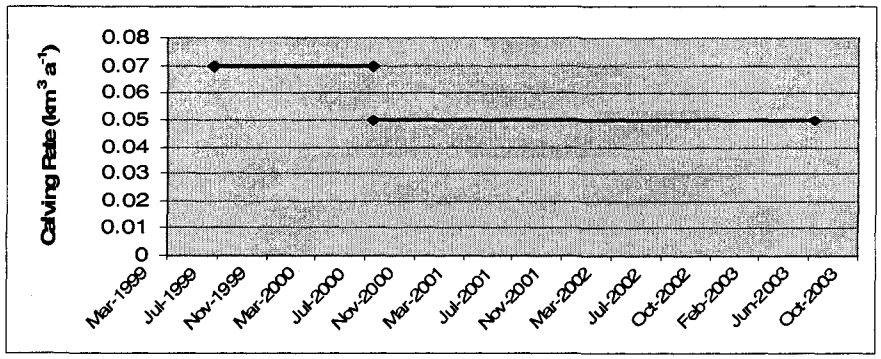

Figure 18. Cañon Glacier calving rates between 1999 and 2003.

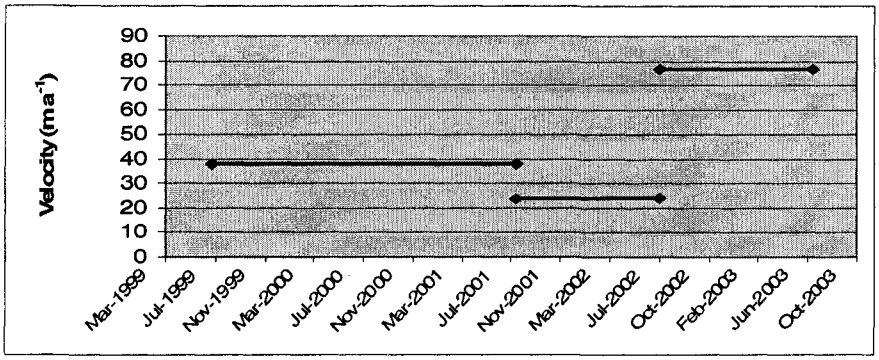

Figure 19. Parrish Glacier velocities between 1999 and 2003.

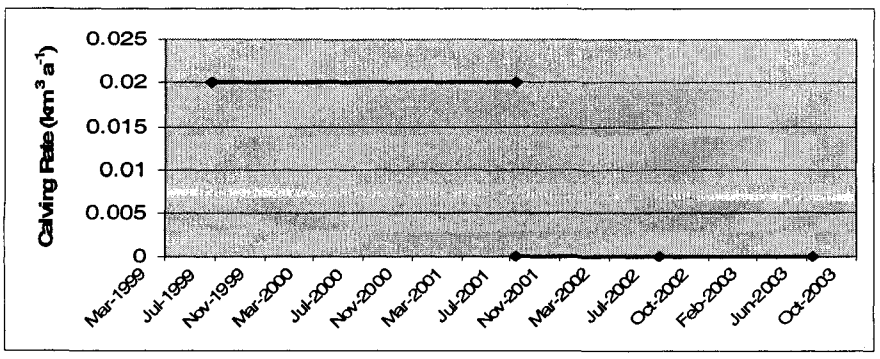

Figure 20. Parrish Glacier calving rates between 1999 and 2003.

The largest annual glacier terminus region velocities found between 1999 and 2003 were on Eugenie and Otto Glaciers. These velocities were in the ~400 – 700 m a^{-1} range, of which the largest were at Otto Glacier. These two glaciers account for ~65% of the total annual calving estimated (0.8 ± 0.2 km^3 a^{-1} – 1999 to 2002) from the nine glaciers in this study.

Otto Glacier flows west from the western Grant Ice Cap into Otto Fjord which extends for ~100 km before opening into Nansen Sound. Otto Glacier was reported to be surging by Hattersley-Smith (1964, 1969) with the surge commencing between 1950 and 1959. Aerial photographs show the lower 25 km of the glacier had become highly crevassed by 1959 and the terminus had advanced by ~3 km; in 1950 the terminus region was stagnant and incised by many melt water channels. Although the terminus velocity in 1950 is unknown, a terminus velocity of ~2810 m a^{-1}, derived from surface feature found between ~3 km and ~1 km of the terminus over a period of 41 days in July and August 1959, was found here (Figure 21). Image cross-correlation did not produce consistent results between 1959 aerial photographs thus necessitating the manual method of velocity determination. The annual average velocity during this period is unknown. The terminus advanced an additional 2 – 3 km between 1959 and 1964. A series of four parallel radio-echo soundings were flown over the lower 15 km of Otto Glacier in 1964 (Hattersley-Smith et al., 1969) which reveal the terminus to be floating. The grounding line was identified as being situated approximately 3 km from the 1964 terminus position and the glacier was grounded below sea level to approximately 15 km from the terminus (Hattersley-Smith, 1969). Copland and others (2003a) classified this glacier as a surge type glacier, largely on the basis of the previously mentioned documented evidence of a surge. Moreover the available imagery does not allow the discrimination between fast flow being initiated at the terminus or high on the glacier and subsequently migrating towards the terminus. Between 1999 and 2003, the terminus lay several kilometres up-fjord from the 1964 position, and it fluctuated within a narrow region (Figure 22), which is located at an opening in the fjord. The width of the terminus region measured behind the 1964 grounding line position (Figure 22; Table 5) increased ~33% (~1522 m) between 1959 and 2002. An increase in width is also evident at the terminus and is consistent with a transfer of ice mass to the terminus and thickening. Crevasses

perpendicular to flow at the terminus, which are indicative of extending flow (Nye, 1952) (which is consistent with the recorded positive velocity gradient values) are being advected into the terminus region from up glacier of the terminus. Dark spots on the terminus region of Otto Glacier are likely due to surface melt water ponding. None of the imagery of Otto Glacier show open water at the terminus.

Table 5 presents the properties and flow characteristics of Otto Glacier. The 1999 – 2003 annually averaged velocities found here range between ~406 and ~672 m a^{-1}. The centre-line velocity (1999 – 2003) was derived manually from digitised crevasse features between ~5 km and ~2 km from the glacier's terminus because the image cross-correlation software did not produce adequate velocity maps between images from 1999 to 2003 (Figure 22 – intermediate year markings between 1999 and 2003 have been omitted for clarity). The manually derived velocities provide no information about how the velocity varies laterally across the terminus region. Seasonal velocities could not be calculated with the available imagery from 1999 – 2003, so the magnitude of seasonal velocity variation on Otto Glacier is unknown. Velocities determined in March by Short and Gray (2005) for Otto Glacier are similar to the annual velocities calculated here, which indicates that high rates of flow occur throughout the year. The centre-line terminus velocity determined by Short and Gray (2005) for Otto Glacier was 650 m a^{-1} in 2002 and 875 m a^{-1} in 2003 – the difference in velocity between 2002 and 2003 was 225 m a^{-1}. These velocities were determined by speckle tracking using RADARSAT-1 data captured 24 days apart in March of 2002 and 2003. Presumably the large velocities degraded the technique to intensity tracking at the terminus and resulted in the larger velocity determination error of up to ~20 m a^{-1}. The velocities determined here were calculated from optical imagery captured 369 days apart in June 2001 and 2002 and 407 days apart between June 2002 and July 2003. The velocities calculated for Otto Glacier over these time periods were 456 m a^{-1} and 672 m a^{-1} respectively, which corresponds to a velocity difference of 216 m a^{-1}. The similarity in the differences between the 2002 and 2003 velocities calculated here and in Short and Gray (2005) indicates that both studies are identifying the same trend in velocity change. However the optical imagery velocity determination technique used here systematically under-estimates the glacier velocity determined by speckle tracking by ~20 – 30%. The discrepancy between the velocities

reported here and those reported by Short and Gray (2005) is likely related to the difference in techniques used to determine displacement. The 1999 – 2003 velocities calculated here are average velocities between ~5 km and ~2 km from the terminus, whereas the velocities reported in Short and Gray (2005) relate to the terminus, which is a benefit of using the speckle tracking technique on fast flowing glaciers. Moreover the centre-line velocity profiles between ~5km from the terminus and the terminus created by Short and Gray (2005) indicate a velocity increase of up to 30%. This increase in velocity corroborates the increasing velocity gradient found here and likely accounts for the velocity discrepancy. Thus the velocity results found here compared to those found by Short and Gray (2005) are consistent. The largest terminus area change (an increase of 6.97 km^2) occurred between August 17, 1959 and July 24, 1999.

Calving rate estimates for Otto Glacier between 1999 and 2003 are presented in Table 6. The calving rates fluctuate by up to a factor of 2 between successive years. The calving rate was lowest ($0.04 - 0.15 \pm 0.02$ km^3 a^{-1}) between 1999 and 2000 and highest ($0.22 - 0.36 \pm 0.03$ km^3 a^{-1}) between 2002 and 2003. The smaller calving rates coincide with periods of terminus area increase while the highest rates coincide with periods of terminus area decreases. The higher calving rate estimates, which were calculated assuming that flow was by basal sliding only, are likely closer to the actual values because Otto Glacier likely has a floating terminus (Hattersley-Smith et al., 1969); the vertical velocity gradient for a floating terminus is negligible (Sanderson and Doake, 1979). Therefore the average of the annual calving rates from 1999 – 2003, using the upper bounds, is 0.25 ± 0.03 km^3 a^{-1}. Calving rates for Otto Glacier were estimated by Short and Grey (2005) from 24 day winter periods between 2002 and 2004. The calving rates that coincide with the calving rates estimated here are 0.12 ± 0.03 km^3 a^{-1} for 2002; and 0.37 ± 0.09 km^3 a^{-1} for 2003. These values agree within error with the calving rates calculated here (Table 5). The apparent agreement in calving rates needs to be explored, however, because the parameters used in their calculation differ. The velocity at the terminus determined here is less than determined by Short and Gray (2005). Short and Gray's (2005) calving rate estimates assume a uniform ice thickness across the glacier terminus which will result in higher values than are reported in this study, where the glacier bed geometry was modeled as a parabola. The calving rate estimate was assigned

an error of ~25% by Short and Gray (2005) of which an over estimate of thickness by up to ~20% is assigned to the uncertainty in width-averaged glacier depth. Short and Gray (2005) reported a 0.15 $km^3 a^{-1}$ advance of Otto Glacier in 2002 and no change in 2003. Here the terminus area increased by 0.48 $km^3 a^{-1}$ between 2001 and 2002 and decreased by 0.20 $km^3 a^{-1}$ between 2002 and 2003. The terminus volume change rate differences are potentially the result of the time separation between the optical and SAR imagery as previously indicated. The optical imagery used here is more representative of the annual volume change rate because the images are captured approximately a year apart. Lastly, when the velocity gradient found here is extrapolated linearly to the terminus to compensate for discrepancy between velocity calculated here and velocity at the terminus (which is assumed to be larger than the values reported here due to the increasing velocity gradient) the calving rate is determined to be under estimated by up to 25%.

The seasonal terminus area change recorded in 1959 is of the same range as those occurring annually in 1999 – 2003, although the terminus is at a slightly more advanced position in the later period. The annually averaged flow rate during the later period is ~1/3 the 1959 summer values. Although the mean iceberg size and standard deviation from 1959 and 1966 are smaller than the mean iceberg size from some years between 1999 and 2003, the iceberg's irregular shapes and surface crevasse markings (Figure 22; Table 5) in both 1959 and 1999 – 2003 are similar, which indicate a similar calving mechanism. Tabular icebergs have not been observed throughout the study period from this glacier.

Otto Glacier is experiencing a period of fast flow which may be related to a surge. The terminus position between 1999 and 2003 fluctuated in a small window. The 1999 to 2003 average calving rate, 0.25 ± 0.03 $km^3 a^{-1}$, is the second largest calving rate found in this study (after Eugenie Glacier). The variability between inter-annual calving is variable by up to a factor of 2. Summer calving rates could not be estimated between 1999 and 2003 because imagery was not available. Therefore the seasonal variations in calving rate are unknown for this glacier.

Table 5. Otto Glacier Terminus Region Properties & Flow Characteristics

Image Date	1959, July 7	1959, Aug. 17	1999, July 24	2000, June 25	2001, June 11	2002, June 15	2003, July27
Terminus Area Change (km^2)	NA	-0.848 (since July7 1959)	+6.124 (since July7 1959)	+1.278 (since 1999)	-1.215 (since 2000)	+0.477 (since 2001)	+0.631 (since 1999) +0.201 (since 2002)
Terminus Region Width (m)	3010	NA	4414	NA	NA	4532	NA
Centre-line Velocity between ~5km and ~2km of terminus 1999 – 2003 ($m\ a^{-1}$)	NA	~2810 between ~3km and ~1km of terminus (since July 1959)	NA	~544 (since 1999)	~406 (since 2000)	~456 (since 2001)	~672 (since 2002)
Average Centre-line Velocity Gradient between ~5km and ~2km of terminus 1999 – 2003 ($m\ a^{-1}$/km)	NA	~+150 between ~3km and ~1km of terminus (since July 1959)	NA	NA	~+32 (since 1999)	NA	~+39 (since 2002)
Mean Iceberg Size – within 2 km of Terminus (m2)	6,872 σ 7,728	2,804 σ 3,504	23,128 σ 15,693	17,692 σ 11,826	8,703 σ 7,592	22,805 σ 28,245	9,805 σ 7,592

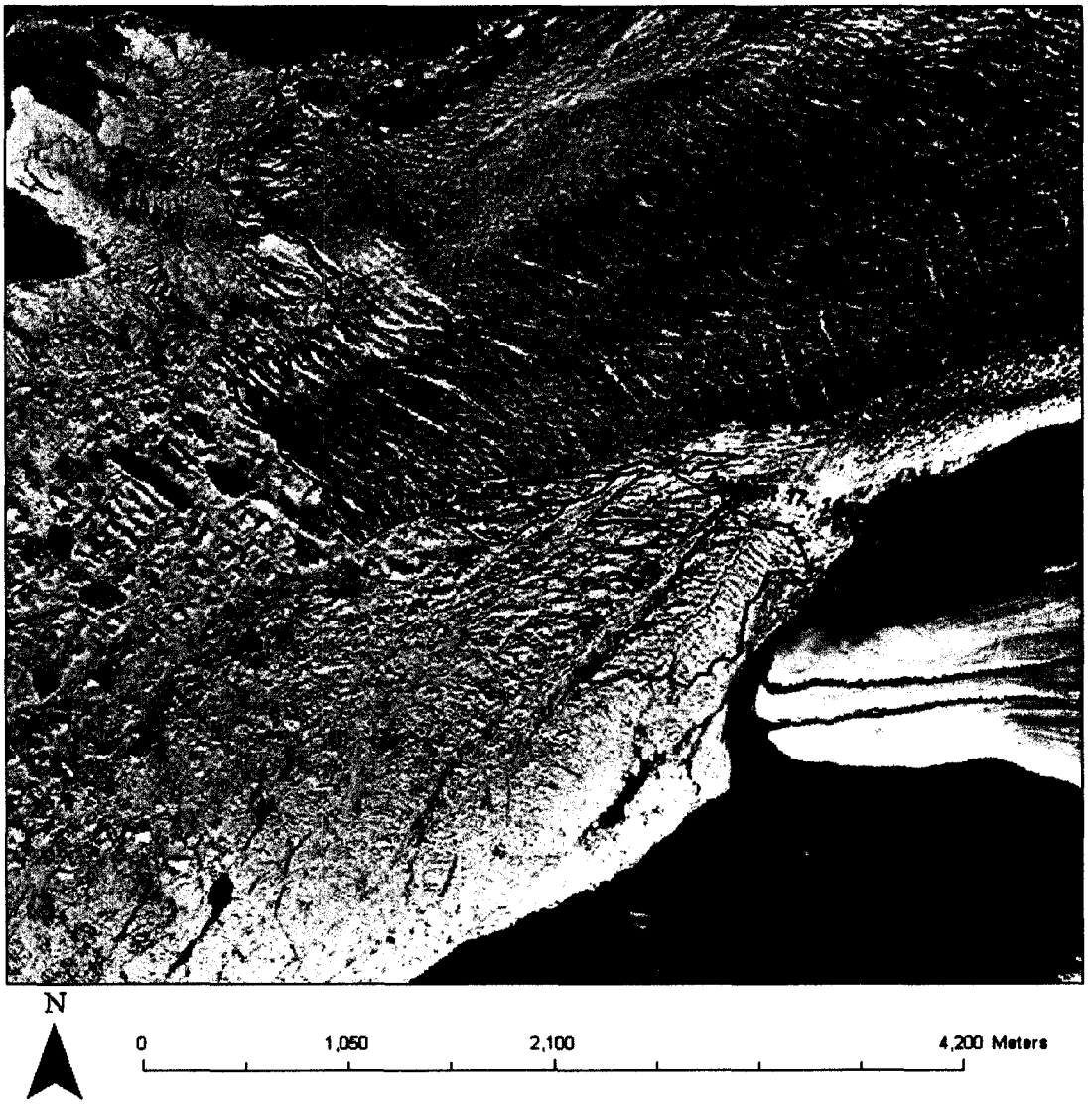

Figure 21. Otto Glacier terminus position and surface feature displacement between July 7 and August 17, 1959 aerial photographs, displayed on the July 7, 1959 aerial photograph (© A16606-029, July 7, 1959).

Figure 22. Selected terminus positions, terminus region width measurement location, between 1959 and 2003 and examples of surface feature displacement between 1999 and 2003 and iceberg crevasse feature from Otto Glacier, displayed on the July 10, 1999 Landsat 7 panchromatic image.

Table 6. Calving rates

Glacier	Image Dates	Centre-line Displacement (km)	Terminus Width (km)	Terminus Area Change (km^2): Increase (I) or Decrease (D)	Parabolic Width Averaged Thickness (km)	Calving Rate ($km^3\ a^{-1}$)
Otto	1999, July 24 to 2000, June 25	0.498	5.4	1.278 (I)	0.080[a]	0.04 – 0.15 ± 0.02
	2000, June 25 to 2001, June 11	0.390		1.215 (D)		0.21– 0.30± 0.02
	2001, June 11 to 2002, June 15	0.460		0.477 (I)		0.09 – 0.20± 0.03
	2002, June 15 to 2003, June 27	0.693		0.201 (D)		0.22 – 0.36 ± 0.03
Eugenie	1999, July 10 to 2000, July 31	0.492	5.0	0.672 (D)	0.100[b]	0.22 – 0.33 ± 0.04
	2000, July 31 to 2001, July 21	0.390		0.839 (D)		0.22 – 0.32 ± 0.05
	2001, July 21 to 2002, July 2	0.386		0.139 (D)		0.15 – 0.25 ± 0.05
	2002, July 2 to 2003, July 8	0.371		0.067 (I)		0.12 – 0.21± 0.04
Eugenie – Seasonal	June 23 to July 21, 2001	0.050		0.400 (D)		0.67 – 0.99± 0.05
Antoinette	July 10, 1999 to June 15, 2001	0.312	2.5	0.721 (D)	0.117[b]	0.07 – 0.09 ± 0.01
	July 19, 2001 to July 2, 2002	0.231		0.005 (I)		0.05 – 0.08 ± 0.02
Antoinette Seasonal	June 15 to July 19, 2001	0.075		0.332 (D)		0.55 – 0.72 ± 0.01
Antoinette Seasonal	July 19 to August 19, 2001	0.110		0.215 (D)		0.53 – 0.76 ± 0.01

Table 6. Calving rates – continued

Lake Tuborg	July 10, 1999 to July 19, 2001	0.235	3.5	0.195 (D)	0.110[b]	0.04 – 0.06 ± 0.06
	July 19, 2001 to July 2, 2002	0.175		0.430 (I)		0.02 – 0.07 ± 0.07
Lake Tuborg – Seasonal	June 15 to July 19, 2001	0.065		0.186 (D)		0.33 – 0.61 ± 0.07
Lake Tuborg – Seasonal	July 19 to August 19, 2001	0.130		0.472 (I)		0 – 0.14 ± 0.07
d'Iberville	July 10, 1999 to June 27, 2001	0.196	2.7	0.845 (D)	0.060[b]	0.04 – 0.05 ± 0.01
	June 27, 2001 to August 4, 2003	0.221		1.437 (D)		0.05 – 0.06 ± 0.01
d'Iberville Seasonal	June 27 – July 20, 2001	0.085		0.030 (D)		0.12 – 0.36 ± 0.01
Parrish	1999, July 10 to 2001, July 21	0.079	2.2	0.308 (D)	0.117[b]	0.02 – 0.03 ± 0.01
	2001, July 21 to 2002, July 2	0.023		0.160 (D)		0 – 0.03 ± 0.01
	2002, July 2 to 2003, July 9	0.079		0.143 (I)		0 – 0.01 ± 0.01
Cañon	July 10, 1999 to July 31, 2000	0.143	5.2	0.056 (D)	0.070[b]	0.03 – 0.07 ± 0.03
	July 31, 2000 to July 9, 2003	0.285		0.071 (D)		0.02 – 0.05 ± 0.03
John Richardson Bay (East)	July 10, 1999 to July 2, 2002	0.046	2.1	0.131 (D)	0.077[b]	0.004 – 0.006 ± 0.006
Sawyer Bay	July 10, 1999 to July 4, 2003	0.167	3.0	0.123 (I)	0.060[b]	0 – 0.01 ± 0.01

[a]Centre-line thickness from Gogineni (1995 – Cited in Short and Gray, 2005).
[b]Centre-line thickness from Dowdeswell (personal communication – 2006).

Eugenie Glacier, which flows eastward into Dobbin Bay from the south-east Agassiz Ice Cap, underwent a dramatic transformation from inactive to active flow sometime between 1966 and 1999. The absence of any surge features on 1959 aerial photographs and relatively few on the 1999 satellite imagery led Copland and others (2003a) to identify Eugenie Glacier as non-surge type. The terminus in 1999 was digitate and the lower section of the glacier had become crevassed compared to 1959 and 1966 imagery. There is no record of a rapid terminus advance, which is often (but not always) associated with a tidewater glacier surge (Murray et al., 2003b). Radio-echo soundings flown over this glacier in 2000 indicated that the terminus was probably floating (Dowdeswell, personal communication – 2006). The position of the grounding line was not identified. The glacier was however identified as being grounded at sea-level 25 km from the terminus. The width of Eugenie Glacier, measured at a consistent position ~3 km from the centre-point of the 1959 terminus (Figure 23), decreased by ~250 m (~5%) between 1959 and 2003, which indicates thinning. The width change between 1959 and 1966 falls within measurement error; the width successively decreased between 1999 and 2003. The crevasses on the terminus region of Eugenie Glacier are not continuous across the glacier. The mushrooming of the terminus caused by the glacier entering a widening portion of the fjord causes extension in both longitudinal and transverse directions, which is consistent with thinning at the terminus. Longitudinal crevasses penetrate into the terminus in all images from the 1999 to 2003 period. The July 2001 image shows sea-ice at the terminus and further into the fjord only beginning to melt and show open water. Pooling of surface water evident in some of the crevasses throughout the satellite imagery indicates that summer surface melting is occurring. The fjord is free of sea-ice at the terminus of Eugenie Glacier in the 1966 and 2000 imagery.

Table 7 lists the terminus properties and flow characteristics of Eugenie Glacier. The surface centre-line annual velocities were approximated manually from digitised crevasse features between ~5 km and ~2 km from the glacier's terminus because the image cross-correlation software did not produce adequate velocity maps from images from the period 1999 to 2003 (Figure 24 – intermediate year surface markings between 1999 and 2003 have been omitted for clarity). The largest annual velocity found between 1999 and 2003 was 464 m a^{-1} from 1999 – 2000 and the smallest was 367 m a^{-1} from

2002 – 2003. The velocities seem to have decreased progressively from 1999 to 2003. The lowest inter-annual velocity is ~20% lower than the highest velocity. A sub-annual centre-line velocity of ~650 m a^{-1} at the terminus was estimated between the end of June and the end of July 2001 (Figure 25) using image cross-correlation software. This corresponds to an approximately 1.5 to 2 fold increase over the 2000 – 2001 and 2001 – 2002 annual velocities. The sub-annual velocity was scaled to an annual average from a displacement of ~50 m. Therefore the error associated with this velocity estimate is relatively high (±30%) compared to the errors in velocity estimates derived from images captured ~ 1 year apart (up to ±6%). The longitudinal velocity gradient between 1999 and 2003 is positive, which indicates acceleration towards the terminus and is characteristic of an actively flowing floating terminus (Short and Gray, 2005). The velocity gradient reduces between 1999 and 2003. The terminus area of Eugenie Glacier decreased by -2.028 km^2 between 1959 and 1966; most of the area loss was regained by 1999. Eugenie Glacier's terminus area decreased again by almost this same amount by 2002, and a small area increase occurred in 2003.

The calving rates calculated for Eugenie glacier between 1999 and 2003 are presented in Table 5. The largest calving rate, 0.22 – 0.32 ± 0.04 km^3 a^{-1}, was measured between 1999 and 2000. There was a large amount of variation in calving rates, with differences between successive years being as large as ~22%. As the terminus is presumed to be floating, the upper calving rate estimate is likely closest to the true rate. The June to July 2001 calving rate is approximately 3 times larger than the largest ~annual calving rates.

Although significant flow change has probably occurred between 1966 and 1999 the terminus has fluctuated within a narrow region between 1959 and 2003. The terminus of Eugenie Glacier is located at a position where the fjord widens. In 1959 and 1966, the surface of Eugenie Glacier's terminus region was crosscut by many melt water channels reaching the terminus and showed no apparent crevassing (Figure 23 & 26). Figure 26 is an example of over-exposed Corona imagery; however melt water channels are apparent and the shape of the terminus remains the same. By 1999 the flow regime had changed. The surface was extremely crevassed in the 1999 – 2003 period, with crevassing extending up to 8 km from the 1999 terminus. The melt water channels have

disappeared and the terminus is more digitate. Melt water pooling is also visible on the 1959 and 1966 imagery, but because the terminus region is not crevassed the melt water channels run to the terminus of the glacier. The mean and standard deviations of sizes of icebergs found within 2km of the termini, originating from all of the imagery, fall within the same range (Table 7). In addition, all of the icebergs share an irregular shape and surface markings. Although the surface markings on the icebergs found in 1959 are likely related to melt channels and those found in the 1999 to 2003 period are likely related to crevassing. Tabular icebergs have not been observed throughout the study periods.

Changes recorded over the surface of Eugenie Glacier indicate that an increase in flow rate has occurred between 1966 and 1999. The average 1999 to 2003 annual calving rate of 0.28 ± 0.05 $km^3 a^{-1}$ is the largest calving rate found in this study. The variability between inter-annual velocity and terminus changes at Otto Glacier are less significant than at Otto Glacier because calving rates are progressively decreasing by up to 30% between successive years. An early summer calving rate in 2001 was ~3 fold larger than the annually averaged calving rates.

Table 7. Eugenie Glacier Terminus Region Properties & Flow Characteristics

Image Date	1959, July 7	1966, August 15	1999, July 10	2000, July 31	2001, June 23	2001, July 21	2002, July 2	2003, July 8
Terminus Area Change (km^2)	NA	-2.028 (since 1959)	-0.178 (since 1959) +1.850 (since 1966)	-0.672 (since 1999)	-0.400 (June 23 to July 21, 2001)	-0.839 (since 2000)	-0.139 (since 2001)	-1.583 (since 1999) +0.067 (since 2002)
Terminus Region Width (m)	5021	4996	4845	4829	NA	4838	4760	4767
Centre-line Velocity ($m\ a^{-1}$) between 5 km & 2 km of terminus	NA	NA	NA	~464 (since 1999)	~650 (June 23 to July 21, 2001)	~400 (since 2000)	~407 (since 2001)	~367 (since 2002)
Average Centre-line Velocity Gradient ($m\ a^{-1}/km$) between 5 km & 2 km of terminus	NA	NA	NA	~+21.3 (since 1999)	NA	NA	~+10.3 (since 2000)	NA
Mean Iceberg Size–within 2 km of Terminus (m^2)	17,405 σ 22,137	13,108 σ 6,322	20,402 σ 17,444	NA	NA	20,472 σ 8,732	14,655 σ 12,423	14,891 σ 10,689

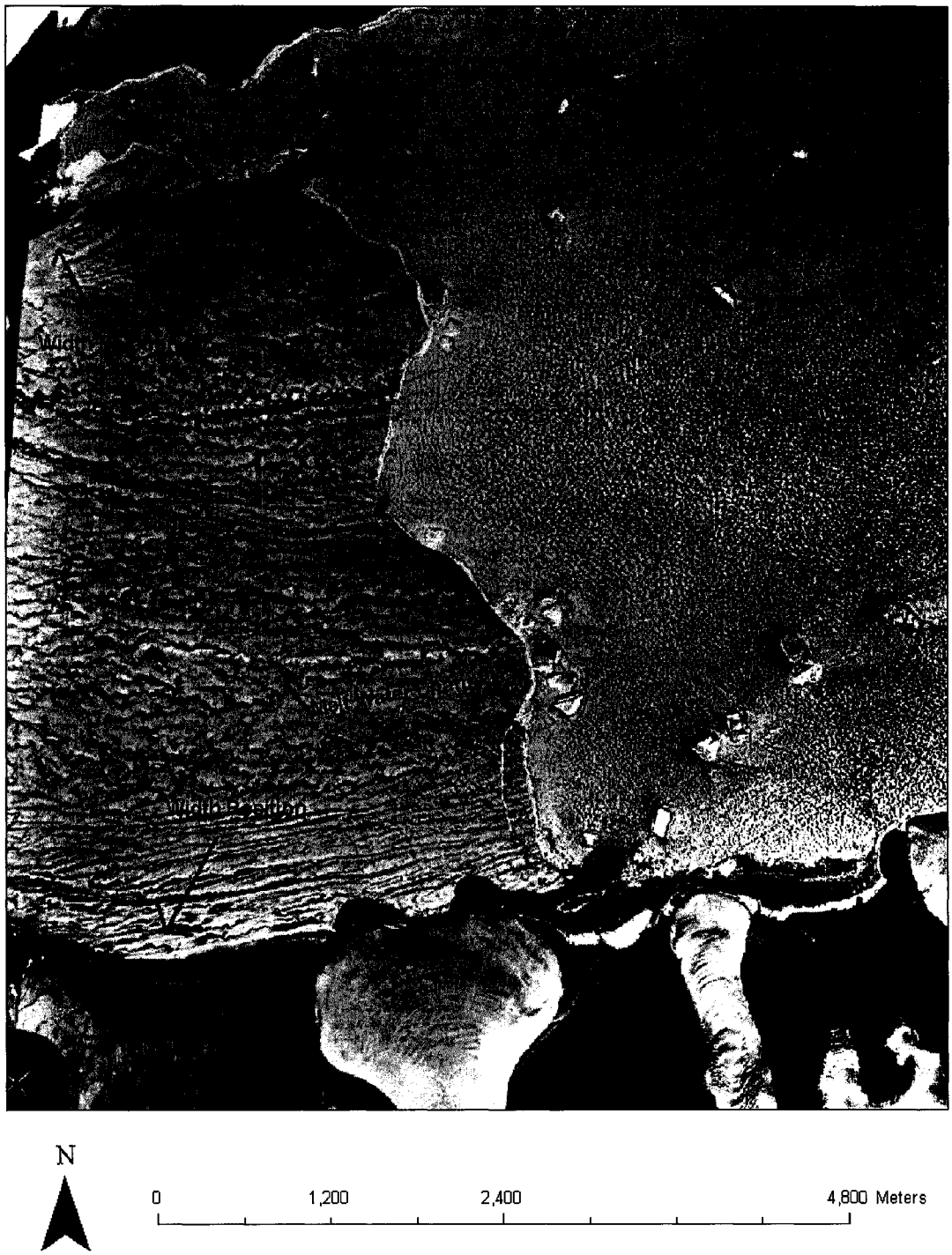

Figure 23. 1959 aerial photograph (© A16612-049, July 7, 1959) of Eugenie Glacier indicating melt water channels and terminus width measurement position.

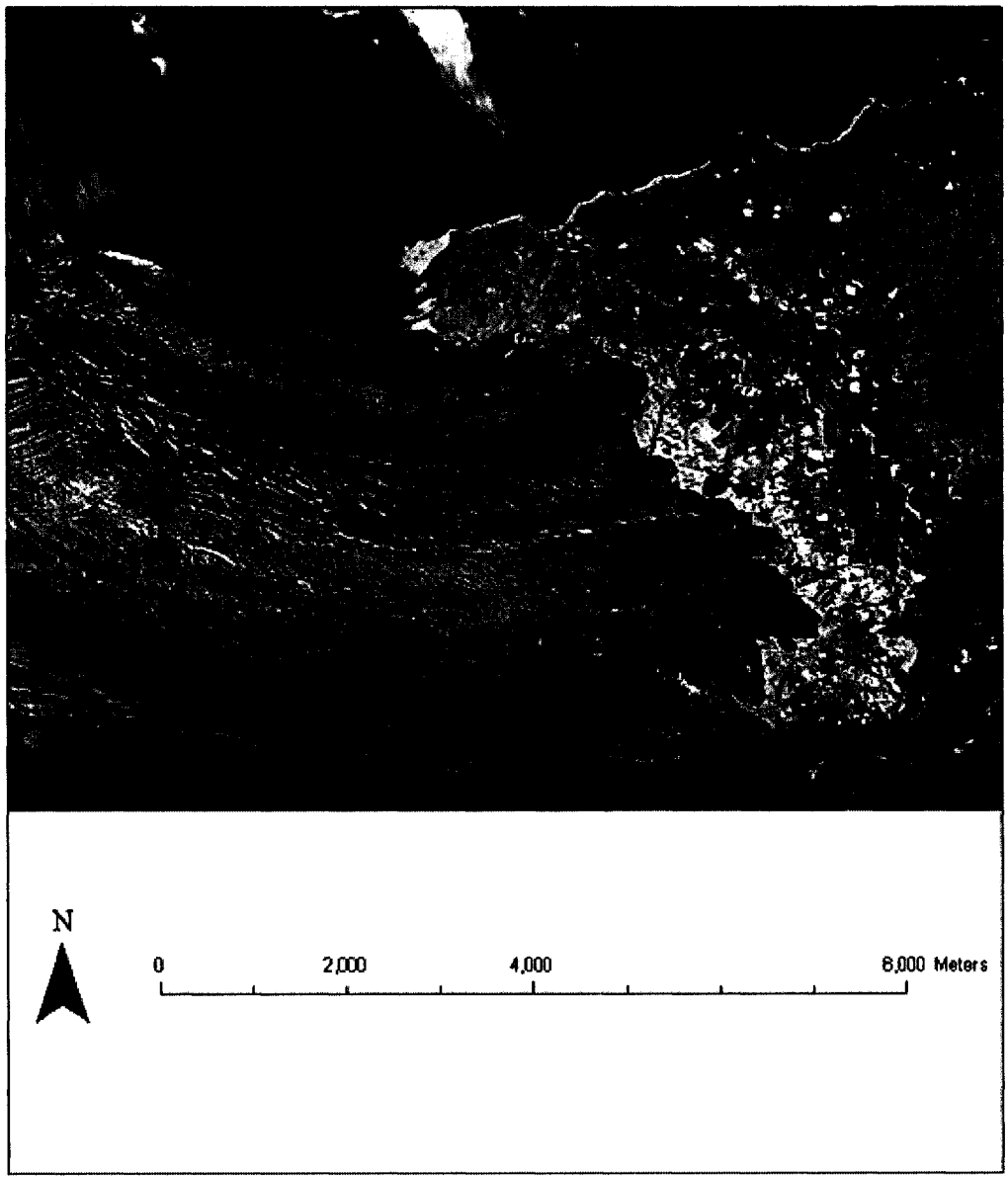

Figure 24. Select terminus positions and examples of surface features used to determine surface displacement from Eugenie Glacier displayed on the July 10, 1999 Landsat 7 panchromatic image.

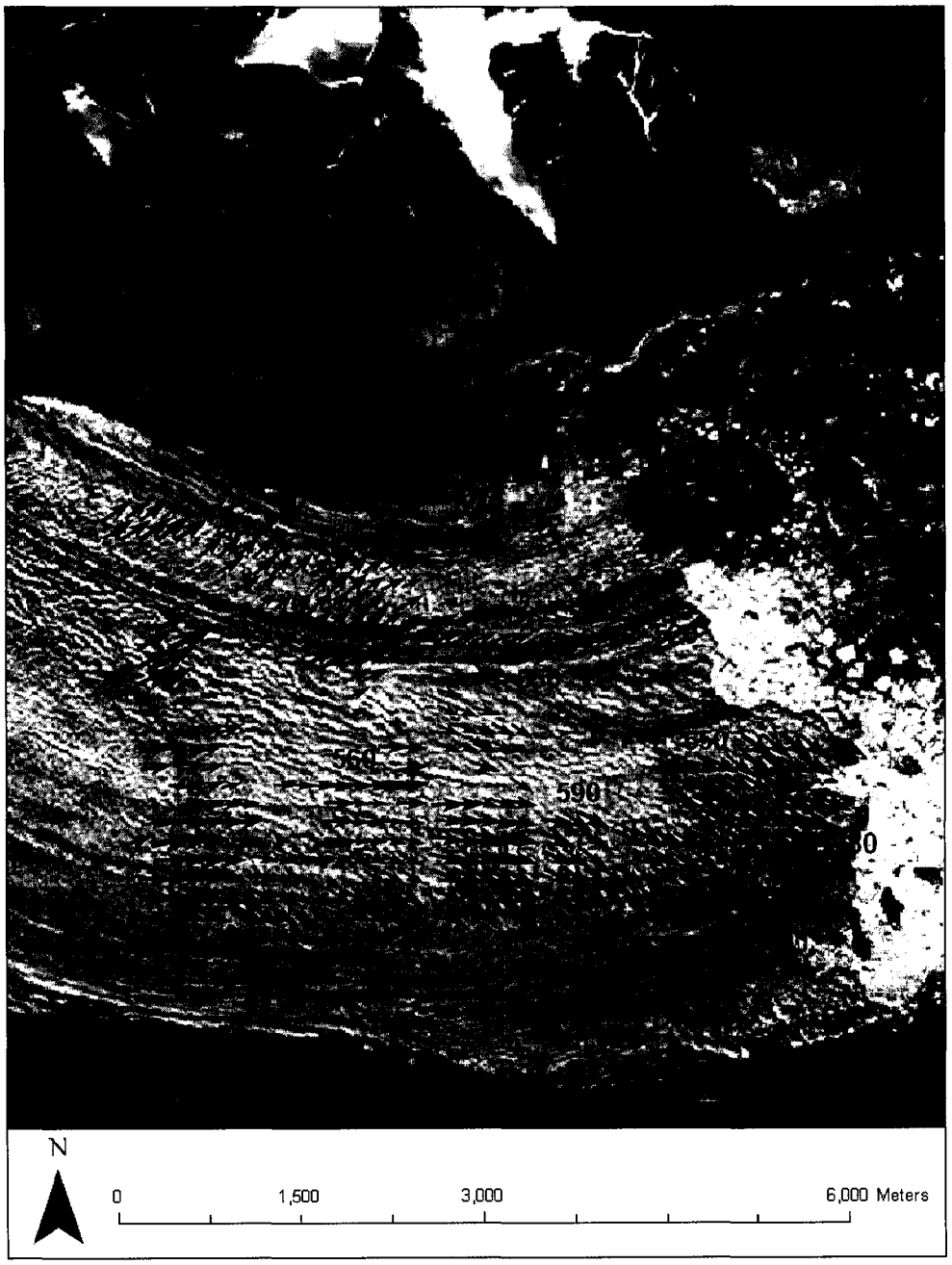

Figure 25. Selected image cross-correlation intra-annual velocity results (m a^{-1}) for Eugenie Glacier between June 23 to July 21, 2001 *displayed on the July 21, 2001 Landsat 7 panchromatic image. Velocities indicated on the map are for the adjacent vectors.*

Figure 26. August 15, 1966 Corona imagery of Eugenie Glacier showing image over-exposure typical of the 1966 Corona imagery.

A group of glaciers that display moderate annual velocities (~100 – 200 m a-1) between 1999 and 2003 comprises ~ ½ of the glaciers analysed here. These glaciers are Antoinette, Lake Tuborg (unofficial name), d'Iberville and Cañon. Furthermore, where available imagery allows the determination of summer velocities, these glaciers display order of magnitude velocity increases over annual velocities. The average of the annual calving rates from these glaciers reveals that they produce approximately 33% of the total from the nine glaciers in this study.

Antoinette Glacier and an unnamed glacier terminate in close proximity at the East end of Greely Fjord. These glaciers have been experiencing annual flow rates of ~200 m a^{-1} and have also experienced up to an order of magnitude summer velocity increases over their annual velocities. It is unknown whether the high inter-annual flow rates are the result of surge activity or fast flow resulting from their tide-water nature. The similarity of surface appearance and terminus position between 1959 and 2002 indicates that these glaciers have been experiencing similar rates for the duration of the study.

Antoinette Glacier flows northwest at its terminus and terminates at the end of its constraining valley. The abrupt opening is likely preventing further advance. Antoinette Glacier was not identified as surge type by Copland and others (2003a). Hattersley-Smith and others (1969) indicated a centre-line glacier thickness of the floating terminus of ~125 m at ~2 km from the 1966 terminus; consistent echo returns from bedrock appear at ~7.5 km from the terminus, ~80 m below sea-level, indicating that the glacier is grounded below sea-level. The centre-line thickness at the terminus in 2000 was ~175 m, thickening to ~200 m 1.5 km from the terminus (Dowdeswell, personal communication – 2006). The difference in thickness between 1966 and 2000 indicates the terminus region has grown thicker. The terminus was identified as floating in 1966 by Hattersley-Smith and others (1969) but was not identified as either floating or grounded in 2000 (Dowdeswell, personal communication – 2006). The increase in glacier thickness between 1966 and 2000 has likely moved the grounding line towards the terminus. The terminus region width is measured at ~ 2 km from the terminus (Figure 27). The width (Table 8) decreases between 1959 and 1999 – 2002 by ~ 3 times the margin definition (~30 m) error which suggests a thickness decrease but is contradicted by the RES data.

Unfortunately the 1966 Corona imagery of west side of Antoinette Glacier's the terminus region was covered in shadow which prevented terminus width measurement. Therefore the width change between 1966 and 2000 cannot be compared to the thickness change found with RES data between 1966 and 2000. Antoinette Glacier is marked by crevasses extending back further than 7 kilometres throughout the study period. Several kilometres up glacier from the terminus the crevasses are aligned roughly perpendicular to the valley walls. This type of crevasse is suggestive of extending flow, which is consistent with a floating terminus or a terminus that is approaching floatation. The crevasses rotate in orientation at ~1.5 km from the terminus (Figure 28), potentially in response to a deflection of the flow line related to greater buoyancy and terminus retreat on the north-east side of the terminus. Surface water can be seen pooling on the lateral edges of the glacier in the 1959 aerial photograph (Figure 27), but is more prevalent in the 1999 – 2002 imagery. Greely Fjord is open water in the August 19, 2001 imagery but open water is not recorded in any other images.

Glacier properties and flow characteristics for Antoinette Glacier are found in Table 8. The largest annual velocity (~ 240 m a^{-1}) was found between July 19, 2001 and July 2, 2002 between 3 and 2 km from the terminus (Figure 27 – intermediate year surface markings between 1999 and 2002 have been omitted for clarity). The July 19, 2001 – 2002 velocity is a ~50% increase from the 1999 – June 15, 2001 velocity found with image cross-correlation software over the same region (Figure 29). The positive longitudinal velocity profile between ~4 km of the terminus and ~1 km of the terminus indicates that the terminus region is experiencing extending flow between 1999 and 2001, which may be due to a fast flowing floating terminus. A limited amount of displacement correlations at 1 km from the terminus indicates the velocity is decreasing from 2 km to 1 km from the terminus. The 1999 – 2001 inter-annual displacement correlations found with image cross-correlation software do not vary significantly laterally, indicating that the centre-line velocity may represent the width averaged velocity for the centre portion of the glacier. No correlations were made in the glacier's lateral zones however. Therefore the lateral velocity variation across the whole width of the glacier is unknown. The 2001 summer centre-line velocity at the terminus, determined with image cross-correlation between June 15 and July 19, 2001 is 800 m a^{-1} and 1300 m a^{-1} between July

19 and August 19, 2001 (Figure 30 and 31 respectively). The small errors in summer displacements (~±20% and ~±14% respectively) indicate that the summer velocities are indeed much larger than annual velocities. The longitudinal velocity gradient changed between negative and positive as the summer of 2001 progressed. The 2003 winter velocities (February to March) determined with speckle tracking techniques by Short and Gray (2005) are ~130 m a^{-1} at 2 km from the terminus and ~160 m a^{-1} at 1 km from the terminus and then decrease to ~100 m a^{-1} at the terminus. The winter velocities found by Short and Gray (2005) were from slightly more than half a year after the last inter-annual velocities determined here, the similarity in values indicates that both this study and that of Short and Gray (2005) are identifying the same velocity trends. The terminus area changes less than 1 km^2 between 1959 – 2002 images (Figure 27), with area change from the summer of 2001 falling within the annual range of area changes. The area changes occur mostly at the centre of the terminus and do not significantly change the position of the terminus in relation to the valley walls.

The calving rates for Antoinette Glacier between 1999 and 2002 are found in Table 6. The 1999 – June 2001 annual calving rate is 0.09 – 0.07 ± 0.01 km^3 a^{-1}, which is ~10% larger than the July 2001 – 2002 calving rate. The 2001 seasonal calving rates are ~ 8 times larger than the inter-annual calving rates, almost entirely due to the increase in summer velocity. The upper calving rates may be closer to the actual values because the terminus is likely floating or approaching floatation. If the results from Short and Gray (2005) describe the actual inter-annual velocity behaviour over the last 2 km of the terminus region between 1999 and 2002, then the calving rates estimated here are potentially over-estimated by up to 20%.

A large crevasse penetrating into the 1999 terminus is reminiscent of a rift, potentially indicating that the terminus is floating or approaching floatation. Icebergs near the terminus (<0.5 km) through the study period bear crevasse markings. However large tabular icebergs have not been observed. A detailed analysis of iceberg size was not completed because icebergs within 2 km from the terminus could not be adequately determined as originating from Antoinette Glacier.

Table 8. Antoinette Glacier Properties & Flow Characteristics

Image Date	1959, July 27	1966, August 14	1999, July 10	2001, June 15	2001, July 19	2001, August 19	2002, July 2
Terminus Area Change (km^2)	NA	-0.808 (since 1959)	+0.507 (since 1959)	-0.721 (since 1999)	-0.332 (since June 2001)	-0.215 (since July 2001)	+0.005 (since July 2001)
Terminus Region Width (m) 2km from terminus	2541	NA	2305	2279	2317	2329	2353
Centre-line Velocity ($m\ a^{-1}$)	NA	NA	NA	~150 measured at ~1 km from terminus (since 1999)	~800 at terminus (since June 2001)	~1300 at terminus (since July 2001)	~240 measured between ~3 km & ~2 km from terminus (since July 2001)
Average Centre-line Velocity Gradient ($m\ a^{-1}$/km) measured between 2 km & 1 km from terminus	NA	NA	NA	~-10 (since 1999)	~-200 (since June 2001)	~+250 (since July 2001)	NA

Figure 27. 1959 aerial photograph (© A16694-040, July 27, 1959) of Antoinette (bottom of image) and Lake Tuborg Glaciers showing the terminus regions and the position of width measurements.

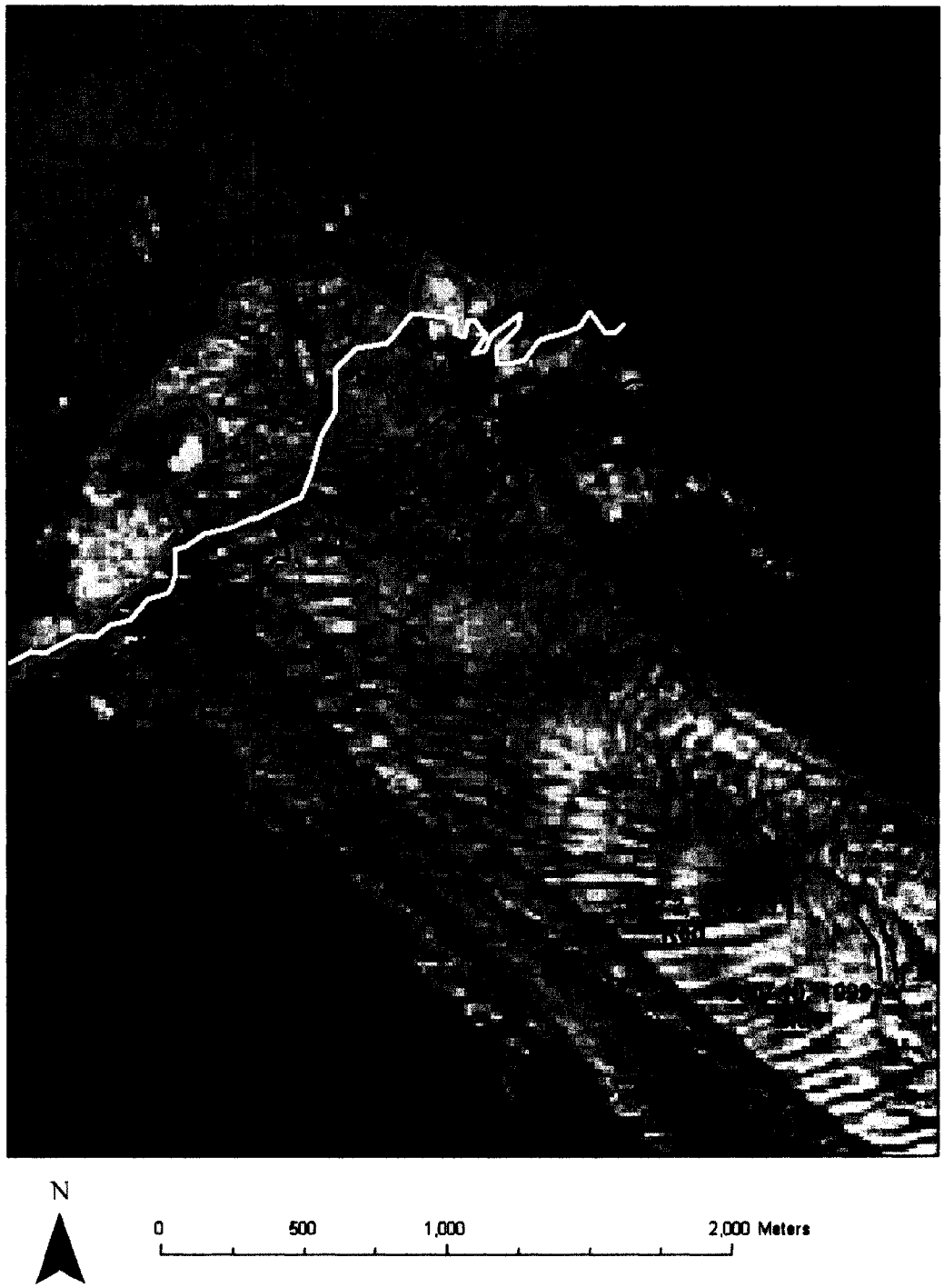

Figure 28. Selected terminus positions and examples of surface features from Antoinette Glacier displayed on the July 10, 1999 Landsat 7 panchromatic image.

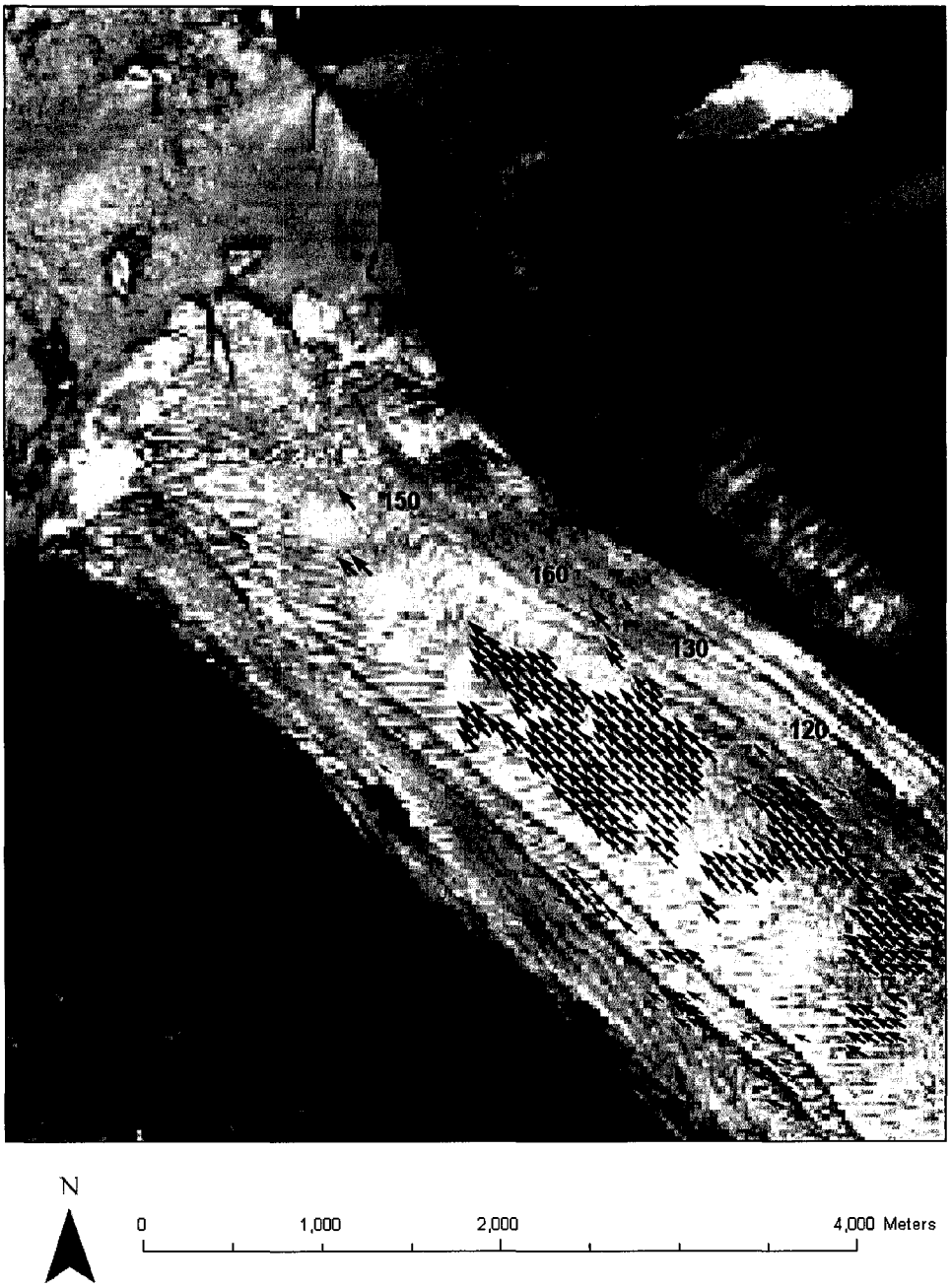

Figure 29. Image cross-correlation velocity results (m a^{-1}) with approximate centre-line velocities at 1 km intervals indicated for Antoinette Glacier between July 10, 1999 and June 15, 2001 displayed on the July 10, 1999 Landsat 7 panchromatic image.

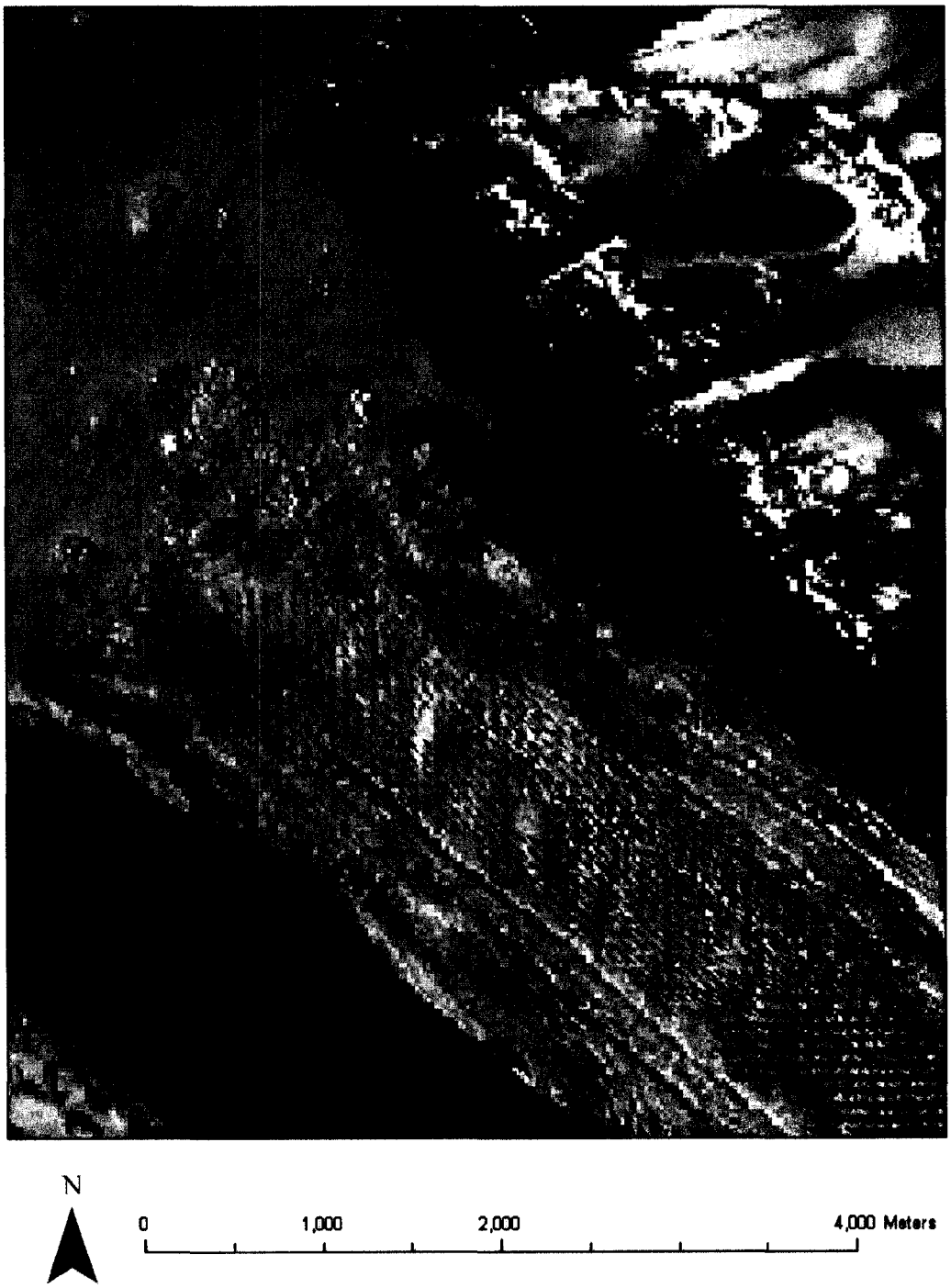

Figure 30. Image cross-correlation velocity results (m a^{-1}) with approximate centre-line velocities indicated at 1 km intervals for Antoinette Glacier between June 15 and July 19, 2001 displayed on the June 15 ASTER imagery.

Figure 31. Image cross-correlation velocity results (m a^{-1}) with approximate centre-line velocities indicated at 1 km intervals for Antoinette Glacier between July 19 and August 19, 2001 displayed on the July 19 ASTER imagery.

The unnamed glacier that separates Lake Tuborg from Greely Fjord is referred to in this study by the unofficial name of Lake Tuborg Glacier. Lake Tuborg Glacier terminates at the end of a constraining valley which opens into Greely Fjord, a position that is likely constraining further advance. Lake Tuborg Glacier was identified as possibly surge type by Copland and others (2003a) because it had a heavily crevassed terminus region and a highly digitate tidewater terminus in both 1959 and 1999. The digitate terminus was maintained in all imagery of Lake Tuborg Glacier including the 1966 Corona series imagery and satellite imagery from 1999 and 2002. Radio-echo soundings were flown over this glacier for the first time in the summer of 2000. The flight line over Lake Tuborg Glacier runs parallel to the centre-line on the south-east side, approximately 1/3 of the distance from the centre-line to the south-east margin, for the last ~5 km of the glacier. Much of the ~5 km terminus region is probably floating (Dowdeswell, personal communication – 2006). The terminus width measured at a consistent position (Figure 27; Table 9) at the approximate position of the grounding line. The width is similar in 1959, 1966 and 1999 but decreased by ~3% between 1999 and 2002, which is approximately 3 times larger than margin definition (~30 m), which suggests a thickness decrease. Greely Fjord is open water in the August 19, 2001 imagery but open water is not recorded in any other images.

Glacier properties and flow characteristics of Lake Tuborg Glacier are found in Table 9. The largest terminus area change, an increase of 2.066 km^2, occurred between 1959 and 1966, and was followed by a decrease in area of 0.516 km^2 between 1966 and 1999 (Figure 32 – Intermediate year omitted for clarity). The centre-line inter-annual velocity found by image cross-correlation between July 10, 1999 and July 19, 2001 (Figure 33) was ~120 m a^{-1} and the lateral velocity diminishes by a small amount laterally at the terminus (<~12%). The largest inter-annual velocity was found between August 19, 2001 and July 2, 2002, which was ~180 m a^{-1} determined manually from features found between ~2 and ~1 km from the terminus (Figure 32 – intermediate year surface markings between 1999 and 2002 have been omitted for clarity). The 2001 summer centre-line velocity at the terminus, determined manually from features found between ~2 and ~1 km from the terminus, between June 15 and July 19, 2001 was 700 m a^{-1} and was 1530 m a^{-1} between July 19 and August 19, 2001. The small errors in

summer displacement (~±34% and ~±17% respectively) indicate that the summer velocities calculated here are indeed larger than annual velocities. February to March 2003 surface velocities at the terminus, determined by speckle tracking of SAR imagery by Short and Gray (2005), for Lake Tuborg Glacier were ~160 m a^{-1}. These velocities show little variation between ~0.5 km and 3.5 km from the terminus, which is consistent with the 1999 – 2001 inter-annual velocities found here. The speckle tracking velocities were found during the winter approximately 6 months after the capture of the 2002 optical image which was used to determine the 2001 – 2002 velocity found here. The similarity in velocities indicates that both studies are identifying the same trends in velocity over the terminus region. The crevasses that were tracked manually between July and August of 2001 (Figure 32) were ~10 m further apart at the end of this time period, which translates to an increase in velocity by ~117 m a^{-1}. The sea-ice present in the July 2001 image has completely melted by the August 2001 image, exposing open water. The correlation between large velocity and velocity gradient increase over the inter-annual values and sea-ice removal suggests that the removal of the buttressing effect caused by the sea-ice may, at least partially, be responsible for these increases. The crevasse pattern is of crevasses running perpendicular to flow across much of the terminus region. This pattern is indicative of extending flow across the terminus region perpendicular to the centre-line, likely as a result of the floating terminus and the increase in velocity towards the terminus measured intra-annually.

Calving rates for Lake Tuborg Glacier between 1999 and 2002 are found in Table 6. The off-centre radio-echo sounding thickness was used as the parabolic width averaged thickness in calculating calving rates. The inter-annual calving rates for this period are similar, with the July 10, 1999 to July 19, 2001 values of 0.07 – 0.05 ± 0.06 km^3 a^{-1} being the largest. The summer intra-annual calving rates are ~2.5 larger than the inter-annual calving rates, largely resulting from the increase in velocity. The terminus is very likely floating, which indicates over this portion of the terminus there is likely little vertical ice deformation, making the upper estimate of calving rates likely closer to the actual rates. The extremely digitate terminus caused a very long terminus length which produced a large terminus area change error. This amount of error is a limitation in defining calving rate for Lake Tuborg Glacier.

More surface water pooling is evident in 1999 – 2002 than in 1959. Melt water channels are seen on the digitate terminus extensions in 1999 and after, likely indicating a lower rate of flow compared to 1959. The monthly terminus area changes found in the summer of 2001 are similar in magnitude to the annual changes from 1999 to 2002. Icebergs near the terminus (<0.5 km) through the study period bear crevasse markings but large tabular icebergs have not been observed. A detailed analysis of iceberg size was not completed because icebergs within 2 km from the terminus could not be adequately determined as originating from Lake Tuborg Glacier.

Table 9. Lake Tuborg Glacier Properties & Flow Characteristics

Image Date	1959, July 27	1966, August 15	1999, July 10	2001, June 15	2001, July 19	2001, August 19	2002, July 2
Terminus Area Change (km^2)	NA	+2.066 (since 1959)	+1.550 (since 1959)	-0.195 (since 1999)	-0.186 (since June 2001)	+0.472 (since July 2001)	+0.430 (since July 2001)
Terminus Region Width (m)	2772	2764	2801	2757	2774	2732	2725
Centre-line Velocity ($m\ a^{-1}$) measured between ~2 km & ~1 km from terminus	NA	NA	NA	NA	~140 (since 1999) at ~1 km from the terminus ~700 (since June 2001)	~1530 (since July 2001)	~180 (since July 2001)
Average Centre-line Velocity Gradient ($m\ a^{-1}$/km) measured between ~2 km & ~1 km from terminus	NA	NA	NA		~+10 (since 1999)	~+117 (since July 2001)	NA

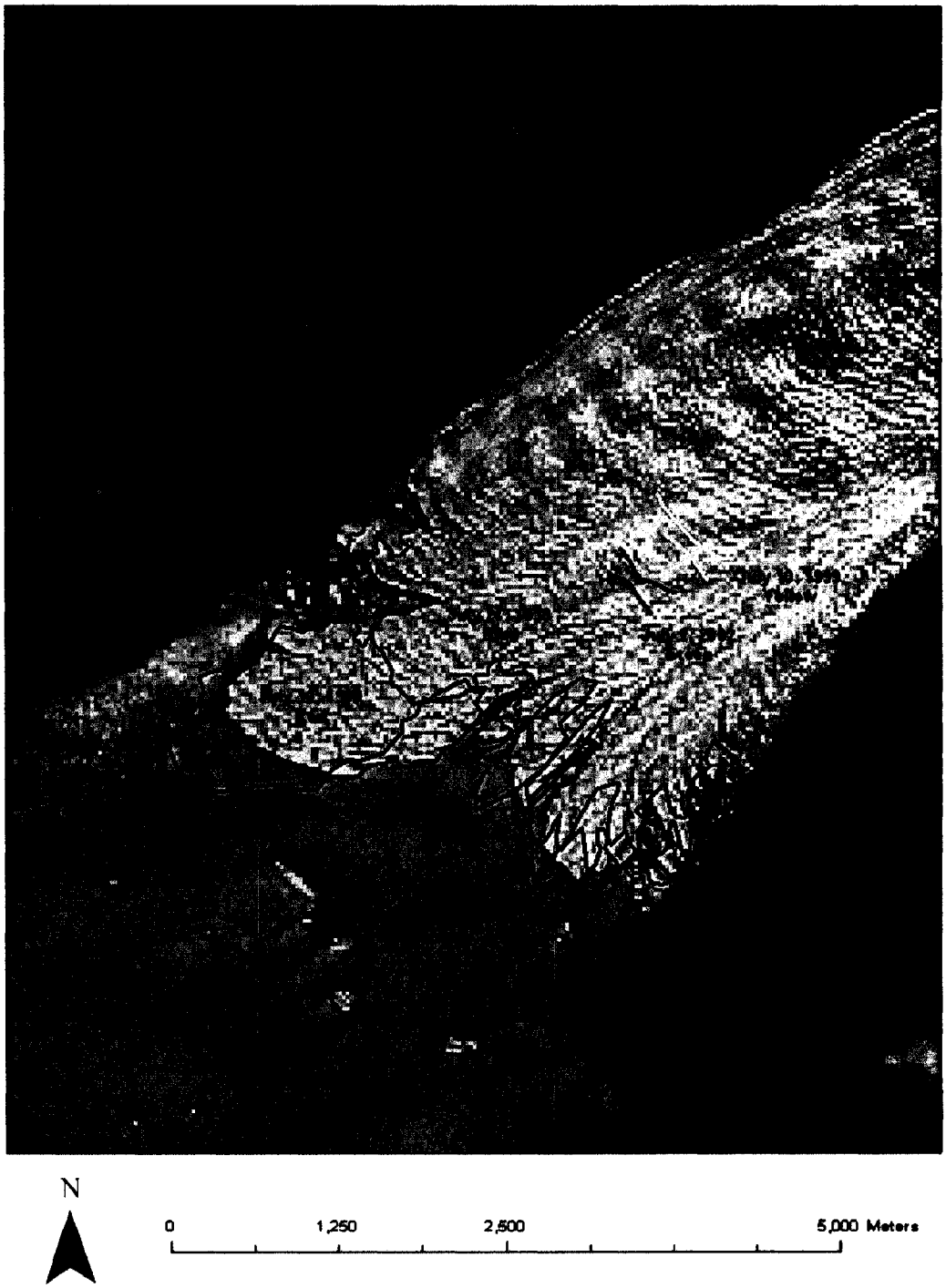

Figure 32. Lake Tuborg Glacier select terminus positions and an example of repeated crevasse patterns displayed on the July 10, 1999 Landsat 7 panchromatic image.

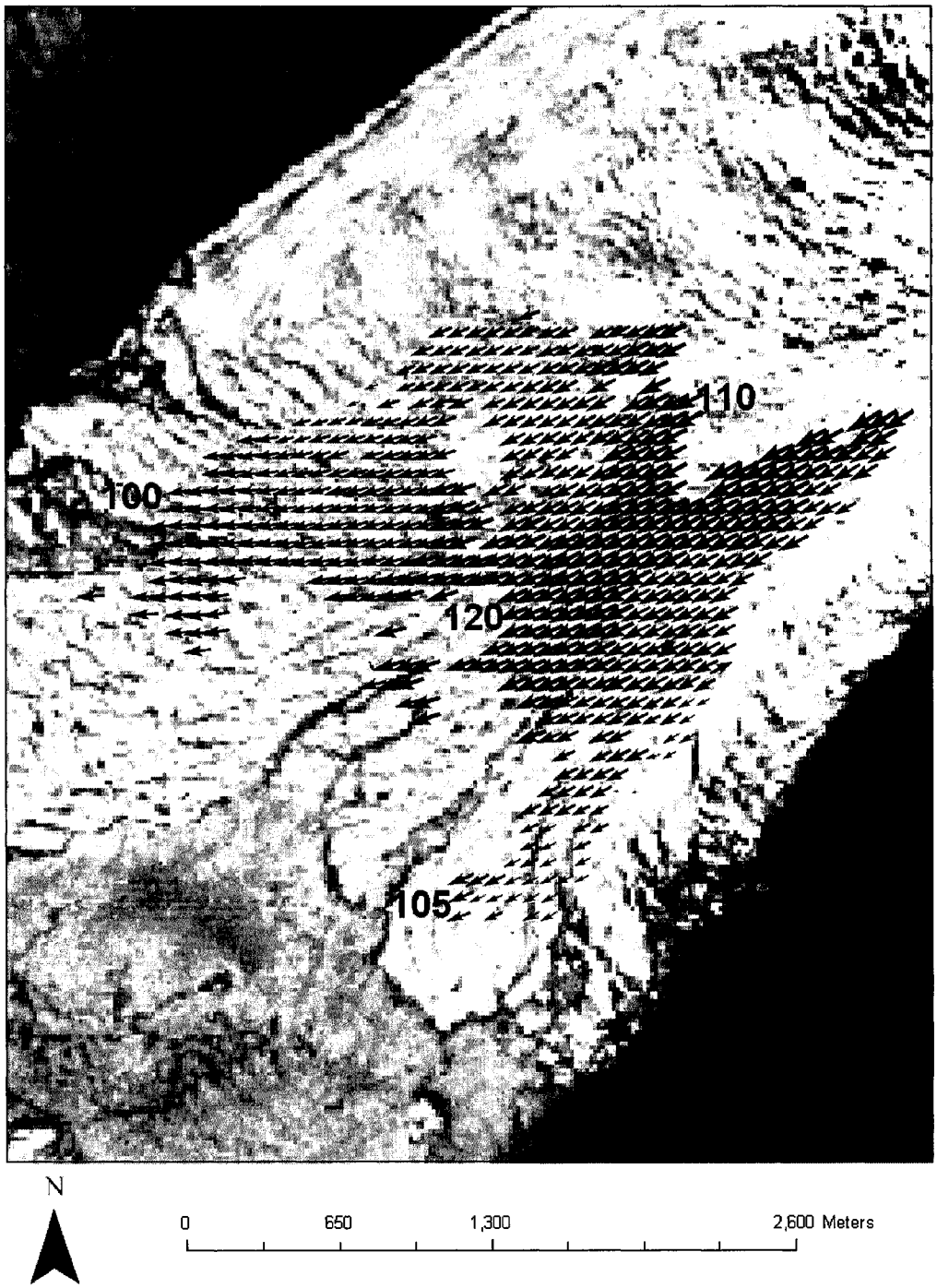

Figure 33. Image cross-correlation velocity results (m a^{-1}) for Lake Tuborg Glacier between July 10, 1999 and July 19, 2001 displayed on the July 10, 1999 Landsat 7 panchromatic image.

D'Iberville Glacier flows north-westwards from the northern side of Agassiz Ice Cap. A digitate tidewater terminus, distinct shear margins and looped moraines on the glacier in 1959 are indicative of recent surge activity, however these features were absent on the 1999 imagery. D'Iberville Glacier is considered to be in the quiescent phase of a surge cycle circa 1999 (Copland et al., 2003a). Results from radio-echo soundings indicate a grounded terminus in 1966 (Hattersley-Smith et al., 1969) and a terminus that was probably floating in 2000 (Dowdeswell, personal communication – 2006). The 1966 radio-echo soundings indicate that the terminus was grounded below sea-level as far as 15 km from the terminus. The terminus thickness was not identified, however. D'Iberville Glacier's width, measured at a consistent position ~4 km up glacier from the 1959 terminus (Figure 34), increased significantly (~20%) between 1959 and 1966, then diminished slightly to a width that varies by less than margin definition during the 1999 – 2003 period. The increase in width of the terminus region is consistent with ice mass being transferred to the receiving area during a surge. The width decrease between 1966 and 1999, although potentially indicating a small thickness decrease, may be enough to change the terminus from grounded to floating. Throughout the study period, crevasses running perpendicular to flow extend to both sides of the glacier and cross in the centre region. This crevasse pattern is indicative of extending flow and friction with the valley walls. The intensity of crevassing however diminishes throughout the study period, with the glacier surface appearing much smoother in 2003, potentially indicating a reduction in velocity and magnitude of extending flow. The fjord at the terminus of d'Iberville Glacier is sea-ice free in the 1959 and 2003 imagery.

Table 10 lists terminus properties and glacier flow characteristics for d'Iberville Glacier. The terminus area decreased between 1959 and 1966, increased between 1966 and 1999, then decreased between 1999 and 2003. Each of these area changes was roughly the same size (approximately 2.0 – 2.3 km^2). The area change was largely the result of change in the central portion of the glacier, thus the lateral terminus position was in roughly the same position throughout the study period (Figure 35 – intermediate year surface markings between 1999 and 2003 have been omitted for clarity). The terminus region velocity map was determined by image cross-correlation between 1999 and 2001. The centre-line velocity was ~100 m a^{-1} and the south-west portion of the terminus is

flowing at a slower velocity, ~35 m a^{-1} or ~65% less than the centre-line velocity (Figure 36). The longitudinal velocity gradient, measured between 1 km of the terminus and the terminus between 1999 and 2001, was increasing towards the terminus which indicates extending flow and is potentially indicative of a floating terminus on an active glacier. The centre-line velocity nearing the terminus, measured manually between ~2 and ~1 km of the terminus, was ~105 m a^{-1} between 2001 and 2003 and was increasing towards the terminus by ~15 m a^{-1}. The 2001 intra-annual velocity, also measured manually, between June 27 and July 20 is ~1350 m a^{-1} with a velocity gradient of ~111 m a^{-1}. Open water is visible at the terminus which suggests thinning of the remaining sea-ice compared to the unbroken sea-ice coverage in the June 2001 image and a reduction of a buttressing effect. The terminus region 1974 – 1975 inter-annual velocity was ~457 m a^{-1} and July-August velocity was ~500 m a^{-1}, which were determined from aerial photographs captured in 1974 and 1975 (Holdsworth, 1977). The 1999 – 2003 inter-annual velocities are markedly lower than for the advancing terminus in 1974 – 1975, a behaviour that is contradictory to the standard model of the tidewater glacier cycle. The inception of the surge, if the cause of the fast flow was indeed a surge, was not recorded. Thus the duration of the active surge (or fast flow) phase is unknown. However, the slowing of flow recorded between 1974 – 1975 and 2003 is consistent with prolonged post surge velocity decrease proposed by Murray et al. (2003a) for glaciers in Arctic regions. The high winter velocity and relatively small increase in summer velocity over winter velocity in 1974 indicates that surface melt water input in the summer to the sub-glacial system is likely playing a minor role in increasing flow in the 1974. This behaviour suggests that melt water penetration is less influential in increasing velocity during periods when inter-annual flow is already high, which in this case may be related to surging. Short and Gray (2005) determined surface velocities for d'Iberville Glacier with speckle tracking technique from RADARSAT – 1 image pairs captured in February and March. In 2003 and 2004 d'Iberville Glacier had winter surface velocity along its 33 km profile of 35 – 80 m a^{-1} with a centre-line velocity of ~40 m a^{-1} at the terminus in both years. These winter velocities are likely lower than the inter-annual velocities calculated here because of the effect that high summer velocity has in increasing the inter-annual average over the winter velocity. The annual velocity increase of 85% to 90% over winter velocity found

for d'Iberville Glacier in 2003 better conform to the results found by Jania (2002) from Spitsbergen Glaciers than those from Otto Glacier.

Calving rates for d'Iberville Glacier are found in Table 6. The largest intra-annual calving rate is 0.06 – 0.05 ± 0.01 $km^3 a^{-1}$ found between June 27, 2001 and August 4, 2003, which is ~ 35% larger than the 1999 to 2001 calving rate. The calving rates found here for 1999-2003 are approximately half of the calving rate of 0.11 ± 0.011 $km^3 a^{-1}$ found by Holdsworth (1977) for 1974 – 1975 when the glacier was flowing at a ~4-5 fold faster rate and had an advancing terminus. The intra-annual calving rate found in June and July, 2001 is ~2.5 times larger than the largest 1999 to 2003 inter-annual calving rate which is mostly related to the intra-annual increase in velocity over the inter-annual rate. Concerning the velocity profile across the terminus region shown on the image cross-correlation velocity map between 1999 and 2001 (Figure 36), the velocity on the west 1/3 of the terminus is ~1/3 the centre-line velocity. This velocity reduction potentially over-estimates the calving rate by up to ~10% because calving rate was calculated with centre-line velocity. However an exact reduction in the calving rate cannot be estimated without more information regarding the lateral terminus thickness. The upper calving rate estimate is likely closer to the actual value because the terminus is likely floating.

During periods when the central portion of the terminus has bulged, longitudinal crevasses or rifts penetrate into this part of the terminus region. The central extension of the terminus region calved as several large tabular icebergs in 2002 that were marked by crevasses, the largest of which was ~0.55 km^2 (Figure 37) an event that has not been recorded on any other imagery. The tabular icebergs cause an order of magnitude increase in iceberg mean area from 2002 compared to other years, which otherwise was within one standard deviation (Table 10). The terminus area changes found for d'Iberville Glacier are the largest found in this study (slightly larger than Eugenie Glacier) which are in the 2 km^2 range. The changes are of approximately the same size range between 1959 – 1966 and 1999 – 2003.

Table 10. D'Iberville Glacier Properties & Flow Characteristics

Image Date	1959, July 27	1966, August 15	1999, July 10	2001, June 27	2001, July 20	2002, July 2	2003, August 4
Terminus Area Change (km^2)	NA	-2.074 (since 1959)	+0.187 (since 1959) +2.261 (since 1966)	-0.845 (since 1999)	-0.030 (since June 2001)	-0.948 (since July 2001)	-2.281 (since 1999) -0.488 (since 2002)
Terminus Region Width (m)	2312	2897	2808	2794	2804	2796	2802
Centre-line Velocity at ($m\ a^{-1}$) between ~1 & ~2 km from terminus	NA	NA	NA	~100 (since 1999) at the terminus	~1350 (since June, 2001)	NA – Cloud	~105 (since July, 2001)
Average Centre-line Velocity Gradient ($m\ a^{-1}/km$)	NA	NA	NA	~+7 between ~1 km from the terminus and the terminus (since 1999)	~+111 between ~1 & ~2 km from terminus (since June, 2001)	NA	~+15 between ~1 & ~2 km from terminus (since June, 2001)
Mean Iceberg Size (m^2)	13350 σ 13162	16099 σ 23342	7596 σ 8836	14336 σ 747	NA	109854 σ 208601	16001 σ 14543

Figure 34. 1959 aerial photograph (© A16692-032, July27, 1959) showing the position at which the terminus region width was measured for d'Iberville Glacier. This imagery shows the fjord at the terminus to be sea-ice free.

Figure 35. Select terminus positions and examples of surface features from d'Iberville Glacier displayed on the August 4, 2003 ASTER image. This image shows the fjord at the terminus to be free of sea-ice.

Figure 36. Image cross-correlation velocity results (m a^{-1}) for d'Iberville Glacier between July 10, 1999 and June 27, 2001 displayed on the July 10, 1999 Landsat 7 panchromatic image.

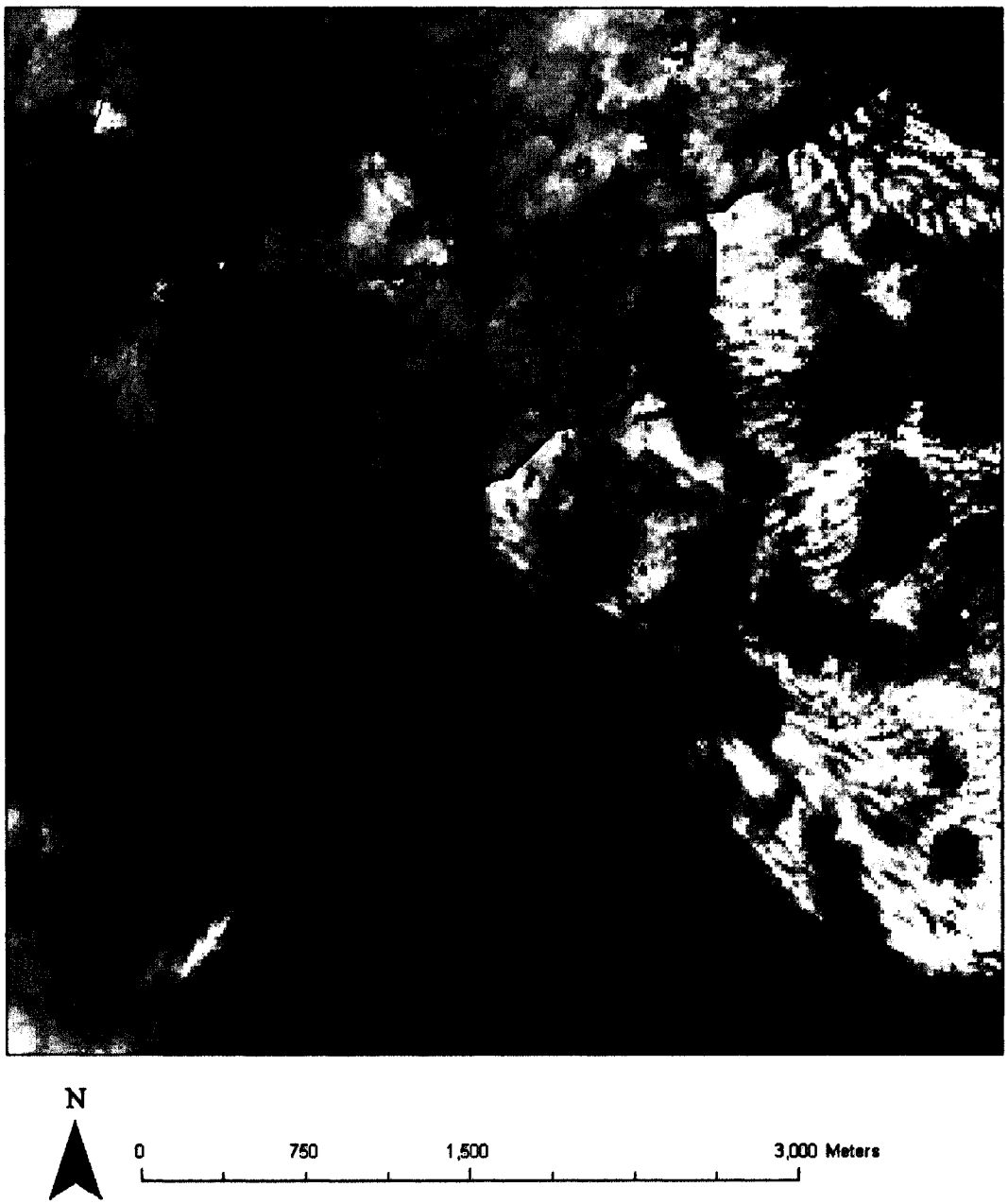

Figure 37. D'Iberville Glacier's large iceberg with crevasse features captured on the July 2, 2002 Landsat 7 panchromatic image.

Cañon Glacier flows south-westward from the south-western Agassiz Icecap into Cañon Fjord. The glacier terminates at a position in the fjord where it widens considerably which is potentially preventing further advance. Interpretation of RES data acquired in 2000 indicates the terminus was probably floating (Dowdeswell, personal communication – 2006). Terminus region width changes lie within margin definition and likely do not reflect any thickness changes of the lower portion of the glacier (Table 11). Crevassing, which appears throughout the study period, is restricted to the central portion of the glacier and shows the crevasses diminish in frequency as the terminus is approached (Figure 38). Limited networks of melt water channels are visible on the surface as well as ponding of melt water throughout the study. There are several crevasses penetrating into the terminus in 1959 which indicate rifting is likely an important mechanism in the formation of tabular icebergs (Figure 38). The Corona imagery from 1966 is over-exposed to the point that no glacier surface features can be determined, thus the evolution of crevasse pattern and orientation between 1959 and 1999 is unknown. The fjord at the terminus of Cañon Glacier is sea-ice free in the 1966 and 2000 imagery.

Table 11 lists terminus properties and glacier flow characteristics for Cañon Glacier. The terminus area has decreased by 0.627 km^2 between 1959 and 2003 (Figure 39 – intermediate year surface markings between 1999 and 2003 have been omitted for clarity), however none of the terminus area changes recorded between any of the imagery changes the terminus position appreciably. Figure 40 displays image cross-correlation velocity results for Cañon Glacier between July 10, 1999 and July 31, 2000. During this time period the centre-line velocity at the terminus was 136 m a^{-1} and the velocity gradient, measured over the last kilometre of the glacier, was ~-5 m a^{-1}. Although the terminus is considered to be floating there must be enough lateral friction over the terminus region to prevent acceleration. The proposed high amounts of lateral friction correspond well with the velocities on the southern and northern portions of the terminus region being approximately half the centre-line velocity. A velocity of ~97 m a^{-1} (determined manually between ~1.5 and 2.5 km from the terminus) was found between 2000 and 2003 with a negative velocity gradient of ~-10 m a^{-1} found over the same position on the terminus. The negative velocity gradients therefore stay roughly the same

between ~1.5 and 2.5 km from the terminus from 1999 to 2003. The 2000 to 2003 velocity is ~40 m a^{-1} less than from the same position between 1999 and 2000, indicating that the terminus region velocity has slowed slightly between 1999 and 2003. Short and Gray (2005) determined surface velocities for Cañon Glacier using the speckle tracking technique of SAR image pairs captured in February and March of 2003. Speckle tracking results show velocities ranging from 75 – 200 m a^{-1} along Cañon Glacier's length in 2003, with a velocity of ~75 m a^{-1} at the terminus which decreases from ~100 m a^{-1} 4 km from the terminus. This deceleration is consistent with image cross-correlation results found in this study several years earlier. The lower winter velocities compared to the annual velocities found here suggest a summer velocity increase. Repeat summer imagery was not available which precluded the determination of seasonal velocities. Therefore the magnitude or sign of summer velocity change could not be directly estimated. The July 31, 2000 ASTER image of Cañon Fjord is completely sea-ice free, but without repeat summer imagery from 2000 the effect on velocity and velocity gradient is impossible to determine.

Calving rates for Cañon Glacier are found in table 6. The largest inter-annual calving rate is found between July 10, 1999 and July 31, 2000 which is 0.07 – 0.03 ± 0.02 km^3 a^{-1}. The calving rate calculated between 2000 and 2003 is ~30% smaller than the 1999 – 2000 calving rate. Concerning the velocity profile across the terminus region shown on the image cross-correlation velocity map between 1999 and 2000 (Figure 40), the velocity on the north and south edges of the terminus is ~1/2 the centre-line velocity. Using linear interpolation this lateral velocity reduction likely causes the calving rate to be over-estimated by up to ~15%. However an exact reduction in the calving rate cannot be estimated without knowledge of the terminus thickness laterally across the terminus. The terminus of Cañon Glacier was considered probably floating, so the higher estimate of calving rate is likely closer to the actual value.

A tabular iceberg (~0.23 km^2), which bears no surface markings, is visible in the 1959 imagery and is likely the result of rifting into a floating terminus. The 1999 – 2003 imagery contains no tabular icebergs. The effect of the tabular iceberg is recorded in the mean iceberg size from 1959 being approximately an order of magnitude larger than the 1999 to 2003 iceberg mean size (table 11). Rifting occurs to differing degrees on the

1999 – 2003 imagery, but seems to be less prominent than in 1959. The appearance of rifts suggests the terminus has remained floating throughout the study period. The stable terminus position throughout the study period indicates that the infrequent production of tabular icebergs is likely not affecting the average calving rate over the study period. Furthermore the similarity of the terminus appearance between 1959, 1966 and 1999 – 2003 suggests the velocity has not changed appreciably.

Table 11. Cañon Glacier Properties & Flow Characteristics

Image Date	1959, July 17	1966, August 14	1999, July 10	2000, July 31	2003, July 9
Terminus Area Change (km^2)	NA	-1.388 (since 1959)	-0.499 (since 1959) +0.889 (since 1966)	-0.056 (since 1999)	-0.128 (since 1999) -0.071 (since 2000)
Terminus Region Width (m)	4473	4468	4493	4466	4494
Centre-line Velocity at Terminus ($m\ a^{-1}$)	NA	NA	NA	~136 between 1 km & 0 km of Terminus (since 1999)	~97 between ~2.5 and ~1.5 km of terminus (since 2000)
Average Centre-line Velocity Gradient ($m\ a^{-1}/km$)	NA	NA	NA	~-5 between 1 km & 0 km of terminus (since 1999)	~-10 – between ~2.5 and ~1.5 km of terminus (since 2000)
Mean Iceberg Size (m^2)	17942 σ 37297	3870 σ 4738	2583 σ 1609	5378 σ 5751	1875 σ 447

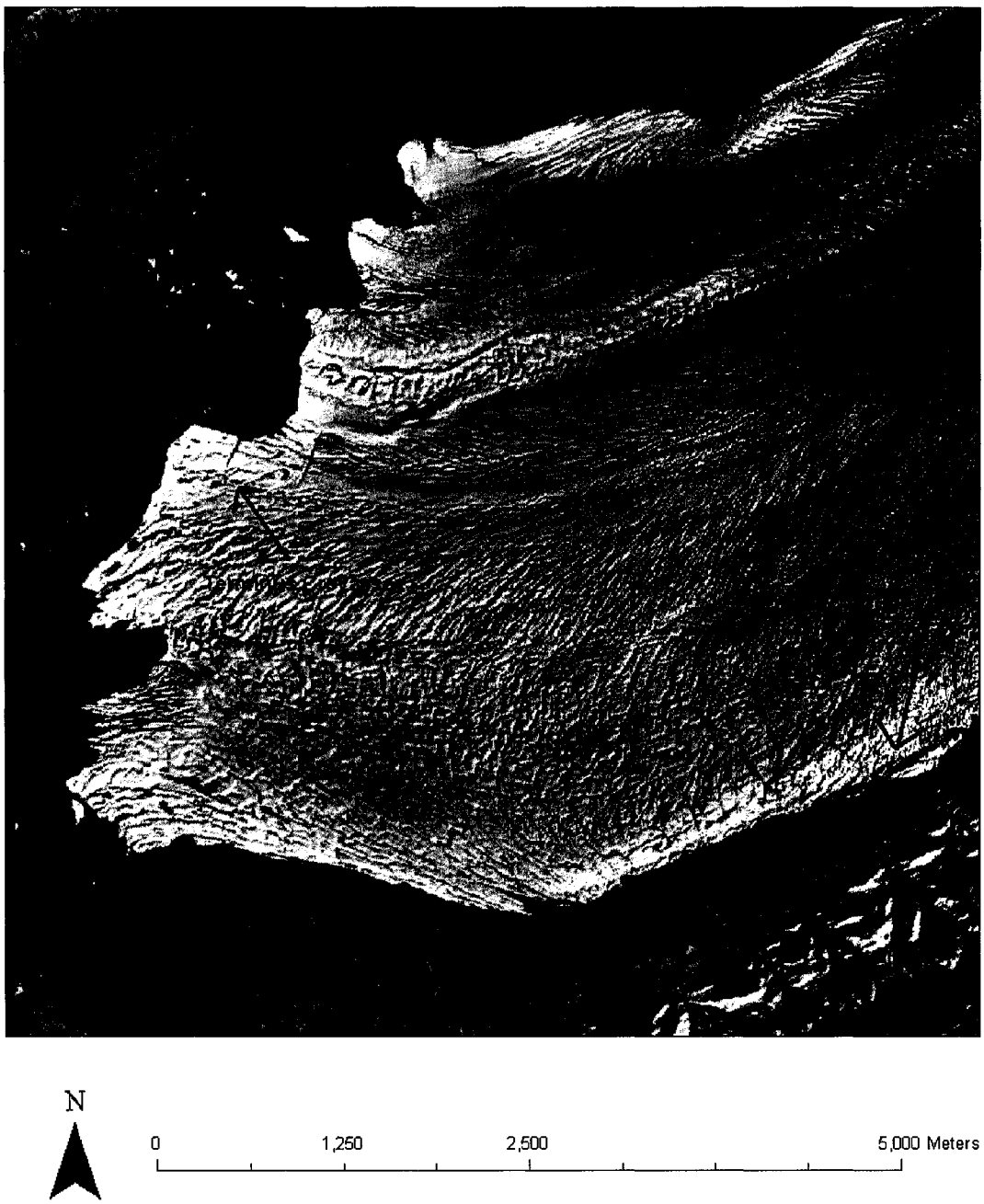

Figure 38. 1959 aerial photograph (© A16681-085, July 17, 1959) of Cañon Glacier showing the terminus width measurement position, a crevasse penetrating into the terminus and a sea-ice free Cañon Fjord .

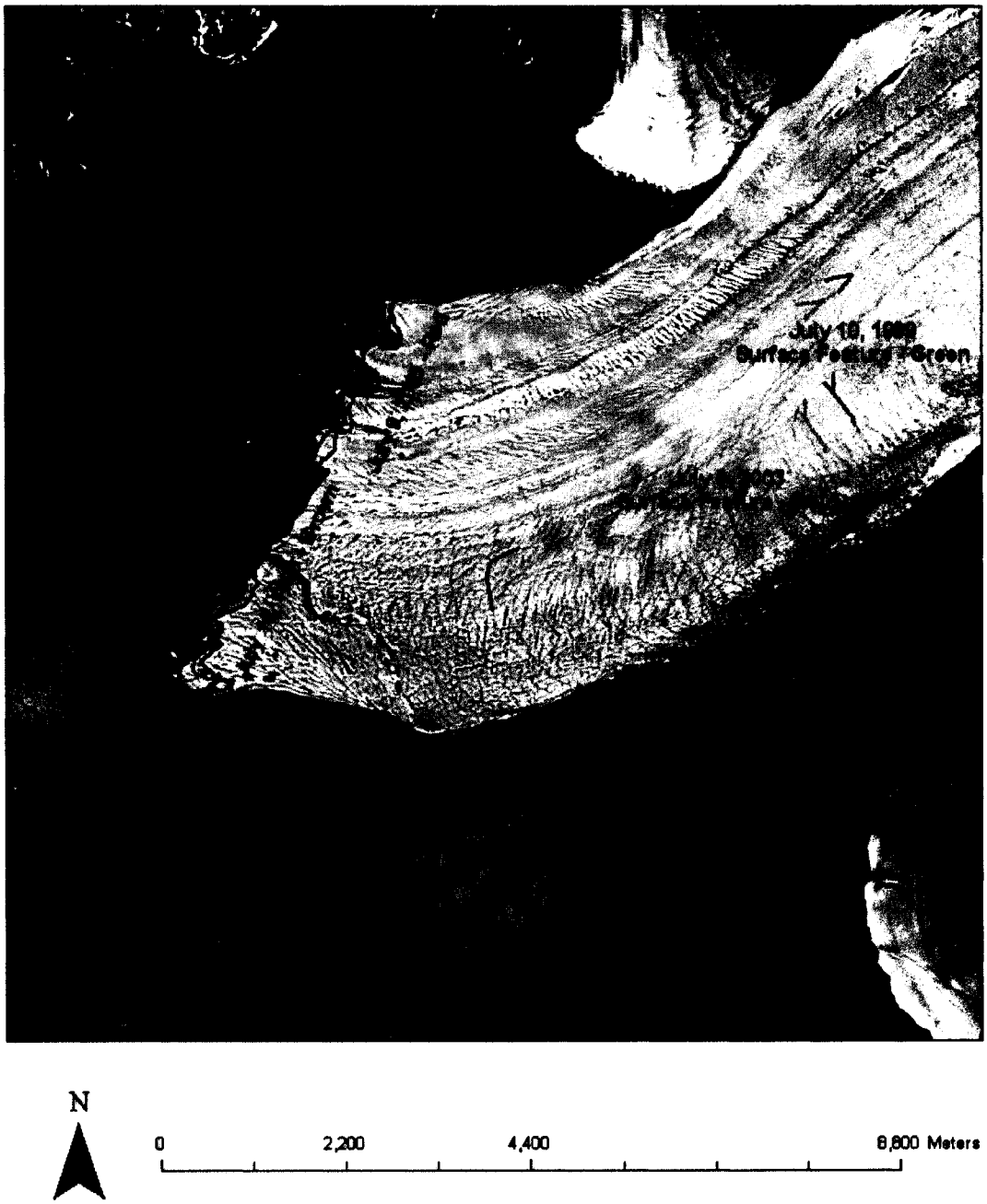

Figure 39. Select terminus positions and examples of surface features on Cañon Glacier displayed on July 10, 1999 Landsat 7 panchromatic imagery.

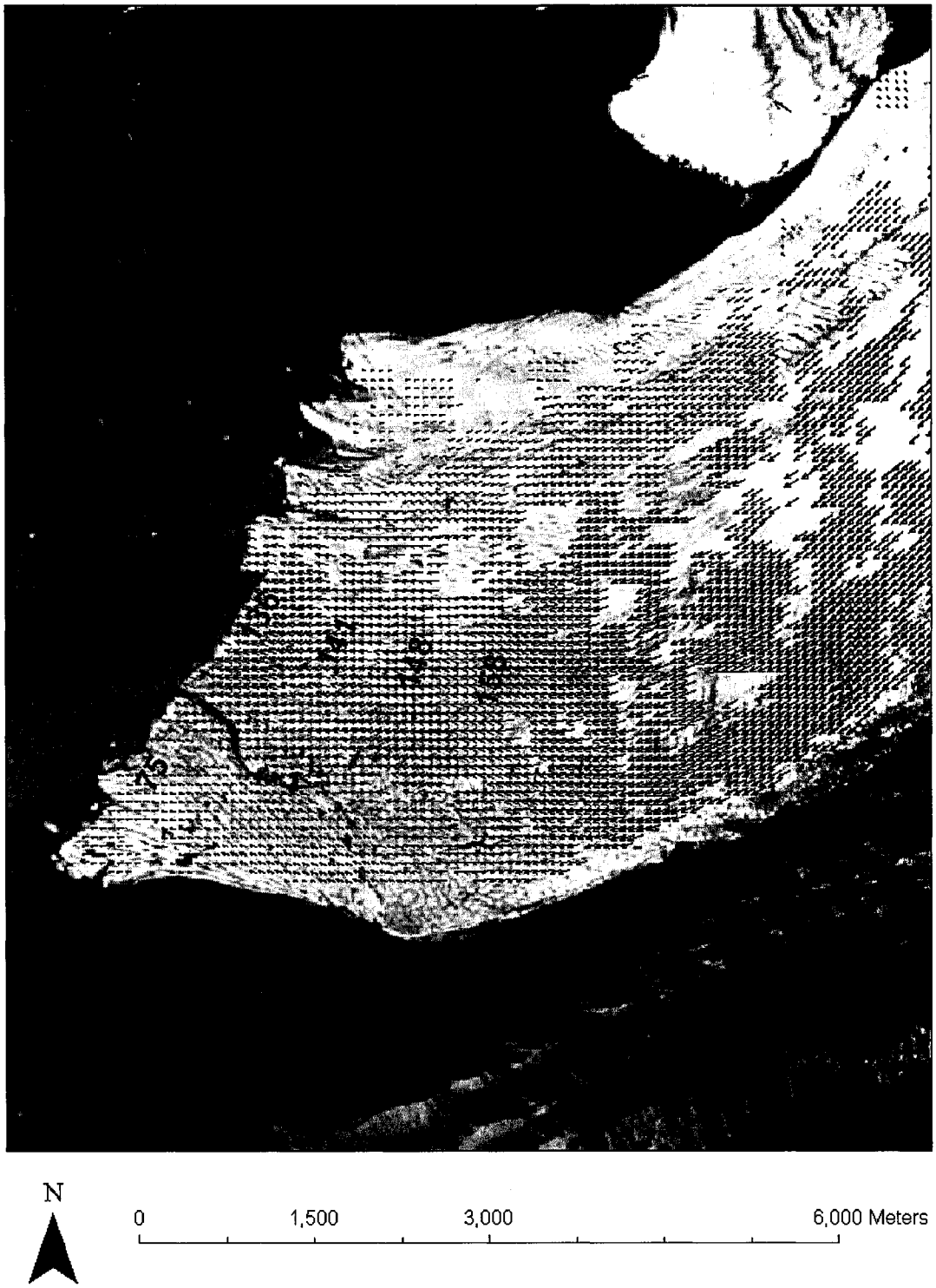

Figure 40. Image cross-correlation velocity results (m a^{-1}) for Cañon Glacier between July 10, 1999 and July 31, 2000 displayed on the July 10, 1999 Landsat 7 panchromatic image.

The final three glaciers analysed in this study are Parrish, John Richardson Bay (East) and Sawyer Bay Glaciers. The latter two glaciers exhibited stable terminus positions between 1959 and 2003 where as Parrish Glacier has recorded a 2 km terminus retreat. The 1999 to 2003 centre-line terminus velocities range between 20 – 80 m a^{-1}. The average 1999 – 2002 calving rate from these three glaciers comprises the remaining ~2% of the calving rate found from the nine glaciers analysed here, of which the majority originates from Parrish Glacier.

Parrish Glacier flows south from southern Agassiz Ice Cap. Folding and shearing on the glacier terminus are suggestive of past surge behaviour, however active surge behaviour has not been observed directly which led Copland and others (2003a) to consider this glacier to be in the quiescent phase of the surge cycle. No crevassing was evident on the terminus during the study period. There are melt water channels and standing water on the glacier surface in 1959 (Figure 41) which both appear to have diminished in quantity by 1999. The terminus was probably not floating in 2000 determined from the interpretation of radio-echo sounding profiles (Dowdeswell, personal communication – 2006). The fjord at the terminus of Parrish Glacier is covered in sea-ice in all imagery.

Table 12 lists terminus properties and glacier flow characteristics for Parrish Glacier. The terminus area of Parrish Glacier decreased in area by 5.356 km^2 between 1959 and 2002 (Figure 42 – intermediate year surface markings between 1999 and 2003 have been omitted for clarity). A modest increase in area of 0.143 km^2 between 2002 and 2003 was recorded. The width of Parrish Glacier (Figure 42), measured at a consistent position ~2 km up glacier from the 1959 terminus, decreased by approximately 20% between 1959 and 2001, which is suggestive of a thickness decrease. The width at the same position showed an increase between 2001 and 2003 returning the width to within margin definition error of the 1999 value. Terminus area thinning and retreat fits well with classical quiescent phase glacier behaviour. The inter-annual centre-line velocity near the terminus between 1999 and 2001 was ~38 m a^{-1} (Figure 43). The velocity is not uniform across the terminus and diminishes to ~20 m a^{-1} on the south-east side of the terminus. The centre-line velocity increased between 1 and 0.3 km of the terminus by ~7 m a^{-1} during the same time period. The centre-line velocity decreased between 2001 and

2002 before increasing to ~77 m a^{-1} between 2002 and 2003. These velocities were determined by manually measuring feature displacement between ~2 and ~1 km from the terminus between 2001 and 2003. The diffuse nature of the surface features precludes the manual measurement of the velocity gradient between 2001 and 2003. Intra-annual velocity could not be determined because repeat summer imagery was not available.

Table 6 reports 1999 – 2003 inter-annual calving rate estimates for Parrish Glacier. The calving rate is largest from July 10, 1999 to July 21, 2001 at 0.03 – 0.02 ± 0.01 km^3 a^{-1}. The terminus was thought to be grounded in 2000, thus the lower estimates of calving rates are likely closer to the actual values. Concerning the velocity profile across the terminus region shown on the image cross-correlation velocity map between 1999 and 2001 (Figure 43), the velocity on the south-west 1/3 of the terminus is ~1/3 the centre-line velocity. The lateral velocity reduction likely causes the calving rate to be over-estimated by up to ~10%. However an exact reduction in the calving rate cannot be assigned without knowledge of the glacier's thickness laterally across the terminus. Lastly, the small values of glacier displacement and terminus area change in relation to terminus area change identification error indicates that the calving rates, although very likely positive, could not be adequately differentiated from zero between 2001 and 2003.

Tabular icebergs recorded in 1959 are not recorded in the 1999 – 2003 imagery. The effect of the tabular iceberg is recorded in the mean iceberg size from 1959 which is approximately an order of magnitude larger than the 1999 to 2003 iceberg mean size (table 12). The tabular icebergs captured on the 1959 imagery did not bear any surface markings except one which contain a prominent melt water channel on its surface (Figure 41). This type of calving suggests that the terminus was either floating or approaching floatation in 1959.

Table 12. Parrish Glacier Properties & Flow Characteristics

Image Date	1959, July 15	1999, July 10	2001, July 21	2002, July 2	2003, July 9
Terminus Area Change (km^2)	NA	-4.888 (since 1959)	-0.308 (since 1999)	-0.468 (since 1999) -0.160 (since 2001)	-0.349 (since 1999) +0.143 (since 2002)
Terminus Region Width (m)	2768	2218	2129	2163	2190
Centre-line Velocity at Terminus ($m\ a^{-1}$)	NA	NA	~38 (since 1999)	~24 (since 2001)	~77 (since 2002)
Average Centre-line Velocity Gradient ($m\ a^{-1}/km$)	NA	NA	~+7 measured between 1 km & 0.3 km from terminus (since 1999)	NA	NA
Mean Iceberg Size (m^2)	89436 σ 46692	21702 σ 8821	8394 σ 9487	8054 σ 8197	5570 σ 5573

Figure 41. Parrish Glacier July 15, 1959 aerial photograph displaying melt water channels and tabular icebergs (© A16721-086, July 15, 1959).

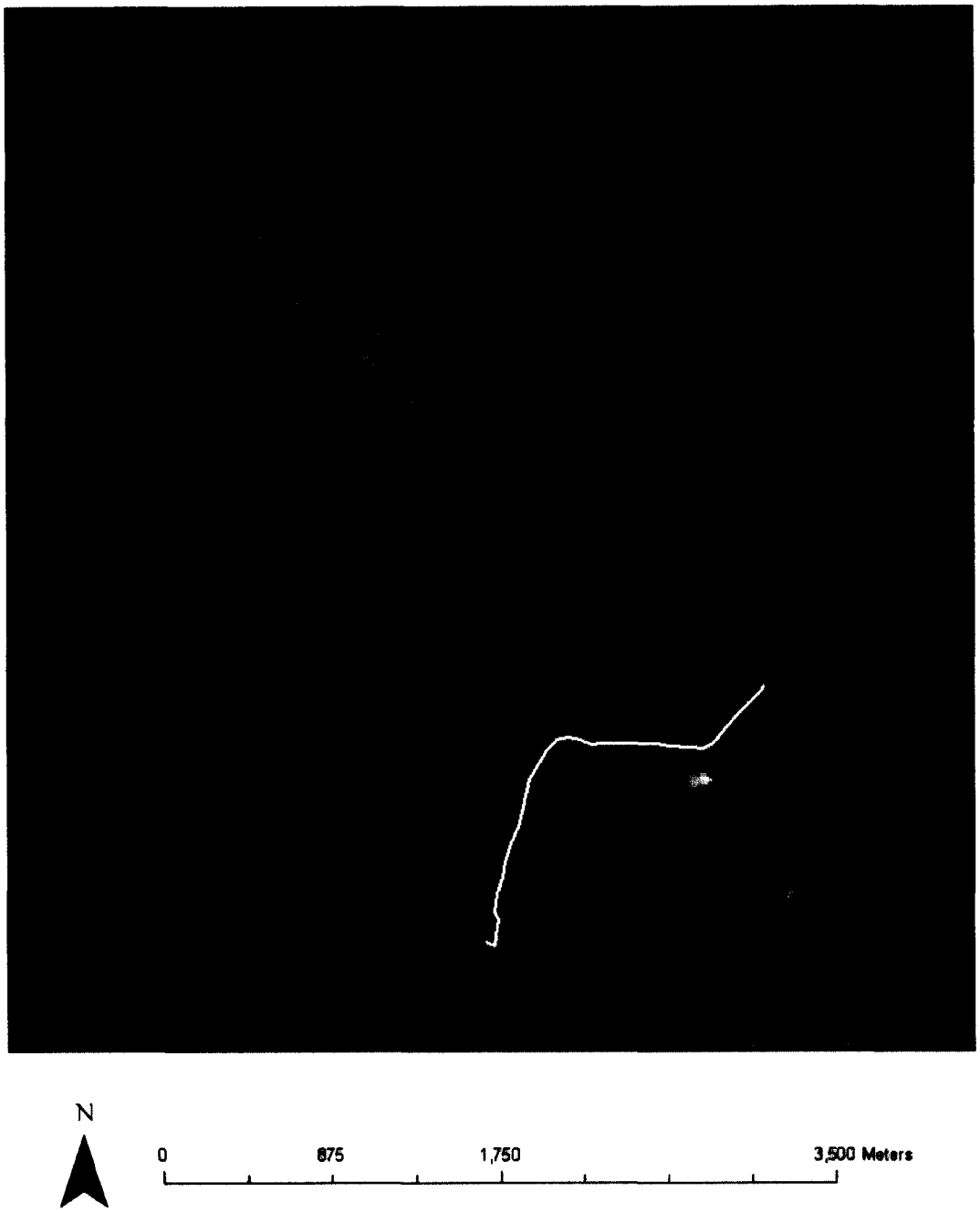

Figure 42. Parrish Glacier selected terminus positions with the terminus region width measured perpendicular to glacier flow adjacent to but not crossing the July 9, 2003 terminus position. Examples of surface features used to determine surface velocity are also shown. All features are displayed on the July 10, 1999 Landsat 7 panchromatic image.

Figure 43. Image cross-correlation velocity results (m a^{-1}) for Parrish Glacier between July 10, 1999 and July 21, 2001 displayed on the July 10, 1999 Landsat 7 panchromatic image. Centre-line velocities are displayed at the east margin.

John Richardson Bay Glacier (East) flows southward from the eastern Agassiz Ice Cap. From this point forward all references to John Richardson Bay Glacier refer to the eastern branch. Surge features have not been observed on this glacier's surface, which led Copland and others (2003a) to classify it as non-surge type. The available imagery reveals that no crevasses were evident on the glacier's terminus during the study period. The surface contained many melt water channels in 1959 (Figure 44) and in the imagery from 1999 – 2003 (e.g. Figure 45). The majority of these seem to flow efficiently to the terminus; little melt water ponding is visible on the terminus region. An airborne radio-echo sounding profile was captured for John Richardson Bay Glacier during the summer of 2000. The interpretation of this determined the terminus to be not floating (Dowdeswell, personal communication – 2006). The width of John Richardson Bay Glacier, measured at a consistent position 2 km from the centre point of the 1959 terminus (Figure 45; Table 13), has increased by 236 m or ~10% between 1959 and 2000. Shadow covered the west side of the glacier in all images except those from 1959 and 2000, which excluded these from width measurement. The width increase is ~8 times larger than the error associated with margin identification and therefore likely identifies terminus thickness increase. The fjord at the terminus of John Richardson Glacier is covered in sea-ice in all imagery.

Table 13 lists terminus properties and glacier flow characteristics for John Richardson Bay Glacier. The terminus lies at a prominent constriction in the fjord, and has consistently lost area throughout the study period. However the area lost has been relatively small – -0.875 km^2 between 1959 and 2003 (Figure 45). Image cross-correlation software produced a centre-line velocity at the terminus between 1999 and 2002 of approximately 14 m a^{-1} (Figure 46). The 1999 to 2003 image cross-correlation results were inconsistent and were not used. Not enough correlations were available at the terminus, between 1999 and 2002 imagery, to indicate if the velocity changed laterally. The velocity gradient, calculated between 1999 and 2002, was ~-2 m a^{-1} measured between ~1 km from the terminus and the terminus. The negative velocity gradient is consistent with terminus region thickening and compressive flow. Summer velocity determination was not preformed because the very small inter-annual displacements determined between 1999 and 2002 suggest that intra-annual velocities

would be too small to measure. The majority of melt water channels exit the glacier over the terminus suggesting that melt water input to the bed is limited and thus flow by basal sliding (and increased velocity related to water input) in the summer months may also be limited.

The calving rate estimate for John Richardson Glacier is found in table 6. The 1999 – 2002 calving rate is 0.006 – 0.004 ± 0.006 $km^3 a^{-1}$. The terminus of this glacier is considered to be grounded, which indicates that the lower of the two calving rates presented here is likely closer to the actual value. Due to the small displacement and terminus area change relative to the error associated with terminus area change determination the calving rate could not be adequately quantified as non-zero.

No large changes in surface appearance or terminus position occured between 1959 and 1999 – 2003 indicates the terminus has remained grounded throughout the study period and calving rate in 1959 are likely very similar to those determined for 1999 – 2003. Tabular icebergs were not identified as being produced at John Richardson Bay Glacier throughout the study period. The mean iceberg sizes are relatively small and do not display order of magnitude differences (Table 13).

Table 13. John Richardson Bay Glacier (East) Properties & Flow Characteristics

Image Date	1959, July 5	1999, July 10	2000, July 31	2002, July 2	2003, July 5
Terminus Area Change (km^2)	NA	-0.735 (since 1959)	-0.083 (since 1999)	-0.131 (since 1999) -0.048 (since 2000)	-0.140 (since 1999) -0.009 (since 2002)
Width (m)	3540	NA	3776	NA	NA
Centre-line Velocity at Terminus ($m a^{-1}$)	NA	NA	NA	~14 (since 1999)	NA
Average Centre-line Velocity Gradient ($m a^{-1}/km$)	NA	NA	NA	~-2 between 1 km & 0 km of Terminus (since 1999)	NA
Mean Iceberg Size (m^2)	1025 σ 326	18734 σ 2855	5611 σ 3235	NA	7578

Figure 44. 1959 aerial photograph (© A16604-020, July 5, 1959) of John Richardson Bay Glacier (East).

Figure 45. Select terminus positions, melt water channels and terminus region width measurement position for John Richardson Bay Glacier (East) displayed on July 31, 2003 ASTER imagery.

Figure 46. Image cross-correlation velocity results (m a^{-1}) for John Richardson Glacier (East) between July 10, 1999 and July 2, 2002 displayed on the July 10, 1999 Landsat 7 panchromatic image. Centre-line velocities are indicated on the map.

The glacier flowing into Sawyer Bay east of Benedict Glacier has not been officially named. For ease of reference this glacier is referred to as Sawyer Bay Glacier. Sawyer Bay Glacier flows southward from the southern Agassiz Ice Cap and partially shares its terminus with Benedict Glacier (Figure 47). The aerial photograph (Figure 48) and satellite imagery of Sawyer Bay Glacier's surface show a smooth quality to the terminus region. The same imagery shows crevassing and surge features, including looped moraines, on the adjacent Benedict glacier, indicating that the Sawyer Bay Glacier is indeed not crevassed. Surge features have not been observed on this glacier's surface, which led Copland and others (2003a) to classify it as non-surge type. Glacier surface features on the 1966 Corona imagery could not be identified due to image saturation. This glacier was determined to have a grounded terminus in 2000 from interpretation of RES data (Dowdeswell, personal communication – 2006) that was collected on a flight-line south-west of the centre-line. The width of Sawyer Bay Glacier, measured at a consistent position approximately 3 km up glacier from the 1959 terminus centre point (Figure 49), is variable and does not show any directional change throughout the study period. Moreover the 1959 and 2003 widths are within margin definition indicating that glacier thickness is likely similar. Sawyer Bay Glacier's width was measured at this location to avoid spurious width measurements that could potentially arise from changes in Benedict Glacier's terminus geometry. The fjord at the terminus of Sawyer Bay Glacier is sea-ice free in 1966 and 2001.

Table 14 lists terminus properties and glacier flow characteristics for Sawyer Bay Glacier. The terminus area change of Sawyer Bay Glacier fluctuates between 1959 and 2003 with a maximum increase of 0.615 km^2 between 1999 and 2001, but shows no evidence of consistent increase or decrease (Figure 49). The 2003 terminus was in roughly the same position as it was in 1959. The prevention of further advance may be the result of the position of the terminus at a widening portion of the fjord caused by the merging of Sawyer Bay and Benedict Glaciers' termini. From 1999 to 2003 the centre-line surface velocity, determined by image cross-correlation software, 0.5 km from the terminus was ~42 m a^{-1} (Figure 50). The velocity measured ~1 km from the terminus decreases to the west side of the glacier by approximately 33%. The longitudinal velocity gradient, determined from the image cross-correlation velocity map, is ~-3 m a^{-1}

measured between 1.5 km of the terminus and 0.5 km of the terminus. This velocity gradient is consistent with the high amounts of basal friction expected from a grounded terminus. Repeat summer imagery from the same year was not available therefore intra-annual velocities could not be calculated.

The calving rate for Sawyer Bay Glacier is found in Table 6. The calving rate between 1999 and 2003 is $0.01 - 0 \pm 0.01$ km^3 a^{-1}. These values were computed using the RES glacier terminus thickness without adjusting it with a parabolic width averaged thickness because the RES was collected midway between the centre-line and south-west margin of Sawyer Bay Glacier. Concerning the velocity profile across the terminus region shown on the image cross-correlation velocity map between 1999 and 2001 (Figure 50), the velocity on the west 1/3 of the terminus is ~1/4 the centre-line velocity. This velocity reduction likely causes the calving rate to be over-estimated by up to ~10%. However an exact reduction in the calving rate cannot be assigned without knowledge of the terminus thickness laterally across the terminus and a better understanding of the velocity on the lateral portions of the terminus region. The lower calving rate estimate is likely closer to the actual value because this glacier is considered to have a grounded terminus. Due to the small displacement and terminus area change relative to the error associated with terminus area change determination the calving rate could not be adequately quantified as non-zero.

Tabular icebergs were not produced throughout the study period and the mean iceberg size is relatively small and does not show order of magnitude variation (Table 14). Judging by the lack of terminus area change or glacier appearance the calving rate calculated between 1999 and 2003 is likely representative of the whole study period.

Table 14. Sawyer Bay Glacier Properties & Flow Characteristics

Image Date	1959, July 28	1966, August 15	1999, July 10	2001, July 21	2003, July 4
Terminus Area Change (km^2)	NA	-0.410 (since 1959)	+0.129 (since 1959) +0.539 (since 1966)	+0.615 (since 1999)	+0.123 (since 1999) -0.492 (since 2001)
Terminus Region Width (m)	1616	1648	1544	1521	1601
Surface Velocity at Terminus ($m\ a^{-1}$)	NA	NA	NA	NA	~42 (since 1999)
Average Centre-line Velocity Gradient ($m\ a^{-1}/km$)	NA	NA	NA	NA	-3 between 1.5 km & 0.5 km from Terminus (since 1999)
Mean Iceberg Size (m^2)	14545	9617 σ 3400	5847 σ 2400	3298 σ 1806	0

Figure 47. Benedict and Sawyer Bay Glaciers' terminus regions including Benedict Glacier's terminal moraine displayed on the July 4, 2003 ASTER imagery.

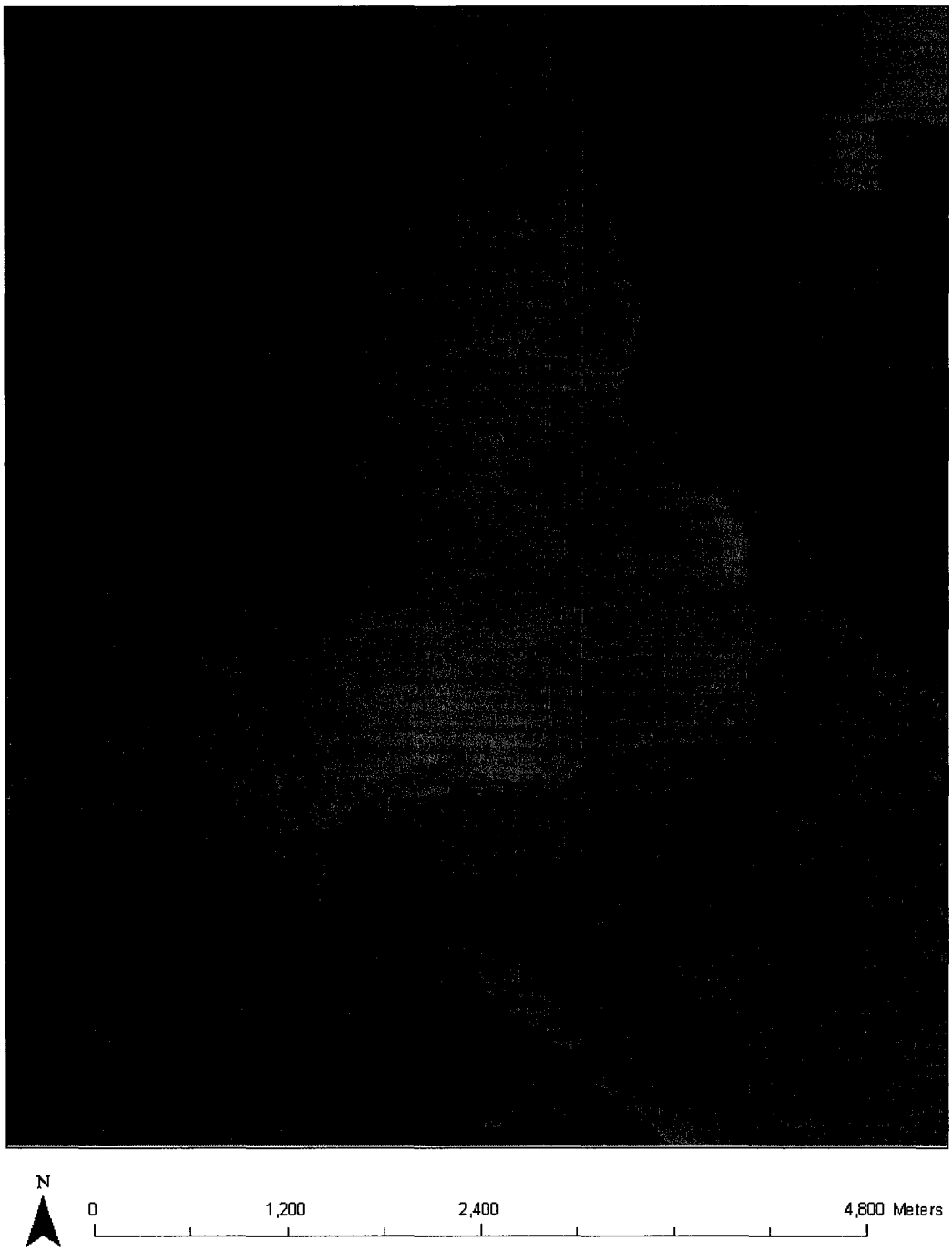

Figure 48. 1959 aerial photograph (© A16708-099, July 28, 1959) of Sawyer Bay Glacier.

Figure 49. Select terminus positions and terminus region width measurement position for Sawyer Bay Glacier displayed on July 4, 2003 ASTER imagery.

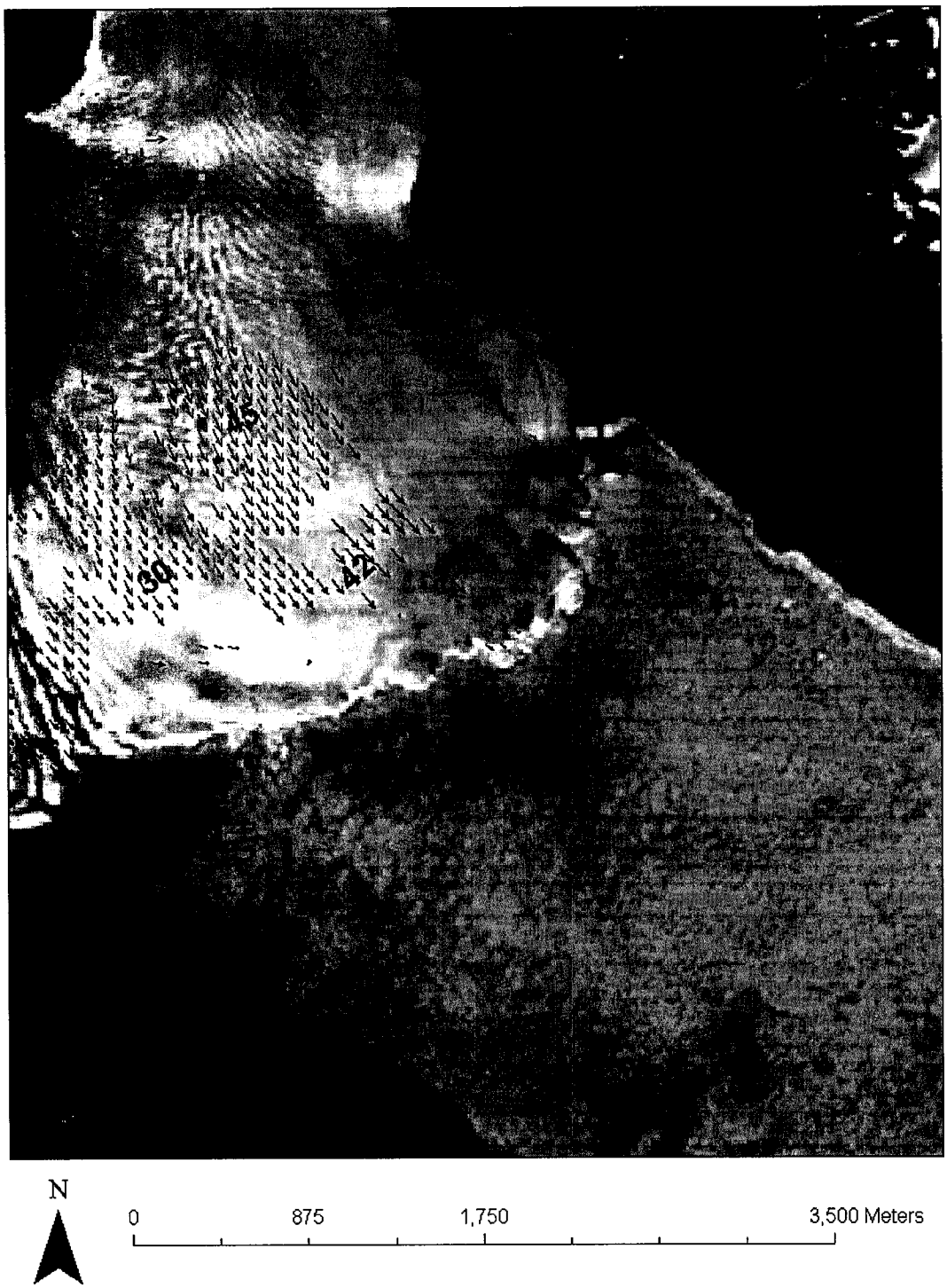

Figure 50. Image cross-correlation velocity results (m a^{-1}) for Sawyer Bay Glacier between July 10, 1999 and July 4, 2003 displayed on the July 10, 1999 Landsat 7 panchromatic image.

Ice cap calving rates

The sum of the annually averaged calving rates of individual glaciers draining the Agassiz Ice Cap, during the period 1999 to 2002, was estimated to be 0.6 ± 0.2 km^3 a^{-1}. This estimate should represent the majority (likely greater than 90%) of the calving from the Agassiz Ice Cap because it includes all of its major tidewater glaciers. The calving rate estimate for Sawyer Bay Glacier, a minor glacier draining the ice cap, was excluded from the total because its calving rate could not be differentiated from zero. The majority of the calving occurs from the larger tidewater glaciers, of which the Eugenie Glacier alone accounts for 47% of the 1999 to 2002 calving flux. The average calving rate from the Otto Glacier from 1999 to 2003 was estimated to be 0.25 ± 0.03 km^3 a^{-1}. This is likely to be a large fraction of the mass loss by iceberg calving from the western Grant Ice Cap because Otto Glacier is the only one of the three tidewater glaciers draining this ice cap that does not terminate in a fjord that is permanently covered by sea-ice. The range of likely ice cap calving rates was computed using the maximum and minimum estimates of calving rates from each glacier. The maximum calving rate estimate results from the assumption that the glacier was either floating or flowing entirely by basal sliding or subglacial sediment deformation. The minimum calving rate results from the assumptions that the glacier terminus was grounded and that the glacier was flowing entirely by ice deformation. The available imagery was not collected in a temporally uniform manner. Therefore calving rates could not be estimated from all glaciers for periods of ~ 12 months. Estimates of the annual average calving rates were computed for Antoinette, Lake Tuborg, d'Iberville and Parrish Glaciers for the period 1999 to 2001, and for Cañon Glacier for the period 2000 to 2003.

Calving rates during the period 1999 to 2003 are highly variable. The largest amount of variation occurs in the two fastest flowing glaciers, Otto and Eugenie Glaciers, which account for ~63% of the estimated calving from the nine glaciers considered in this study. The mean calving rate from Otto Glacier is 0.25 ± 0.08 km^3 a^{-1} (1 standard deviation) and that from Eugenie Glacier is 0.28 ± 0.05 km^3 a^{-1}. The calving rates in the period from June to August are from two to eight times larger than the annual averages. Terminus area change and velocity variation both contribute to calving rate variability at

both annual and seasonal timescales. However, large summer velocities are mainly responsible for the large summer calving rates.

DISCUSSION

Glacier flow rates and flow rate variability

Before the advent of satellite remote sensing, measurements of glacier velocities in the Canadian Arctic were confined to studies using stake networks on smaller glaciers and on safely accessible outlet glaciers. These studies measured annual surface velocities that were typically in the 10 – 50 m a^{-1} range (e.g. Koerner, 2002; Copland et al., 2003b). Surging glacier flow has been of special interest to researchers because of the high velocities that are achieved and the potential for producing large calving rates. Annually averaged velocities of 250 to 1000 m a^{-1} (e.g. Copland et al., 2003a; Holdsworth, 1977) have been recorded for several probable surging glaciers in the Canadian Arctic. The fastest recorded velocity (~2800 m a^{-1}) was measured at Otto Glacier in the summer of 1959 (Hattersley-Smith, 1969).

Several studies have indicated that velocities of land terminating glaciers in the Canadian Arctic increase during the summer (e.g. Iken, 1972; Bingham et al., 2003) with peak summer velocities reaching as much as 400% above winter velocities (Copland et al., 2003b). To date, however, there have been few studies of the seasonal velocity variability of large, fast flowing tidewater glaciers in the region. Holdsworth (1977) showed that the 1975 summer (July-August) velocity of d'Iberville Glacier, which may have been experiencing a surge at the time, was ~9% higher than the average velocity over the whole of the year 1974-75. Moreover the 1974-75 annual average velocity (~457 m a^{-1}) indicates that the winter velocity was likely quite large.

Recently, Short and Gray (2005) employed the speckle tracking technique to RADARSAT-1 synthetic aperture radar imagery (24 day image capture separation) to determine late winter (February-March) velocities and calving rates for several tidewater glaciers (>1.5 km in width) on Ellesmere Island. These short-term measurements provide limited information about either annually averaged velocities or the magnitude of seasonal velocity variation. Velocities of several hundred metres per year were found to be common on these tidewater glaciers, a result that is confirmed here. The glaciers

included in the present study can be grouped into three categories on the basis of their annually averaged velocities: (i) glaciers that have relatively fast annual flow mean rates (~500 – 700 m a^{-1}): Eugenie and Otto Glaciers; (ii) glaciers with moderate annual mean flow rates (~100 – 200 m a^{-1}): Lake Tuborg, Antoinette, d'Iberville, and Cañon Glaciers; and (iii) glaciers with relatively slow annual flow rates (~10 – 100 m a^{-1}): Parrish, John Richardson Bay and Sawyer Bay Glaciers. Radio-echo soundings indicate that Otto Glacier (Hattersley-Smith et al., 1969), Eugenie, Lake Tuborg, d'Iberville and Cañon Glaciers may have floating termini, whereas Parrish, John Richardson Bay and Sawyer Bay are probably grounded at their termini (Dowdeswell, personal communication – 2006). It is not clear whether the terminus of Antoinette Glacier is floating or grounded. Thus most of the glaciers with annual flow rates > ~100 m a^{-1} may have floating termini.

The largest velocities calculated here are the velocities of Lake Tuborg and Antoinette Glaciers in the period July to August 2001 and of d'Iberville Glacier in the period June to July 2001. These summer velocities are approximately an order of magnitude larger than the annually averaged velocities (100 – 200 m a^{-1}) of these glaciers. At Lake Tuborg and Antoinette Glaciers, the early summer (June to July) velocities are ~half of the late summer velocities. By comparison, the early summer flow rates of Eugenie Glacier increase only marginally over the annually averaged rate during the summer. Imagery of d'Iberville and Eugenie Glaciers was not available for August 2001, so the late summer velocity could not be determined and the question of whether the velocity continued to increase during this period is unanswered. The seasonal velocity variation of the other glaciers in this study could not be determined because repeat summer imagery was not available.

Variations in a glacier's flow rate are related to variations in its force balance (O'Neel et al., 2005). A glacier's down slope flow caused by gravitational driving stress is balanced by resistive stresses, provided that conservation of momentum can be treated as a static equilibrium (Paterson, p258). This assumption can be used for slow flowing fluids such as glaciers, assuming depth independent strain (geometrical deformation caused by stress). Resistive stresses are derived by using the constitutive relation to invert spatial derivatives of horizontal surface velocities (O'Neel et al., 2005). However, the force balance for individual glaciers is dictated by the local valley and bed geometry.

Thus the discussion of the variations in both summer and annual velocity reported here should be framed in terms of the components of force balance, and their relative contributions to the stresses resisting the down-slope motion of the glacier.

Changes in a glacier's driving stress can occur. Driving stress is directly related to the surface slope and glacier thickness. Under conditions of fast flow ice thickness and surface slope can change rapidly (potentially days to weeks), but under conditions of slow flow these variations will occur over a prolonged period (potentially years). The relative importance of longitudinal and transverse resistive stresses is altered by the degree of sliding, and longitudinal stress acting on the terminus is altered by changes in buttressing. However, to maintain the static equilibrium, when one stress decreases another must increase to compensate. The amount of sliding can be mediated by surface melt water penetrating to the bed in summer, sliding on materials that alter their deformation with water content and/or the composition of the thermal regime of at the base of a glacier. Alteration in resistive stress can also be caused by a change in the buttressing effect caused by the presence/absence of sea-ice or the change in the geometry of a glacier's terminus. A glacier's terminus region, either floating or grounded, has contact with confining valley walls which resist flow.

Summer melt water penetration to a glacier's bed has been shown to increase the sub-glacial water pressure (e.g. Iken, 1983) in alpine glaciers thus enhancing glacier sliding (and surface velocity) by separating a glacier from its bed, which reduces basal drag. In Greenland, Zwally and others (2002) have shown that seasonal flow acceleration near the ice sheet equilibrium line correlates with variations in the intensity of surface melting, with larger increases accompanying higher amounts of summer melting. Thus inter-annual variations in the amount of melt water penetration to the bed correlate with inter-annual velocity variations. The near coincidence of the period of flow acceleration with that of surface melting is further evidence that glacier sliding is enhanced by surface melt water input to the basal environment. Recently (Amundson et al., 2006) showed that basal shear stresses in a central region of the land terminating Black Rapids Glacier in Alaska decreased progressively while lateral stresses increase between spring and summer while velocity increased progressively (1.2 and 1.5 times respectively compared to winter values). The seasonal velocity increases are likely associated with the eventual

decoupling of the ice from its bed in certain locations due to the influx of water. The velocity progression recorded on Black Rapids Glacier is similar to that recorded on Antoinette and Lake Tuborg Glaciers, and suggests a similar mechanism of velocity increase. However in the case of floating termini the velocity increase is transferred across the grounding line.

The enhancement of sliding by increased sub-glacial water pressure does not however indicate that sliding of large glaciers only occurs during the summer months when the glacier is de-coupled from its bed. Zwally and others (2002) hypothesised that glacier sliding on a wet base maintained at the pressure melting point (PMP) is important year round. Otherwise, if a glacier's bed is below its freezing point, shear predominates near the bed (Paterson, p.255), and lower velocities may result. Depending on the amount of resisting stress or bed properties, a glacier may slide at a relatively slow rate. However glacier sliding over a deformable sub-glacial sediment layer, to which the addition of surface melt water would increase the sliding efficiency by saturating the sediment, could explain the high annual velocities. In the lower portions of tidewater glaciers that are experiencing large amounts of dynamic thinning in Greenland, annual flow rates increase only marginally in the summer (Rignot and Kanagaratnam, 2006). The reason for this behaviour is unknown, but likely stems from high rates of sliding and or deformation of sub-glacial sediment or basal ice throughout the year. Water at the base of a glacier can promote sliding and can be modelled with effective pressure (ice over-burden pressure minus the water pressure). To test the sliding hypothesis, Vieli and others (2000) used an effective-pressure-dependent sliding law model coupled with a highly deformable basal layer applied to a numerical glacier-flow model for a tidewater glacier in Svalbard. The results indicate that enhanced basal sliding on a thin highly deformable basal layer is likely an important aspect of the seasonal velocity change because model velocities closely match field velocities.

Back pressure exerted on a glacier by sea-ice or a floating glacier tongue may regulate a glacier's velocity. In Greenland the stability of glaciers with floating tongues is dependent on the back-pressure provided by the sea-ice in front of the glacier (Reeh et al., 2001). Furthermore calving only takes place during the seasonal break-up of the near shore fast-ice. Back pressure changes on a glacier's terminus can diminish due to the

seasonal melting or thinning of sea-ice. However Luckman and Murray (2005) indicate that little evidence for a reduction in this form of back pressure is evident in the terminus change at Jakobshavn Isbræ in 1995. Joughin and others (2004) indicated that "back-stress" exerted from resistance from fjord walls and pinning points regulates Jakobshavn Isbræ's terminus position. When a section of a floating tongue is removed less lateral friction is exerted on the tongue and velocity increases. However to restore equilibrium in the new configuration, longitudinal shear stresses must increase, which increases the resistive force from lateral drag. This theory is supported by losses of sections of the floating terminus coinciding with velocity increases at Jakobshavn Isbræ, and elsewhere (e.g. De Angelis and Skvarca, 2003).

Here, only minor changes in terminus area (calving zone of <200 m long) occur between 1999 and 2003. At the fastest flowing (annually) glaciers analysed here, Otto and Eugenie Glaciers, the terminus area changes between 1999 and 2003 do not appear to be associated with inter-annual velocity changes. The velocity at Eugenie Glacier did increase early in the summer of 2001 when sea-ice was still present in the fjord but the terminus area change remained within the limits of the 1999 to 2003 fluctuations. Furthermore sea-ice was present in front of the Otto Glacier in July and August 1959, but whether the large velocity recorded during this period was a seasonal increase over annually averaged velocity or a surge is unknown. At Antoinette and Lake Tuborg Glaciers in 2001 sea-ice cover was present in June and July, but had completely disappeared by August, which correlates to the period when the largest velocities were recorded. At d'Iberville Glacier sea-ice cover was present in both June and July. However, the velocity increase at d'Iberville Glacier was as large as those from Antoinette and Lake Tuborg Glaciers where sea-ice disappeared. Thus it would seem that the reduction in the buttressing effect provided by the removal of sea-ice is not necessary for the order of magnitude summer velocity increase over the annually averaged velocities. Unfortunately August 2001 imagery was not available for d'Iberville and Eugenie Glaciers. Therefore if the velocity continued as recorded at Antoinette and Lake Tuborg Glaciers is unknown. Furthermore, whether the large velocity increases on Antoinette, Lake Tuborg and d'Iberville Glaciers is related to the

fact that they drain the north central portion of Agassiz Ice Cap is unknown because of the lack of August imagery from the other moderate and fast annually flowing glaciers.

Evidence for the glacier sliding mechanism is also apparent in the data set analysed here. The glaciers with the largest velocities (both seasonal and annual) have significant amounts of surface crevassing. The crevasses provide ample opportunity for the entrance of surface melt water to the basal environment which could promote sliding in a fashion suggested by Zwally and others (2002). Furthermore, the ponding of melt water viewed on many of these glaciers is suggestive of high basal water pressure (assuming that surface water viewed is in hydrostatically linked to the glacier's basal environment). Lastly many of the slow flowing glaciers analysed here had melt water channels running on the surface to the terminus, which suggests surface melt water is not entering the basal environment in large volumes.

The implications of calving rate variation

The calving rates reported here are highly variable. Inter-annual differences can be as large as two fold and the summer rates are ~2 – 8 times larger than the annual values. Previously, calving rates from Devon Ice Cap (Burgess et al., 2005) and from various glaciers from Ellesmere Island (Short and Gray, 2005) have been estimated using imagery captured over periods less than a month, and on the assumption that the measured ice surface velocities approximated the long term average. The calving rate estimates were made using velocity measurements derived during the winter months from 1-3 day repeat synthetic aperture radar interferometry (InSAR) (Burgess et al., 2005) or 24 day repeat SAR speckle tracking velocities (Short and Gray, 2005). In light of the significant amount of variability in calving rates found here the approach of assuming that the velocity estimates used in these studies provide a good estimate of the long term mean velocity is potentially problematic. However, the annually averaged calving rates reported here were derived for a relatively narrow time window (three or four years) and from a relatively small sample of glaciers. Therefore the results found here may not be sufficient to characterise the calving rate variability over longer time scales.

The best estimate of iceberg calving from the Agassiz Ice Cap (approximately 19,500 km^2) between 1999 and 2002 is 0.6 ± 0.2 km^3 a^{-1}, with ~47% of calving occurring

from Eugenie Glacier. Although several smaller tidewater glaciers on Agassiz Ice Cap were not included in this study, their contribution to the total calving flux from the ice cap is likely negligible. For example, eight major tidewater glaciers accounted for ~90% of the total ice mass discharged by calving from the Devon Island Ice Cap (Burgess et al., 2005). On Agassiz Ice Cap the five largest tidewater glaciers (Eugenie, Antoinette, Lake Tuborg, d'Iberville and Cañon) account for a similar fraction (~97%) of the calving from the eight glaciers considered. The calving rate from the Devon Island Ice Cap (approximately 14,400 km^2) estimated by Burgess and others (2005) between 1960 and 1999 assuming invariable flow rates was 0.57 $km^3\ a^{-1}$. The large calving rates estimated for the Agassiz Ice Cap indicate that iceberg calving is likely a significant component of mass balance. However without estimating the surface mass balance for Agassiz Ice Cap, the relative importance of the iceberg calving term is unknown. The results found here indicate that calving rates can vary substantially both annually and seasonally, which suggests that iceberg calving has the potential to bring about rapid changes in the overall mass balance of these ice caps.

Variations in glacier calving rate associated with changes in flow dynamics

Surge-type glaciers have the potential to produce a significant increase in the iceberg calving rate when they are actively surging (e.g. Dowdeswell, 1989). Tidewater glaciers may undergo periods of fast flow during the retreat phase of the tidewater glacier cycle that can potentially result in large calving rates that may continue for long periods, similar in form to the Alaskan Columbia Glacier (Meier and Post, 1987). Furthermore non-cyclical non-surge type flow rate variability in the form of multiyear periodic, pulse-like increases in velocity may occur (Mayo, 1978). However, accurately determining whether a tidewater glacier is surging or experiencing grounding line instability is often difficult from the data available. For example the two glaciers with the largest annually averaged velocities (and calving rates) considered in this study (Otto and Eugenie Glaciers) could potentially be either surging or experiencing fast flow related to their tidewater nature. With no image data for the period between 1964 and 1999, it is difficult to determine whether the high velocities and terminus position change recorded at Otto Glacier between 1999 and 2003 are a continuation of the 1950s era "surge", a second

surge, or a sustained period of fast flow (as opposed to a cyclic flow instability) (e.g. Meier and Post, 1987). At Eugenie Glacier, the lack of diagnostic surge features, a progressive terminus region width decrease and lack of terminus position change suggests that this glacier is no surging even though it is fast-flowing. Thus without detailed altimetry data to monitor changes in ice thickness, a surge should not be ruled out. The switches in flow regime observed at Otto and Eugenie Glaciers could potentially represent a permanent change from slow to fast flow. Finally, the lack of substantial terminus position change (greater than several kilometres) at the majority of the glaciers contained in this study indicates that the data set analysed here is not sufficient to differentiate the effects of glacier surges or tidewater retreat on calving rates.

Floating tidewater glacier tongues and mass balance

An important, but often overlooked, form of ablation from floating termini exists – mass loss by basal melting. This has been shown to be an important ablation term in North and Northeast Greenland (Rignot et al., 1997). The Petermann Glacier in Northern Greenland is a dramatic example of how significant this type of ablation can be, as basal melting accounts for 10 times more ablation than surface melting (Stewart et al., 2004). In a survey of 14 tidewater glaciers in North and Northeast Greenland, Steffen and others (2005) found that grounding line ice flux is ~3.5 times that estimated from iceberg calving. The discrepancy has been attributed to surface and basal melting, with basal melting thought to be the dominant term. Little is known about basal melt rates from floating termini in the Canadian Arctic. Holdsworth (1977) suggested that basal melting must be occurring throughout the year on d'Iberville Glacier because the height of icebergs surrounded by sea-ice decreased progressively during the winter. Of the nine glaciers studied here the largest five likely had floating termini. Lake Tuborg's ~5 km long floating tongue is likely the longest of these. This indicates that future studies into ice cap mass balance should determine the significance of basal melting.

Further work

Calving rates from large tidewater glaciers in northern Ellesmere Island as appear to be highly variable. Thus, calving rates need to be computed using estimates of the long term

average flow velocity of glaciers rather than using velocities measured over short time intervals. Presently little is known about the mechanisms that are responsible for the variability of tidewater glacier flow. To this end, field work will have to be accomplished to better understand the force balance of tidewater glaciers in the Canadian Arctic and its changes over time. The acquisition of repeat laser altimetry surveys may help resolve the nature of glacier fast flow. Surges could potentially be identified by a migrating surge front and may provide an opportunity to better understand how thickness changes may affect terminus buoyancy. A laser altimetry survey, similar to those conducted in Greenland (e.g. Abdalati, et al., 2001), would provide a base-line to which future glacier and ice cap elevations could be quantitatively compared. Finally, an effort to estimate the outstanding components of mass balance should be made and thus quantitatively comment on this region's influence on sea-level change. In light of the significance of basal melt from floating glacier tongues, of which the study area has several, this component of mass balance should actually be measured (and not considered insignificant). A more comprehensive understanding of how the study area is reacting to air temperature variation would require the acquisition and analysis of significantly more precipitation and temperature data than are currently being collected. These data must be collected in conjunction with a sufficient amount of new optical imagery to adequately document the spatial and temporal evolution of glacier surface velocity fields. Unfortunately the acquisition of optical imagery is dictated by orbital repeat times and atmospheric conditions and high latitude variations in illumination dictate whether the data provide adequate ground visibility. In light of the results of this study, optical imagery should be considered necessary for further understanding glacier flow and calving rate variability. However due to the limitations inherent to optical imagery, radar imagery analysis should supplement optical imagery because of its ability to view glaciers through the polar night and cloud cover.

CONCLUSIONS

Iceberg calving rates have been calculated for nine major tidewater glaciers draining the Agassiz and western Grant Ice Caps using estimates of surface velocity and terminus position change derived from repeat optical imagery captured between 1999 and 2003.

The average calving rate from the Agassiz ice cap from 1999 to 2002 was estimated to be 0.6 ± 0.2 km^3 a^{-1}, with ~ 47% of the calving occurring from Eugenie Glacier. Four minor tidewater glaciers were omitted from this estimate of the total calving flux because their influence was thought to be negligible because they were small in size and inactivity. The average calving rate from Otto Glacier from 1999 to 2003 was estimated to be 0.25 ± 0.03 km^3 a^{-1}, which is likely a large majority of the mass loss by iceberg calving from western Grant Ice Cap. The 1999 to 2003 annual calving rates are highly variable, with increases of up to 100% between successive years. The June to August 2001 calving rates are ~2 – 8 times larger than the annual values, largely because of the large summer velocity increases compared to the annually averaged velocities. Summer velocity increases of up ~10 times the annual values have been recorded for the months of July to August, with ~3 fold increases being common from June to July. The summer velocity increases suggest surface melt water penetration may play a dominant role in enhancing basal sliding but velocity increase caused by removing of the buttressing effect from sea-ice or floating tongue geometry change should not be discounted. Few cases of terminus retreat or large amounts of terminus position variability occurred in the study area between 1959 and 2003.

REFERENCES

Abdalati, W., W. Krabill, E. Fredrick, S. Manizade, C. Martin, J. Sonntag, R. Swift, R. Thomas, C. Wright, and J. Yungel. 2001. Outlet glacier and margin elevation changes: Near coastal thinning of the Greenland Ice Sheet. *Journal of Geophysical Research*, **106**, 33729-33741.

Amundson, J. M., M. Truffer and M. P. Lüthi. 2006. Time-dependent basal stress conditions beneath Black Rapids Glacier, Alaska, USA, inferred from measurements of ice deformation and surface motion. *Journal of Glaciology*, **52**, 347-357.

Bernstein, R. 1983. Image geometry and rectification, In Manual of Remote Sensing (R. N. Colwell, ed.), American Society of Photogrammetry, Falls Church, VA, pp.881-884.

Bingham, R. G., P. W. Nienow and M. J. Sharp. 2003. Intra-annual and Intra-seasonal flow dynamics of a High Arctic polythermal valley glacier. *Annals of Glaciology*, **37**, 181-188.

Burgess, D. O., M. J. Sharp. 2004. Recent changes in areal extent of the Devon Ice Cap, Nunavut, Canada. *Arctic, Antarctic, and Alpine Research*, **36**, 261-271.

Burgess, D. O., M. J. Sharp, D.W.F. Mair, J. A. Dowdeswell, T. J. Benham. 2005. Flow dynamics and iceberg calving rates of Devon Ice Cap, Nunavut, Canada. *Journal of Glaciology*, **51**, 219-230.

Church, J., et al. 2001. Changes in sea level in *Climate Change 2001: The Scientific Basis: Contributions of Working Group I to the Third Assessment Report of the Intergovernmental Panel on Climate Change*, edited by J. Houghton et al., 639-694, Cambridge University Press, Cambridge, U.K. 892pp.

Copland, L., M.J. Sharp, J.A. Dowdeswell. 2003a. The distribution and flow characteristics of surge-type glaciers in the Canadian High Arctic. *Annals of Glaciology*. **36**, 73-81.

Copland, L., M. J. Sharp, P. W., Nienow. 2003b. Links between short-term velocity variations and the subglacial hydrology of a predominantly cold polythermal glacier. *Journal of Glaciology*, **49**, 337-348.

De Angelis, H. and P. Skvarca. 2003. Glacier surge after ice shelf collapse. *Science*, **299**, 1560-1562.

Dowdeswell, J. A. 1989. On the nature of Svalbard icebergs. *Journal of Glaciology*, **35**, 224-234.

Dowdeswell, J. A. and 10 others. 2002. Form and flow of the Academy of Sciences ice cap, Severnaya Zemlay, Russian High Arctic. *Journal of Geophysical Research*, **107**(B4). (10.1029/2000JB000129.)

Dowdeswell, J. A., T. J. Benham, M. R. Gorman, D. Burgess and M. Sharp. 2004. Form and flow of the Devon Island ice cap, Canadian Arctic. *Journal of Geophysical Research*, **109**(F02002). (10.1029/2003JF000095.)

Gray, A. L., K. E. Mattar, P. W. Vachon, R. Bindschadler, K. C. Jezek, R. Forster, J. P. Crawford. 1998. InSAR results from the RADARSAT Antarctic mapping mission data: estimation of glacier motion using a simple registration procedure. In *Proceedings of the IEEE International Geoscience and Remote Sensing Symposium*, IGARSS'98, 6-10 July 1998, Seattle Wash. IEEE Inc., Piscataway, N.J. Vol.3, pp. 1638-1640.

Gray, A. L., N. Short, K. E. Mattar and K. C. Jezek. 2001. Velocities and flux of the Filchner Ice Shelf and its tributaries determined from speckle tracking interferometry. *Canadian Journal of Remote Sensing*, Vol. 27, No. 3, pp. 193-206.

Hattersley-Smith, G. 1964. Rapid advance of glacier in northern Ellesmere Island. *Nature*, **201** (4915), 176.

Hattersley-Smith, G. 1969. Recent observations of the surging Otto Glacier, Ellesmere Island. *Canadian Journal of Remote Sensing*, **27**, 193-206.

Hattersley-Smith, G., A. Furesy, S. Evans. 1969. Glacier Depths in Northern Ellesmere Island: Airborne Radio Sounding in 1966. Defense Research Establishment Ottawa. DREO Technical Note NO. 69-6.

Holdsworth, G., 1969. Flexture of a floating ice tongue. *Journal of Glaciology.* **8**, 385-397.

Holdsworth, G. 1977. *Ice flow and related measurements of d'Iberville Glacier, Ellesmere Island, NWT, Canada.* Glaciology Division. Inland Waters Directorate, Department of the Environment, Ottawa, Ont.

Howat, I. M., I. Joughin, S. Tulaczyk, and S. Gogineni. 2005. Rapid retreat and acceleration of Helheim Glacier, east Greenland. *Geophysical Research Letters.* **32**, L22502, doi:10.1029/2005GL024737.

Hughes, T. 2002. Calving bays. *Quaternary Science Reviews.* **21**, 267-282.

Iken, A. 1972. Measurements of water pressure in moulins as part of a movement study of the White Glacier, Axel Heiberg Island, Northwest Territories, Canada. *Journal of Glaciology*, **11**(61), 53-58.

Iken, A., H. Röthlisberger, A. Flotron, W. Haberli. 1983. The uplift of Unteraargletscher at the beginning of the melt season – a consequence of water storage at the bed? *Journal of Glaciology*, **29**, 28-47.

IPCC, 2001: *Climate Change 2001: Impacts, Adaptation, and Vulnerability.* McCarthy, J. J., Canziani, O. F., Leary, N. A., Dokken, D. J., White, K. S. (eds.). Cambridge: Cambridge University Press for Intergovernmental Panel on Climate Change. 1032 pp.

Jania, J. 2002. Calving intensity of Spitsbergen Glaciers. In *The Changing Physical Environment: Proceedings from the 6th Ny Aalesund International Scientific Seminar*, 8-10 October 2002. Polar Environmental Centre, Tromso, Norway. Norwegian Polar Institute, NP Report Series 10, pp. 117-120.

Joughin, I., S. Tulaczyk, M., M. Fahnestock, R. Kwok. 1996. Contribution to the glaciology of northern Greenland from satellite radar interferometry. *Science.* **274**, 228.

Joughin, I., R. Kwok, M. Fahnestock. 1998. Interferometric estimation of three-dimensional ice flow using ascending and descending passes. *IEEE Transactions on Geoscience and Remote Sensing*, Vol. 36, No. 1, pp.25-37.

Joughin, I., W. Abdalati, and M. Fahnestock. 2004. Large fluctuations in speed on Greenland's Jakobshavn Isbræ glacier. *Nature*, **432**, 608 – 610.

Joughin I. and D. R. MacAyeal. 2005. Calving of large tabular icebergs from ice shelf rift systems. *Geophysical Research Letters*, **32**, L02501, doi:10.1029/2004GL020978

Kirkbride, M. P. and C. R. Warren, 1999. Tasman Glacier, New Zealand: 20th – Century thinning and predicted calving retreat. *Global and Planetary Change.* **18**, 11-28.

Koch, L. 1928. Contributions to the glaciology of Northern Greenland. *Medd. Groenl.* **65**, 181.

Kock, I., M. Sharp, L. Nicholson, D. Dahl-Jensen. Comparison of climate proxies in short ice core records from the Canadian Arctic with observed climate records. Submitted to Annals of Glaciology (**46**).

Koerner, R. M. 2002. Glaciers of the High Arctic Islands. In *Satellite image atlas of glaciers of the world, North America.* Edited by R. Williams and J. Ferrigno. US Geological Survey, Professional Paper 1386-J, pp. 129–134.

Krabill, W., E. Hanna, P. Huybrechts, W. Abdalati, J. Cappelen, B. Csatho, E. Frederick, S. Manizade, C. Martin, J. Sonntag, R. Swift, R. Thomas, and J. Yungel. 2004.

Greenland Ice Sheet: Increased coastal thinning. *Geophysical Research Letters*, **31**, L24402, doi:10.1029/2004GL021533.

Lawson, W. 1997. Spatial, temporal and kinematic characteristics of surges of Variegated Glacier, Alaska. *Annals of Glaciology*, **24**, 95-101.

Luckman, A. and T. Murray. 2005. Seasonal variation in velocity before retreat of Jakobshavn Isbræ, Greenland. *Geophysical Research Letters*, **32**, L08501, doi:10.1029/2005GL022519.

MacDonald, T. R., J. G. Ferrigno, R. S. Williams Jr., B. K. Lucchitta. 1989. Velocities of Antarctic outlet glaciers determined from sequential Landsat images. *Ant-arctic J. U. S.*, **24**, 105-106.

Mayo, L. R. 1978. Identification of unstable glaciers intermediate between normal and surging glaciers. *Mat. Glyatsiologicheskikh Issled. Khronica Obsuzhdeniya*, 33, pp. 133-135.

Meier, M.F. and A. Post. 1969. What are glacier surges? *Canadian Journal of Earth Sciences*, **6**, 807-817.

Meier, M.F. and A. Post. 1987. Fast Tidewater Glaciers. *Journal of Geophysical Research*, **92**, 9051-9058.

Molnia, B. 2003. Disarticulation and recent rapid retreat of the Bering Glacier, Alaska. The Geological Society of America, XVI INQUA Congress Conference Proceedings. July 24, 2003.

Müller, F. 1969. Was Good Friday Bay Glacier on Axel Heiberg Island surging? *Canadian Journal of Earth Sciences*, **6**(4), Part 2, 891-894.

Murray, T., T. Strozzi, A. Luckman, H. Jiskoot, P. Christakos. 2003a. Is there a single surge mechanism? Contrasts in dynamics between glacier surges in Svalbard and other regions. *Journal of Geophysical Research.* **108**, 2237-2252.

Murray, T., A.J. Luckman, T. Strozzi, A.M. Nuttall. 2003b. The initiation of glacier surging at Fridjovbreen Svalbard. *Annals of Glaciology*, **36**, 110-116.

Nye, J. F. 1952. The mechanics of glacier flow. *Journal of Glaciology*, **2**, 82-93.

Nye, J. F. 1965. The flow of a glacier in a channel of rectangular, elliptic or parabolic cross-section. *Journal of Glaciology*, **5**, 661-690.

O'Neel, S., W. T. Pfeffer, R. Krimmel, M. Meier. 2005. Evolving force balance at Columbia Glacier, Alaska, during its rapid retreat. *Journal of Geophysical Research*, **110**, F03012, doi:10.1029/2005JF000292.

Overpeck, J., K. Hugen, D. Hardy, R. Bradley, R. Case, M. Douglas, B. Finney, K. Gajewski, G. Jacoby, A. Jennings, S. Lamoureux, A. Lasca, G. MacDonald, J. Moore, M. Retelle, S. Smith, A. Wolfe, G. Zielinski. 1997. Arctic environmental change of the last four centuries. *Science*, **278**, 1251-1256.

Paterson, W.S.B., 1994. *The physics of glaciers*. Third Edition. Oxford. Elsevier. 481p.

Post, A. 1969. Distribution of surging glacier in western North America. *Journal of Glaciology*, **8**(53), 229-240.

Reeh, N. 1968. On the calving of ice from floating glaciers and ice shelves. *Journal of Glaciology*, **7**, 215-232.

Reeh, N., C. Mayer, H. Miller, H. H. Thomsen, A. Weidick. 1999. Present and past climate control on fjord glaciations in Greenland: Implications for IRD-deposition in the sea. *Geophysical Research Letters*, **26**(8), 1039-1042, 10.1029/1999GL900065.

Reeh, N, H. H. Thomsen, A. K. Higgins, A. Weidick. 2001. Sea-ice and the stability of north and northeast Greenland floating glaciers. *Annals of Glaciology*, **33**, 474-480.

Rignot, E. J., S. P. Gogineni, W. B. Krabill, S. Ekholm. 1997, North and Northeast Greenland Ice Discharge from Satellite Radar Interferometry. *Science*, **276**, 934-937.

Rignot, E., W. B. Krabill, S. P. Gogineni, I. Joughin. 2001. Contribution to the glaciology of northern Greenland from satellite radar interferometry. *Journal of Geophysical Research*, **106**, 34007-34020.

Rignot, E., P. Kanagaratnam. 2006. Changes in the Velocity Structure of the Greenland Ice Sheet. *Science*, **311**, 986-990.

Scambos, T. A., M. J. Dutkiewicz, J. C. Wilson, and R. A. Bindschadler, 1992. Application of image cross-correlation to the measurement of glacier velocity using satellite image data. *Remote Sensing of Environment*, **42**, 177-186.

Serreze, M. C., J. E. Walsh, F. E. Chaplin III, T. Osterkamp, M. Dyurgerov, V. Romanovsky, W. C. Oechel, J. Morison, T. Zhang, R. G. Barry. 2000. Observational evidence of recent change in the northern high latitude environment. *Climate Change*, **46**, 159-207.

Short, N. H. and A. L. Gray. 2005. Glacier Dynamics in the Canadian High Arctic from RADARSAT-1 Speckle Tracking. *Canadian Journal of Remote Sensing*, **31**, 225-239.

Sanderson, T. I. O and C. S. M. Doake. 1979. Is vertical shear in an ice shelf negligible? *Journal of Glaciology*. **22**, 285-292.

Stewart, C., E. Rignot, K. Steffen, N. Cullen, R. Huff. 2004. Basal topography and thinning of Petermann Gletscher, northern Greenland, measured by ground-based phase-sensitive radar. FRISP Report No. 15, 1-5.

Steffan, K., 2005, http://cires.colorado.edu/science/projects/aoms-steffenK01.html Accessed September 2006.

Strozzi, T., A. Luckman, T. Murray, U. Wegmüller, and C. L. Werner. 2002. Glacier motion estimation using SAR offset-tracking procedures. *IEEE Transactions on Geoscience and Remote Sensing*, **40**, 2384-2391.

Sturm, M. 1987. Observations of the distribution and characteristics of potholes on surging glaciers. *Journal of Geophysical Research*, **92**, 9015-9022.

Trettin, H. P. 1989. The Arctic Islands – in A. W. Bally and A. R. Palmer, eds., The Geology of North America: An Overview. Boulder, CO: Geological Society of America, Vol. A, p. 349-370.

Van der Veen, C.J. 2002. Calving glaciers. *Progress is Physical Geography*, **26**, 96-122.

Vaughan, D. G and C. S. M. Doake. 1996. Recent atmospheric warming and retreat of ice shelves on the Antarctic Peninsula. *Nature*, **379**, 328-331.

Vieli, A., M., Funk, H. Blatter. 2000. Tidewater glaciers: frontal flow acceleration and basal sliding. *Annals of Glaciology*, **31**, 217-221.

Weertman, J. 1973. Can a water-filled crevasse reach the bottom surface of a glacier? International Association of Scientific Hydrology Publication, **95**, 139-145.

Zwally, H. J., W. Abdalati, T. Herring, K. Larson, J. Saba, K. Steffen. 2002. Surface Melt-Induced Acceleration of Greenland Ice-Sheet Flow. *Science*, **297**, 218 – 222.